

RADIATION DAMAGE IN DISCONTINUOUS TANTALUM FILMS

EFFECTS OF PROTON RADIATION DAMAGE ON THE CONDUCTANCE AND
TEMPERATURE COEFFICIENT OF RESISTANCE OF
REACTIVELY SPUTTERED, DISCONTINUOUS TANTALUM THIN FILM RESISTORS

By

WAYNE RAYMOND HARDY, B.Sc., M.Sc.

A Thesis

Submitted to the School of Graduate Studies
in Partial Fulfilment of the Requirements
for the Degree
Doctor of Philosophy

McMaster University

November 1971

DOCTOR OF PHILOSOPHY
(Electrical Engineering)

McMASTER UNIVERSITY
Hamilton, Ontario

TITLE: Effects of Proton Radiation Damage on the Conductance
and Temperature Coefficient of Resistance of
Reactively Sputtered, Discontinuous Tantalum Thin
Film Resistors

AUTHOR: Wayne Raymond Hardy, B.Sc. (Queen's University)
M.Sc. (Queen's University)

SUPERVISOR: Professor J. Shewchun

NUMBER OF PAGES: xvi, 162

ABSTRACT

Tantalum thin film resistors have been reactively sputtered in oxygen and nitrogen simultaneously. The films studied had resistivities ranging from $400 \mu\Omega\text{-cm}$ to $3 \times 10^4 \mu\Omega\text{-cm}$. The corresponding TCR values ranged from $-50 \text{ ppm}/^\circ\text{C}$ to $-2,000 \text{ ppm}/^\circ\text{C}$. Conductance-temperature measurements show that electrical conduction in discontinuous films of metallic islands (typically 100 \AA) largely surrounded by regions of Ta_2O_5 (typically 50 \AA) may be due to a tunneling mechanism of negative TCR operating concurrently with a metallic mechanism of positive TCR via interconnected metallic islands.

Irradiation of these discontinuous films by 150 keV protons produces a conductance increase which is attributed to an enhanced tunneling mechanism via electronic defect levels in the inter-island oxide regions. During irradiation of these films at 30°K , the conductance change increases and approaches apparent saturation. This nonlinearity is attributed to a combination of spontaneous recombination and close-pair thermal annealing. The number of unstable sites surrounding each defect is found to be ≥ 4 . Thermal recovery of the conductance proceeds in two main stages: Stage A (34°K to 150°K) is attributed to close-pair or correlated recombination; Stage B (150°K to 300°K) is attributed to uncorrelated migration of defects to gap-island interfaces, as is indicated by the greatly reduced Stage B annealing which is observed for

continuous, polycrystalline films of Ta_2O_5 , having a typical grain size of 1,500 Å. Negative annealing stages (characterized by a conductance increase) indicate a metallic conduction process via connected metallic islands.

For 286° K irradiation of discontinuous films, the conductance initially increases with fluence in a nonlinear fashion until a threshold fluence is reached, at which point the conductance decreases with fluence. The nonlinearity of the conductance increase is attributed to trapping of mobile radiation-produced defects at gap-island interfaces during irradiation. The subsequent conductance decrease is attributed to a shift in the Fermi level, and thus the height of the tunneling barrier, as the result of the formation of unequal concentrations of stable radiation-produced donor and acceptor defects since unequal concentrations of these defects can be expected to annihilate at the gap-island interface. The absence of this conductance decrease in continuous polycrystalline films is consistent with this model, since the absence of gap-island interfaces is expected to result in equal concentrations of stable donor and acceptor levels being produced.

The observed negative increase in TCR with fluence is attributed to an increase in the proportion of the tunneling mechanism of negative TCR (as the result of radiation-produced defects in the inter-island oxide regions) relative to the proportion of the metallic conduction mechanism of positive TCR.

The difference between the TCR recovery after irradiation at 30°K (little recovery between 150°K and 300°K) and the conductance recovery (about 50 percent of the recovery occurs between 150°K and 300°K) is attributed to the expected greater influence of metallic recovery on the annealing of the film TCR relative to the annealing of the film conductance.

ACKNOWLEDGMENTS

I wish to thank my supervisor, Dr. J. Shewchun, for suggesting this problem and for his support during the ensuing investigation.

Dr. Roger Kelly and Dr. J.A. Davies provided much encouragement as well as many helpful suggestions regarding the experimental results.

Dr. Peter Pronko helped obtain the low temperature experimental data as well as suggesting possible interpretations.

Mr. L. Goodridge assisted in the construction of the accelerator.

Mr. R. Yager constructed the current integrator.

Film depositions by Mr. C. Tam and Mr. D. Kuenzig, Aerovox of Canada Ltd. are gratefully acknowledged.

Financial support for the project was provided by Aerovox of Canada Ltd.

T A B L E O F C O N T E N T S

I.	INTRODUCTION	1
1.1	General	1
1.2	Tantalum Thin Films	2
1.3	Radiation Damage in Thin Films	4
1.4	The Present Investigation	6
II.	EXPERIMENTAL EQUIPMENT	9
2.1	Accelerator	9
2.2	Current Integrator	10
2.3	Room Temperature Target Assembly	14
2.4	Cryogenic Equipment	14
2.5	Electrical Measurements	20
III.	REACTIVELY SPUTTERED TANTALUM THIN FILM RESISTORS	22
3.1	General	22
3.2	Experimental Procedure	22
3.3	Experimental Results	26
3.4	Discussion	43
3.5	Summary	54
IV.	LOW FLUENCE, ROOM TEMPERATURE RADIATION DAMAGE	56
4.1	General	56
4.2	Experimental Results	56
4.3	Discussion	64
4.4	Summary	76
V.	LOW TEMPERATURE IRRADIATION AND ISOCHRONAL ANNEALING EXPERIMENTS	77
5.1	General	77
5.2	Experimental Results	78
5.3	Discussion	91
5.4	Summary	99

VI.	HIGH FLUENCE, ROOM TEMPERATURE RADIATION DAMAGE	102
6.1	General	102
6.2	Experimental Results	103
6.3	Discussion	107
6.4	Summary	124
VII.	EFFECTS OF RADIATION DAMAGE ON FILM TCR	128
7.1	General	128
7.2	Experimental Results	128
7.3	Discussion	134
7.4	Summary	144
VIII.	CONCLUSIONS	146
APPENDIX A	THE RELATIONSHIP BETWEEN THE CHANGE IN FILM CONDUCTANCE DUE TO ENHANCED TUNNELING AND THE RADIATION-PRODUCED DEFECT CONCENTRATION	150
APPENDIX B	DEFECT CONCENTRATION AS A FUNCTION OF FLUENCE	153
APPENDIX C	FUNCTIONAL DEPENDENCES OF FILM CONDUCTANCE	156
REFERENCES		158

LIST OF FIGURES

FIGURE		PAGE
2-1	Circuit of current integrator.	11
2-2	Room temperature target assembly for thin film resistor irradiation.	15
2-3	Cryogenic target assembly.	17
2-4	Power dissipation of cryogenic target assembly.	18
2-5	Temperature response of cryogenic target assembly for typical isochronal annealing pulses.	19
3-1	Electron microscope results for a heat treated Ta film reactively sputtered in a partial pressure of 1.5×10^{-5} torr oxygen and 1.5×10^{-5} torr nitrogen.	27
3-2	Electron microscope results for Ta films reactively sputtered in a partial pressure of 7×10^{-6} torr nitrogen and 4.3×10^{-5} torr oxygen.	33
3-3	Room temperature resistivity and TCR of sputtered tantalum films as a function of total reactive partial pressure of oxygen plus nitrogen.	35
3-4	Arrhenius plot of film conductance, for a film sputtered in a total reactive partial pressure of 4.0×10^{-5} torr.	38
3-5	Film conductance plotted as a function of the square of the absolute temperature.	39
3-6	Room temperature conductance as a function of the square root of the heat treatment time, for a film heat treated at 500°C in an air ambient at atmospheric pressure.	41

FIGURE		PAGE
3-7	Arrhenius plot of the conductance change occurring in a film which was heat treated in air at atmospheric pressure.	42
4-1	σ - ϕ curves for room temperature irradiation of films sputtered in a reactive partial pressure of 2×10^{-5} torr nitrogen and 2×10^{-5} torr oxygen.	58
4-2	σ - ϕ curve for room temperature irradiation of a non heat treated film sputtered in a reactive partial pressure of 2×10^{-5} torr nitrogen and 2×10^{-5} torr oxygen.	59
4-3	Slope of the σ - ϕ curves for room temperature irradiation of films heat treated in air at 500°C , as a function of the total reactive partial pressure, for equal oxygen and nitrogen reactive partial pressures.	61
4-4	Slope of the σ - ϕ curves for room temperature irradiation of films heat treated in air at 500°C , as a function of reactive oxygen partial pressure, the reactive nitrogen partial pressure being kept constant at 7×10^{-6} torr.	62
4-5	Conductance increase at a fluence of 10^{16} p/cm ² as a function of $\frac{1}{E} \ln 130E$, where E is the beam energy.	65
4-6	Electron microscope results for a film sputtered in a reactive partial pressure of 5×10^{-6} torr nitrogen and 5×10^{-6} torr oxygen after irradiation to 10^{16} p/cm ² .	66
5-1	σ - ϕ curves for irradiation of non heat treated, vacuum heat treated, and air heat treated films to 10^{16} p/cm ² at 30°K . These films were sputtered in a reactive partial pressure of 2×10^{-5} torr nitrogen and 2×10^{-5} torr oxygen.	79

FIGURE		PAGE
5-2	σ - ϕ curve (marked x), and rate of conductance increase $d\sigma/d\phi$ as a function of conductance increase σ (marked o), for 34°K irradiation of a non heat treated film sputtered in a reactive partial pressure of 1×10^{-5} torr nitrogen and 3×10^{-5} torr oxygen.	80
5-3	σ - ϕ curve (marked x) for an air heat treated film irradiated at 30°K. The slope of the σ - ϕ curve ($d\sigma/d\phi$) is also shown as a function of σ (marked o). This film was sputtered in a reactive partial pressure of 1×10^{-5} torr nitrogen and 1×10^{-5} torr oxygen.	82
5-4	Integral isochronal annealing curve for an air heat treated film sputtered in a reactive partial pressure of 1×10^{-5} torr nitrogen and 3×10^{-5} torr oxygen.	83
5-5	Differential isochronal annealing curve for an air heat treated film sputtered in a reactive partial pressure of 1×10^{-5} torr nitrogen and 3×10^{-5} torr oxygen.	84
5-6	Differential isochronal annealing curve for a non heat treated film sputtered in a reactive partial pressure of 1×10^{-5} torr nitrogen and 3×10^{-5} torr oxygen.	86
5-7	Differential isochronal annealing curve for an air heat treated film sputtered in a reactive partial pressure of 1×10^{-6} torr nitrogen and 1×10^{-6} torr oxygen.	88
5-8	Differential isochronal annealing curve for a polycrystalline Ta ₂ O ₅ film which was sputtered in a reactive partial pressure of 7×10^{-6} torr nitrogen and 4.3×10^{-5} torr oxygen.	89

FIGURE		PAGE
5-9	Differential isochronal annealing curve for an air heat treated film sputtered in a reactive partial pressure of 3×10^{-5} torr nitrogen and 1×10^{-6} torr oxygen.	90
6-1	σ - ϕ curve for 286°K irradiation of a film sputtered in a reactive partial pressure of 3×10^{-6} torr nitrogen and 3×10^{-6} torr oxygen.	104
6-2	σ - ϕ curves for 286°K irradiation of air heat treated and non heat treated films sputtered in a reactive partial pressure of 1.5×10^{-5} torr nitrogen and 1.5×10^{-5} torr oxygen.	106
6-3	Curves illustrating the threshold fluence for the radiation-produced conductance decrease occurring at 286°K (marked x), and the magnitude of this decrease (marked Δ), as a function of total reactive partial pressure for equal partial pressures of reactive oxygen and nitrogen.	108
6-4	σ - ϕ curve for 286°K irradiation of a polycrystalline Ta_2O_5 film which was sputtered in a reactive partial pressure of 7×10^{-6} torr nitrogen and 4.3×10^{-5} torr oxygen.	109
6-5	Graph showing the σ - ϕ curve for the non heat treated film of Fig. 6-2 replotted as the slope of the σ - ϕ curve $d\sigma/d\phi$ (marked o), and the reciprocal slope of the σ - ϕ curve $d\phi/d\sigma$ (marked x), as a function of the conductance increase σ .	111
6-6	Graph showing the σ - ϕ curve for the air heat treated film of Fig. 6-2 replotted as the slope of the σ - ϕ curve $d\sigma/d\phi$ (marked x), and the reciprocal slope of the σ - ϕ curve $d\phi/d\sigma$ (marked o), as a function of the conductance increase σ .	113

FIGURE		PAGE
6-7	Graph showing the σ - ϕ curve for the air heat treated film of Fig. 6-3 replotted as the slope of the σ - ϕ curve $d\sigma/d\phi$ (marked o), and the reciprocal slope of the σ - ϕ curve $d\phi/d\sigma$ (marked x), as a function of the conductance increase σ .	115
6-8	Graph of the function $\ln\{1/[1-bC(\phi)]\}$ as a function of $bC(\phi)$.	121
6-9	Graph of $\ln(\phi^{\frac{1}{2}}d\sigma/d\phi)$ as a function of $\phi^{\frac{1}{2}}$ for fluences in excess of the threshold value for the radiation-produced conductance decrease.	125
7-1	Curves showing the conductance increase as a function of temperature for a film sputtered in a reactive partial pressure of 2×10^{-5} torr nitrogen and 2×10^{-5} torr oxygen before irradiation (marked x), and after irradiation to 2.4×10^{18} p/cm ² (marked o).	129
7-2	Curves showing the ratio (post-irradiation TCR) to (pre-irradiation TCR) as a function of fluence for films sputtered in a reactive partial pressure of 2×10^{-5} torr nitrogen and 2×10^{-5} torr oxygen. The TCR was measured over the temperature range 303°K to 373°K (marked o), as well as from 33°K to 44°K (marked Δ).	132
7-3	Curve showing the variation with fluence of the percent conductance decrease which occurs at 30°C after a post-irradiation TCR run in which the films were maintained at 130°C for 30 minutes. This curve was for films sputtered in a reactive partial pressure of 2×10^{-5} torr nitrogen and 2×10^{-5} torr oxygen.	133

FIGURE

PAGE

- 7-4 Curve showing the variation with total reactive partial pressure of the percent conductance decrease (measured at 30°C) which occurs after a post-irradiation TCR run in which the films are maintained at 130°C for 30 minutes. These films were sputtered in equal reactive partial pressures of oxygen and nitrogen. 135
- 7-5 Curves showing the recovery which occurs in film conductance and film TCR as a function of temperature after irradiation to 2×10^{18} p/cm² at 34°K. This film was sputtered in a reactive partial pressure of 1×10^{-5} torr nitrogen and 3×10^{-5} torr oxygen. 136

LIST OF TABLES

TABLE		PAGE
3-1	Cross-section of reactive partial pressures of oxygen and nitrogen used in DC sputtering of tantalum thin films.	24
3-2	Comparison of electron diffraction pattern of Figure 3-1 with the standard Ta ₄ O ₃ electron diffraction pattern.	28
3-3	Summary of the structure of selected tantalum films reactively sputtered in oxygen plus nitrogen.	29
3-4	Analysis of tantalum electron diffraction pattern based on BCC lattice with $a_0 = 3.34 \text{ \AA}$.	30
3-5a	Room temperature resistivity and TCR of non heat treated films as a function of reactive oxygen partial pressure, the reactive nitrogen partial pressure being constant.	36
3-5b	Room temperature resistivity and TCR of non heat treated films as a function of reactive nitrogen partial pressure, the reactive oxygen partial pressure being constant.	36
3-5c	Room temperature resistivity and TCR of non heat treated films as a function of reactive oxygen and reactive nitrogen partial pressures, the total reactive partial pressure being constant.	37
3-6	Comparison of Ta(O,N) film resistivity and TCR with previously published results	52
4-1	Slope of the σ - ϕ curves for films heat treated in air, as a function of reactive nitrogen partial pressure, the reactive oxygen partial pressure being constant.	63

TABLE

PAGE

4-2 Slope of the σ - ϕ curves for films heat treated in air, as a function of reactive oxygen and nitrogen partial pressures, the total reactive partial pressure being constant at 4×10^{-5} torr.

63

INTRODUCTION

1.1 General

Due to their small physical size, precision, and long term stability, thin film resistors are used extensively in microelectronic circuits. Tantalum is often used as the basic film material due to the fact that it may be easily anodized. This property allows the resistance of a device to be trimmed very simply to within about 0.1% of the desired value. This trimming process is very important since untrimmed sputtered films generally deviate from the desired resistance value by several percent. An additional reason for employing tantalum as the basic film material is that anodically formed Ta_2O_5 is a relatively good dielectric, making the production of thin film capacitors completely compatible with the production of tantalum thin film resistors.

One of the main applications of thin film resistors is as feedback elements for active devices. In this application, the characteristics of the circuit become relatively independent of the characteristics of the active devices, but the sensitivity of the circuit to changes in the feedback network may approach unity¹. Thus, if a circuit is to be used in a radiation environment, such as occurs in a satellite, it is

important to understand the effects of radiation on the thin film resistors. However, the literature does not contain any significant references to such studies. The present investigation was undertaken in order to fill this apparent gap.

1.2 Tantalum Thin Films

For circuit applications, thin film resistors should have a high value of resistivity and a low temperature coefficient of resistance (TCR), generally within the range of +100 ppm/°C to -100 ppm/°C. Marcus² has employed electron beam evaporation to deposit undoped Ta films which approach bulk Ta in properties (13.6 $\mu\Omega$ -cm at room temperature and a TCR value of 2,000 ppm/°C). However, this resistivity is much too low and the TCR too large for practical use in resistor manufacture. Marcus and Quigley³ have found that films deposited on very clean substrates without the deliberate addition of reactive gases may have a β -type crystal structure⁴. The resistivity of these films is about 200 $\mu\Omega$ -cm and the TCR falls within the range of +100 ppm/°C to -100 ppm/°C⁵. Gerstenberg and Calbick⁶ have shown that the resistivity of sputtered films may be increased to about 300 $\mu\Omega$ -cm by the addition of reactive nitrogen to the sputtering gas. The TCR of about -100 ppm/°C has been attributed to the formation of a nitride compound. These authors⁶ have also demonstrated that the resistivity of the films may be increased further by reactive sputtering in oxygen. These films have resistivities

as high as $10,000 \mu\Omega\text{-cm}$, but the corresponding TCR is as large as $-1,500 \text{ ppm}/^\circ\text{C}$. These electrical parameters have been accounted for by the formation of regions of Ta_2O_5 within the film. Krikorian and Sneed ⁷ have reported that, if the partial pressure of reactive oxygen is sufficiently high, films of insulating Ta_2O_5 are formed. These films have been found to have resistivities as high as $10^{14} \mu\Omega\text{-cm}$ and TCR values as large as $-3,500 \text{ ppm}/^\circ\text{C}$.

The work on the properties of Ta films reported to date in the literature suggests that for thin film resistors requiring a small value of TCR, reactive sputtering with nitrogen may produce suitable films for small values of resistance. However, for large values of resistance, these nitride films may be excessively large physically. Therefore, for large resistances, films reactively sputtered with oxygen should be considered. However, these films would have the disadvantage of a very large negative TCR value.

Consideration of these results suggests that, if Ta films were reactively sputtered in oxygen and nitrogen simultaneously, the resulting films might have a relatively high resistivity and a relatively small TCR. The films used in the present investigation were sputtered in this fashion, and are suitable for use as resistors since they possess values of resistivity and TCR intermediate between films reactively sputtered in oxygen only and those reactively sputtered in nitrogen only.

1.3 Radiation Damage in Thin Films

A general review of radiation damage theory has been given by Thompson⁸. In connection with the effects of radiation damage on the properties of thin metallic films, Ramsay⁹ found that fast neutron irradiation of Ta and TaN films produced a resistance increase of 0.02% at 10^{16} n/cm². Merkle and Singer¹⁰ investigated the effects of 2 MeV α -particle irradiation on films of annealed Au, Cu, and Al. These films ranged in thickness from 2,000 Å to 7,000 Å and were irradiated at 4.2°K. The increase in resistance with fluence was attributed to atomic displacements within the films. Ivanovskii and Radzhabov¹¹ have studied the effects of 2 keV argon ion bombardment on Ti films of 1,000 Å thickness. These films were thermally annealed and degassed prior to irradiation. The resistance increase of 1.3% at a fluence of 1.5×10^{16} ions/cm² was attributed to carrier impurity scattering caused by argon ions deposited within the film. Navinsek and Carter¹² have irradiated Ag, Au, Ti, and W films of 500 Å thickness with argon ions of energy 250 eV to 4 keV. There were three distinct regions of resistance change with fluence. For values of fluence less than 5×10^{15} ions/cm², the resistance of the films decreased. This resistance decrease was attributed to the removal of

adsorbed gases on the surface of the film, thus changing the effect of the surface on carrier scattering. For fluence values between 5×10^{15} ions/cm² and 4×10^{16} ions/cm² the resistance increase was ascribed to "bulk" damage within the film. For higher values of fluence, the resistance increased catastrophically due to sputtering of the film. The failure of Ivanovskii and Radzhavov¹¹ to observe the initial resistance decrease on bombarding Ti films with argon ions might be attributed to the fact that their films were degassed prior to irradiation. Teodosic¹³ found that the irradiation of Ag films of thickness 150 Å to 400 Å by Ag ions of energy 20 keV to 500 keV caused the film resistance to decrease, reach a minimum and then increase with fluence. The initial resistance decrease was attributed to radiation-produced changes in the reflection coefficient for carriers striking the film surface. The subsequent resistance increase was ascribed to bulk damage and sputtering effects.

Although various types of films have been irradiated by different types of particles, no clear picture of irradiation effects on any given type of film emerges. Reports in the literature on the effects of irradiation of thin films do not generally consider the films from the point of view of an electrical device. The exception to this is the work of Ramsay⁹ on neutron irradiation of tantalum films. However, he did not consider the effects of varying any of the parameters usually associated with thin film resistor manufacture,

e.g., the effect of varying the dopant concentration. Neither did Ramsay consider the effect of heat treating the films prior to irradiation. This heat treatment process is generally deemed to be a necessary step in the manufacture of stable tantalum thin film resistors ¹⁴.

In order to completely characterize the behaviour of thin film resistors in a radiation environment, it is necessary to know the effects of radiation damage on the film TCR. Ramsay ⁹ has found that, for irradiation of tantalum thin film resistors to 10^{16} n/cm², there was no change in the negative TCR of the unirradiated films. However, it is not certain whether this constant TCR was an intrinsic property of these films, or whether it was the result of the small damage level used in the investigation, since the corresponding conductance increase of the films was only 0.02%.

1.4 The Present Investigation

This thesis considers the permanent effects of low energy (150 keV) proton radiation damage on the conductance and TCR of reactively sputtered tantalum thin film resistors. This type of radiation was chosen in order to simulate a space radiation environment. Although the electron flux density exceeds the proton flux density in space ¹⁵, the electrons are generally of insufficient energy to cause a significant amount of damage in the resistors. The damage concentration produced by a given fluence of heavy ions may exceed that caused by the same fluence of protons, but since the flux density of heavy

ions is much less than that of protons in outer space¹⁵, and since these heavy ions will be attenuated by almost any material surrounding the devices, this type of radiation is not considered in this thesis.

The equipment used in obtaining the experimental results is described in Chapter II of this thesis. Chapter III describes the discontinuous structure and electrical conduction mechanisms of the reactively sputtered tantalum thin film resistors. These must be understood in order to attempt an explanation of the effects of radiation damage on the conductance and TCR of these devices. Chapter IV considers the effects of room temperature radiation damage on the device conductance for fluences up to 10^{16} p/cm² (this fluence corresponds to a minimum of about three years in outer space). On the basis of these results, a model is proposed to explain the observed increase in film conductance with fluence. Low temperature damage and recovery mechanisms are discussed in Chapter V. These results are used as a basis for a discussion of high fluence (2×10^{18} p/cm²) room temperature damage results considered in Chapter VI. Following this discussion of radiation-enhanced conduction mechanisms within the films, the effects of radiation damage on film TCR are considered in Chapter VII. The thesis concludes with a summary of the experimental results and proposed conduction mechanisms in Chapter VIII.

The work done for this thesis is original since the literature does not contain any references either to the

deposition of discontinuous Ta films by reactive sputtering in oxygen and nitrogen simultaneously, or to radiation damage in such a film structure. The eight publications which have resulted from this thesis characterize the film structure¹⁶ and conductance mechanisms in discontinuous films both before and after irradiation¹⁷⁻²¹, as well as describing an IC current integrator²² and a cryogenic system²³ which is particularly suitable for radiation damage experiments.

II

EXPERIMENTAL EQUIPMENT

2.1 Accelerator

The basic accelerator consisted of a Texas Nuclear Corporation model 9509 Cockroft-Walton accelerator for which the maximum available accelerating voltage was 150 kv. A magnetic beam-switching system was designed and added to this basic accelerator. This system was capable of producing an analyzed beam of singly charged ions up to mass 22 at an accelerating potential of 150 kv. The complete system could produce an analyzed proton beam of 300 μ amp at 150 keV energy. Unless otherwise stated, all experimental results were obtained at a beam current density of 10 μ amp/cm² at 150 keV.

The vacuum system for the accelerator and beam transport system consists of two oil diffusion pumps with their associated cold traps. One pump is located at the grounded end of the accelerator tube, while the second pump is located on the beam line, about two feet from the target chamber. The target section of the beam line contains an additional cold trap which is concentric with the beam line and one foot in length. One end of this beam line trap is adjacent to the target assembly. This arrangement reduces the hydrocarbon layer on the resistors sufficiently that the conductance change produced by this layer at the highest fluence used (2×10^{18} p/cm²) is less than 0.1% of the film conductance. This change in film conductance indicates that the contaminant layer is expected to have a negligible effect on the measurement of radiation-produced conductance changes which

are always in excess of 20% at 2×10^{18} p/cm² (Chapter VI).

2.2 Current Integrator

The first stage of the integrator consists of a Philbrick SP65A operational amplifier employed as a current to voltage converter (Figure 2-1). The open loop gain of this stage is 10^7 , providing a maximum input resistance of 10 ohms; this occurs on the 10^{-8} and 10^{-9} ranges. The 709 operational amplifier of the second stage operates as a linear amplifier, the gain of which depends on the selected input range. The output of this stage is read by means of a panel meter which indicates the input current to the integrator.

The integrating stage consists of a 709 operational amplifier fed from the second amplifier stage by a 47,000 ohm resistor. When the voltage on the integrating capacitor reaches -2.3 volts, the 710 comparator triggers, placing a logical 0 on the J* input of the SN7470 flip-flop. Since the K* input is permanently grounded, the next clock pulse sets \bar{Q} to 1, causing the reset current to flow into the integrating capacitor. During this reset pulse, the output of the integrating operational amplifier will fall below the triggering level of the 710 comparator, causing a 0 to be applied to the J* input of the flip-flop. The next positive going clock pulse will then reset \bar{Q} to 0, switching off the reset current. It should be noted that the exact level at which the discriminator triggers is not critical, since the discharge current flows for a period of one clock pulse. The total charge accumulated is recorded by a scalar which counts the number of times the integrating

capacitor is reset. The number of coulombs/count at the input to the integrator is given by:

$$(\text{full scale current reading}) \times 10^{-1} \text{ sec.}$$

Clock pulses are obtained by squaring the 60 hertz AC line voltage. The frequency stability of the line is better than 0.1% ²⁴. The sine wave is initially squared by means of the 710 comparator. This signal is then passed through two SN7400 gates to provide less than 150 nsec rise time to trigger the SN7470 flip-flop.

The input offset voltage of the SP65A amplifier may be adjusted by means of a 20,000 ohm panel-mounted potentiometer. To make this adjustment, the meter is switched from its normal position to the output of the integrating amplifier stage. At the same time, the integrating capacitor is replaced by a resistor. The offset control is adjusted until a zero meter reading is obtained. The offset adjustment of both 709's is adjusted initially, and then remains fixed.

The chopper stabilized SP65A amplifier has an offset current of 10^{-11} amp. This is the limiting factor on the smallest beam current which can be measured. If these low currents are not to be measured, considerable economy may be attained by replacing the first amplifier stage with a unit having a higher offset current. An amplifier having less gain could also be used if a higher input resistance were tolerable.

As constructed, the measured accuracy of the integrator is within 1%. This accuracy could be increased by replacing

the "line-frequency" clock by a crystal controlled clock. This would also allow for an increase in the clock frequency, permitting current integration over shorter periods of time than is presently possible.

The two SN7400 speed-up gates may be eliminated if the SN7470 flip-flop is replaced by a SN7472 flip-flop. The SN7472 flip-flop triggers on the DC level of the pulse, rather than on the rising edge of the pulse.

The method of discharging the integrating capacitor by a fixed current for a fixed time has an advantage over the capacitor shorting method of Hakansson²⁵ in that the accuracy attainable with the present instrument may be improved simply by increasing the accuracy of the clock. The accuracy of Hakansson's instrument depends on the stability of the SCR holding current and the 710 triggering level with temperature. In the present case, the $V_{CE}(\text{Sat.})$ of the reset transistor may vary with temperature, but the effect of this variation on the over-all accuracy will be small since the transistor saturation voltage is of the order of 0.5% of the reset voltage; variations in the reset current due to changes in the saturation voltage will be much less than this. However, in the present case, the stability of the capacitor discharge voltage is critical; this voltage is obtained from a regulated, temperature compensated power supply²⁶.

2.3 Room Temperature Target Assembly

During irradiation, the sample substrate was mounted on a water cooled copper block maintained at 286°K. This mounting block also served as part of a Faraday cup for measuring the beam current. This assembly is illustrated in Figure 2-2. Electrical contact to the resistor was made by means of pressure contacts which were attached to the Faraday cage. In order to reduce secondary emission, a suppressor electrode immediately preceded the target assembly. Lack of substrate charging during irradiation was indicated by a continuous luminescence of the substrate.

The average temperature of the films increased by $6 \pm 2^\circ\text{K}$ during irradiation by a $15 \mu\text{amp}/\text{cm}^2$ beam of 150 keV protons. This value of temperature change was obtained from a calculation using film conductance as measured immediately after the beam was switched off, the "thermal equilibrium" conductance as measured two minutes later, and the measured TCR value for the irradiated film. It should be noted that this value represents the increase in the average temperature of the film in contrast to the possibly larger instantaneous "temperature" increase around a proton track. This measured value of average temperature increase is in agreement with the calculated ²⁷ value of 3°K .

2.4 Cryogenic Equipment

The equipment for the low temperature radiation damage studies consisted basically of a Malaker Corp. Mark VII-C Cryomite cryogenic cooler which operates on a Stirling cycle. This unit is self contained in a cylindrical assembly which is

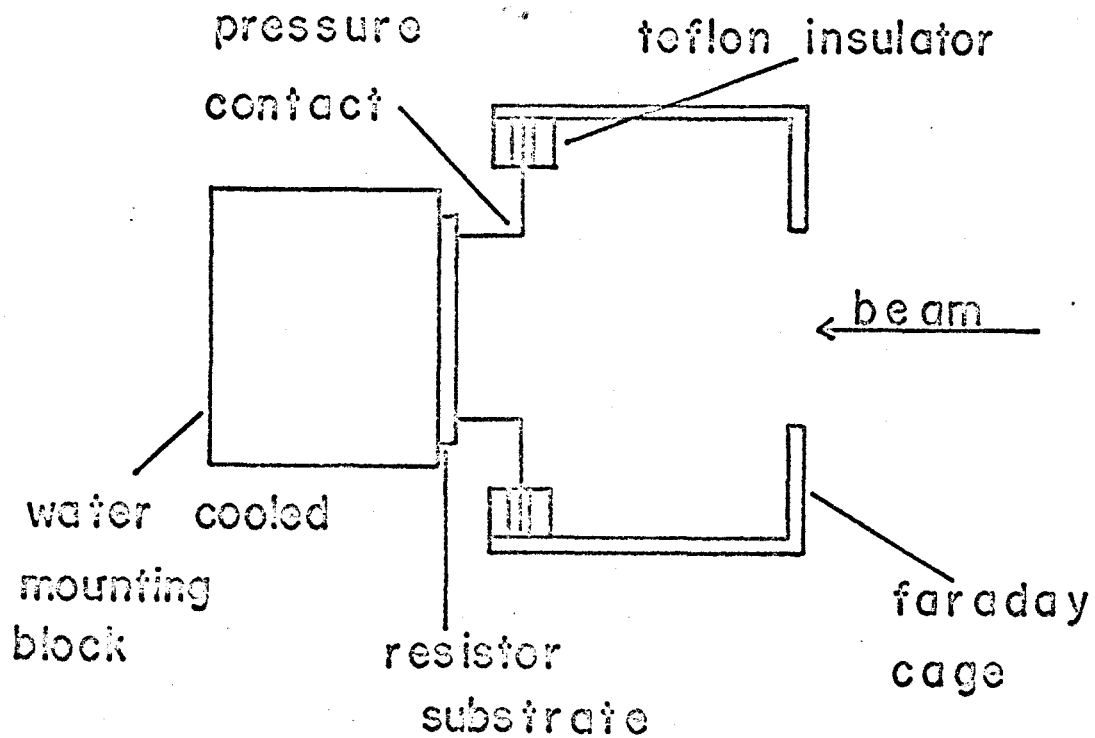


Figure 2-2

Room temperature target assembly for thin film resistor irradiation, illustrating the Faraday cup and the water-cooled mounting block which is maintained at 286°K.

about 26 inches long and 5 inches in diameter with a total weight of 16 pounds. All perceptible vibration during operation was eliminated by securely attaching both the cooler and the beam line to a lab table.

A photograph of the low temperature target assembly is shown in Fig. 2-3. The sample block (No. 8) is attached to the cooler cold head by four nylon bolts. To obtain electrical isolation of the sample block and the cold head while maintaining good thermal contact between them, these units were separated by a 0.001 inch thick mylar spacer covered with Dow-Corning heat sink compound. Heat sink compound was also used between the resistor substrate and the sample block. Pressure contacts mounted on the Faraday cage (No. 11) were used to make electrical contact to the devices.

The sample temperature was regulated by means of a Cryotronics proportional temperature controller which supplied power to a diode (No. 6) mounted adjacent to the sample holder. The sample temperature was measured by means of a platinum resistance thermometer (No. 7). The base temperature of the target assembly is 26° K. This increases with beam current as shown in Fig. 2-4.

For isochronal annealing experiments, a cryogenic system should produce "square" temperature pulses. Fig. 2-5 gives actual recorder traces of temperature cycles for various annealing levels. During warm-up the last 2° K are obtained in 36 seconds, whereas on the cool-down side of the pulse the

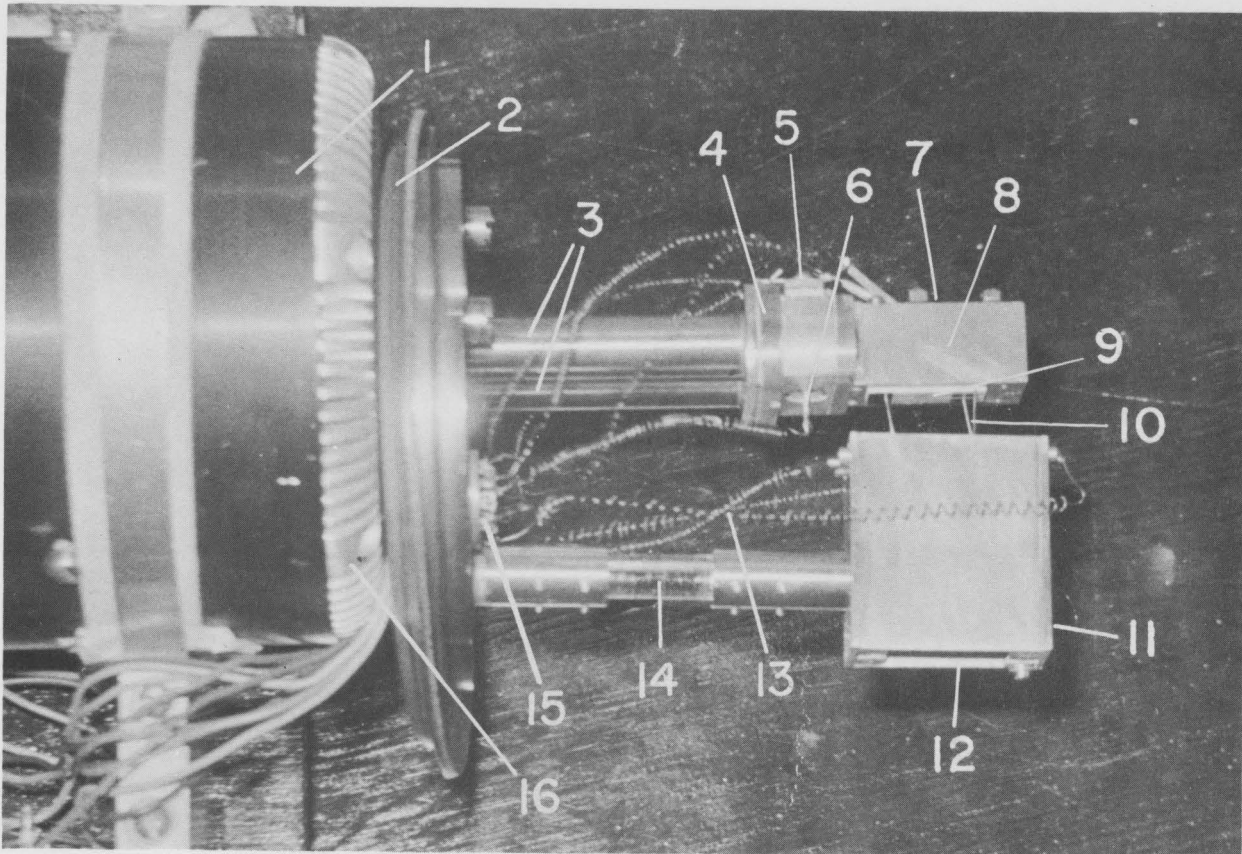


Figure 2-3

1. Body of cooler, 2. Vacuum flange, 3. Circulating tubes for refrigerating gas (helium), 4. Primary cold heat through which refrigerating gas flows, 5. Platinum precision resistor for temperature control, 6. Diode heater for temperature control embedded in a copper block which is attached to cold head, 7. Platinum precision resistor for specimen temperature, 8. Copper block to which specimen is mounted, 9. Specimen, 10. Specimen conductance probes, 11. Faraday cup, 12. Entrance port for incident beam, 13. Electrical leads of coiled copper wire, 14. Glass insulating rod, 15. Multi-pin vacuum electrical feed through, 16. Cryomite cooling fins.

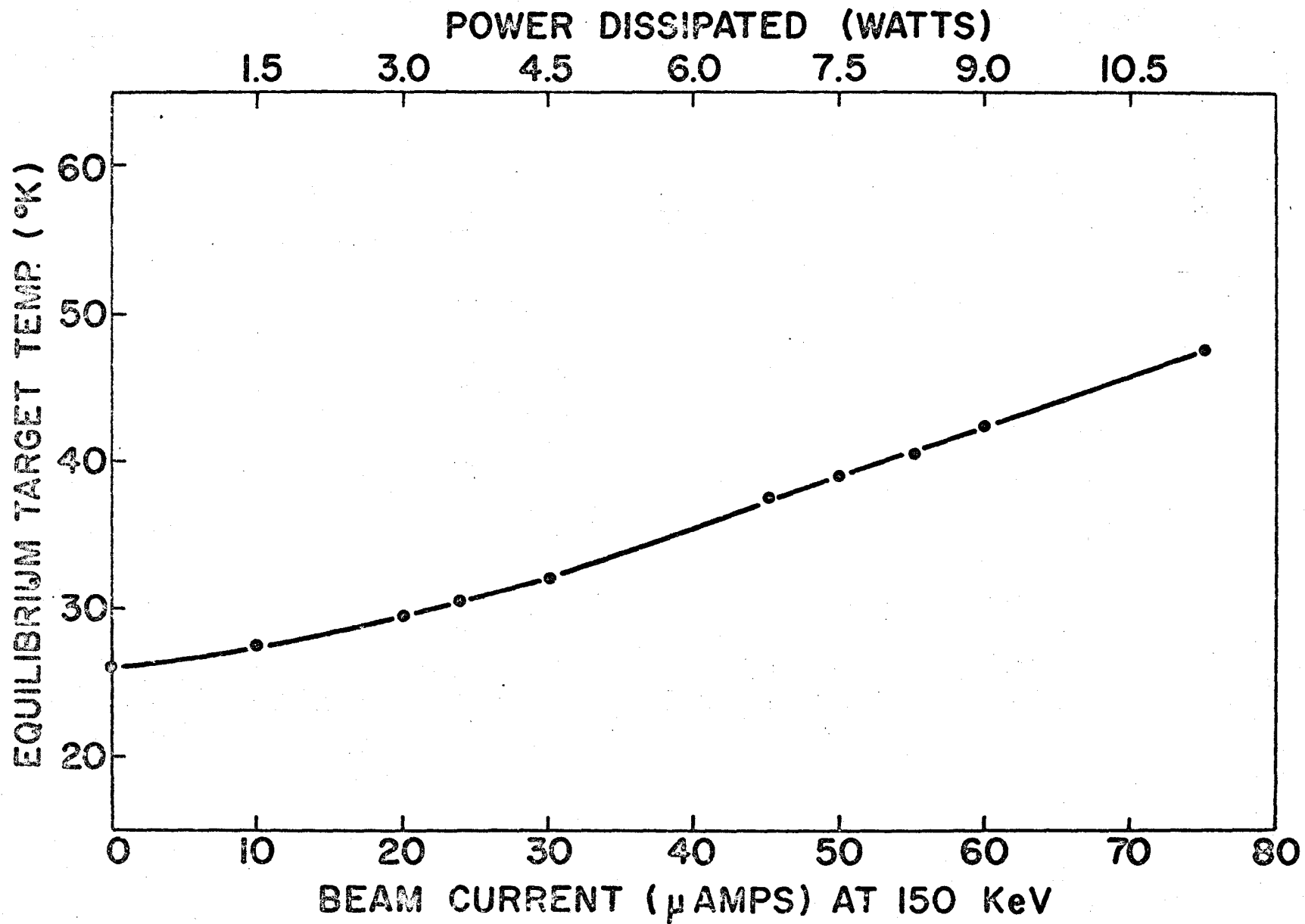


Figure 2-4

Power Dissipation of Cryogenic Target Assembly

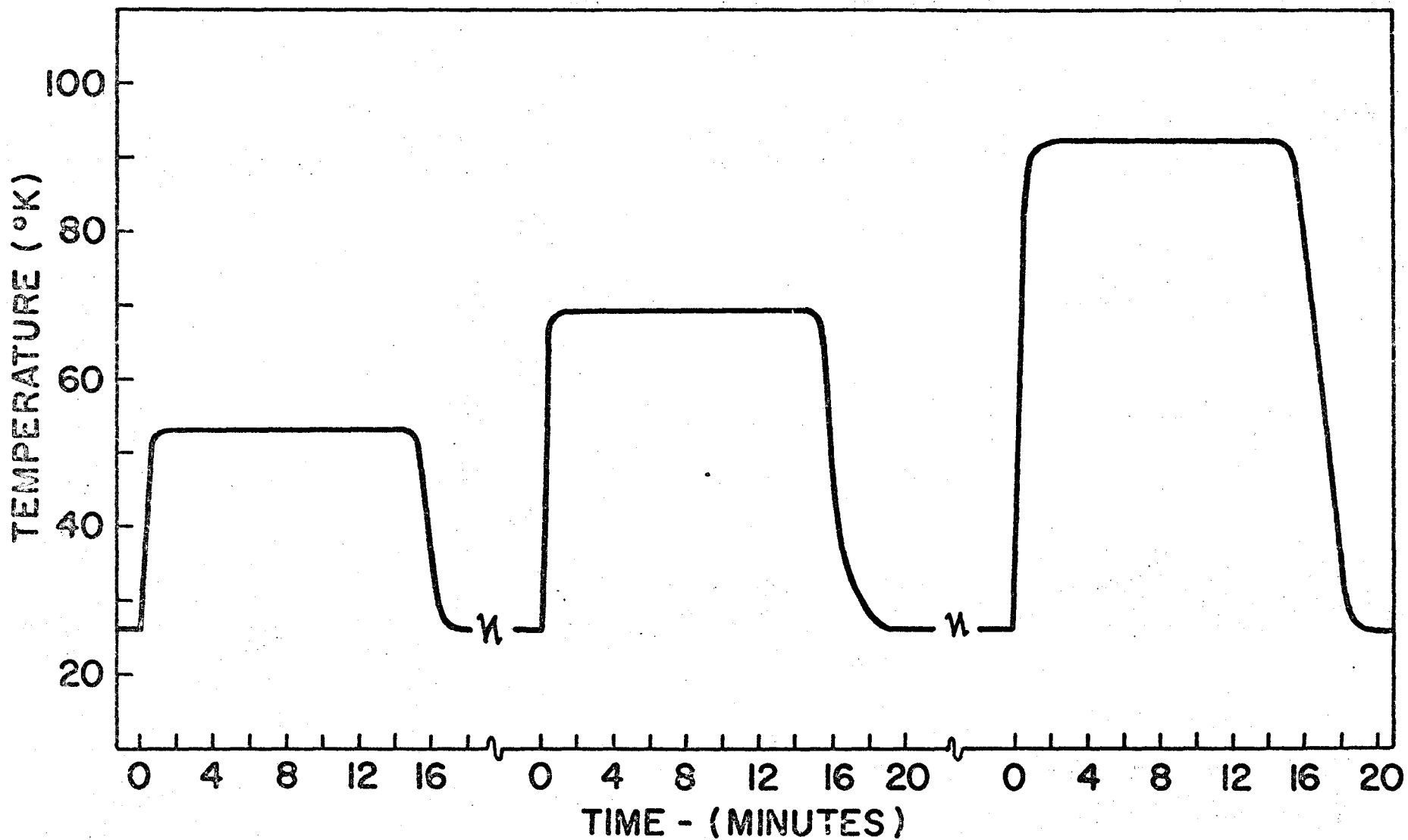


Figure 2-5

Temperature Response of Cryogenic Target Assembly for Typical Isochronal Annealing Pulses

temperature decreases through the first 2°K in $2\frac{1}{4}$ seconds. It can be seen in this figure that the total warm-up time of the cycle is faster than the total cool-down, the reverse of which is true for cryostat systems. In the present case, the cold head could be heated much more rapidly since it is not necessary to boil off a cryogenic fluid. The quench rates are comparable to cryostat systems ²⁸, with a total cool-down time of about 15 minutes from room temperature to 26°K .

This cryogenic system is particularly suitable for isochronal annealing experiments since the temperature pulses are obtained by adjusting the temperature controller to the desired annealing level and allowing the system to automatically execute its approach to the equilibrium annealing temperature. The performance of an annealing sequence is thus rather more simplified than in the case of cryostat-operated heat switches and vapour tubes. Comparison of Fig. 2-5 with annealing pulses obtained from cryostat designs ²⁸ demonstrates that the present system is entirely satisfactory for this type of work.

2.5 Electrical Measurements

All conductance measurements were carried out on a Wayne-Kerr model B641 conductance bridge at a frequency of 1,592 hertz. The accuracy of this bridge is 0.01%.

Measurements of the temperature coefficient of resistance (TCR) of the films were done over the range 30°C to 130°C by heating the films in a Delta model 2300 oven. Before a

measurement was made the film was allowed one-half hour to come to equilibrium at each designated temperature. In the range 273°K to 26°K the film conductance was measured as a function of temperature by cooling the films with the Cryomite refrigerator.

The film resistivity was calculated from the film geometry and the measured resistance. The film thickness was measured by means of a Hilgar-Watts model N130 multiple beam interferometer.

III

REACTIVELY SPUTTERED TANTALUM THIN FILM RESISTORS

3.1 General

This chapter describes the deposition of tantalum thin film resistors by reactive sputtering in oxygen and nitrogen simultaneously. The advantages of this method of film deposition over the commonly used method of sputtering in a single reactive gas are discussed. Electrical conduction mechanisms within the films were investigated by measuring film conductance as a function of temperature. Electron microscopy was employed to examine the structure of the films. A knowledge of these parameters will permit a model to be postulated to account for the effects of radiation damage on the conductance and TCR of the films.

3.2 Experimental Procedure

3.2.1 DC Sputtering and Device Fabrication

The films were deposited onto American Lava No. 743 glazed ceramic substrates by means of DC sputtering in an argon discharge of 30 millitorr pressure. The cathode consisted of a sheet of tantalum placed two inches from the anode. The substrate was biased at -500 volts relative to the anode. This bias was employed to increase the reproducibility of the films by reducing the concentration of unintentional impurities

such as hydrocarbons. This also signifies that a higher partial pressure of reactive oxygen and nitrogen must be used to obtain the same dopant concentration as in films prepared without the use of bias. This is advantageous since it is easier to control a larger partial pressure of reactive gas than a smaller partial pressure.

The first step in fabricating a device consisted of sputtering undoped tantalum onto the glazed surface of the substrate. This film was then thermally oxidized to completion in air. The purpose of this oxide layer was to protect the substrate glaze from the tantalum etchant solution.

The resistor film material was presputtered onto a shutter first and then onto the base oxide layer while the substrate was being maintained at 400°C. The reactive partial pressures of nitrogen and oxygen for a cross-section of substrates studied are detailed in Table 3-1. The resulting films were 1,200 Å thick. Standard photo-etching techniques were then used to produce the desired resistor pattern in the film. Two patterns were used: a straight line pattern of 50 squares and zig-zag pattern of 1,000 squares. Contact pads were then evaporated in the form of nichrome nucleated gold. Films which are irradiated at this stage of the manufacturing process will be referred to as non heat treated.

Table 3-1

CROSS-SECTION OF REACTIVE PARTIAL PRESSURES OF OXYGEN AND
NITROGEN USED IN DC SPUTTERING OF TANTALUM THIN FILMS

Reactive Dopant Partial Pressure
x 10⁻⁵ torr

Substrate No.	Nitrogen	Oxygen
1	.7	0
2	.3	.3
3	.7	4.3
4	.7	.6
5	.7	2.6
6	.3	3.7
7	2.0	1.0
8	2.0	2.0
9	1.0	3.0
10	3.0	1.0
11	.5	3.0
12	1.0	1.0
13	.7	.3
14	.4	.4
15	1.5	1.5
16	2.5	2.5

3.2.2 Device Heat Treatment

After fabrication, the resistance of a device was stabilized by a heat treatment procedure consisting of baking the device in an air ambient at atmospheric pressure and 500°C for fifteen minutes. This step completed the production of a "standard" device. Films which have undergone this standard procedure will be referred to as air heat treated.

In order to systematically investigate the effect of heat treatment on the properties of a device, devices were randomly chosen and subjected to the following experiments: a) heat treatment under a vacuum of 10^{-6} torr at 500°C for 15 minutes; b) heat treatment in air as a function of temperature for a fixed time of 5 minutes; and c) heat treatment in air as a function of time at a fixed temperature of 500°C. The films which have been subjected to heat treatment a) will be referred to as vacuum heat treated.

3.2.3 Electron Microscopy

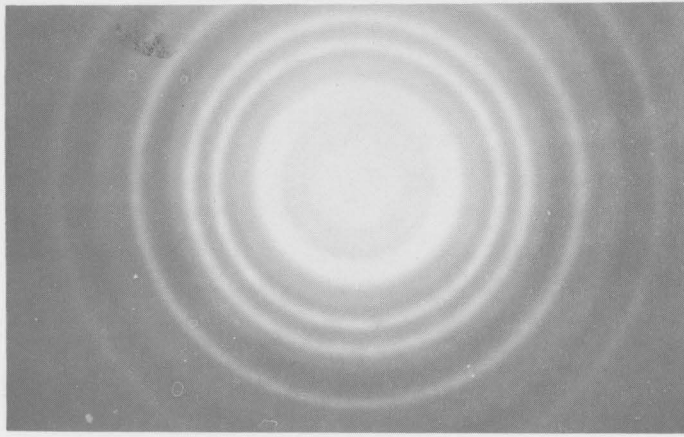
Structural and compositional features of the films were examined by means of bright and dark field electron micrographs, as well as electron diffraction patterns. A Philips EM300 electron microscope, operated at 100 kv was used for these investigations. The films were prepared for observation by sputtering onto substrates onto which 50 Å of carbon had previously been deposited. The sputtered films were then covered with a parlodion solution. After the solvent had evaporated, the parlodion film was removed from the substrate, bringing the

Ta film with it. This double film was then placed on a 300 mesh microscope grid, at which time the parlodion film was dissolved in isoamyl acetate. The Ta film was then ready for observation at room temperature as well as during in situ heating in the microscope at 500°C.

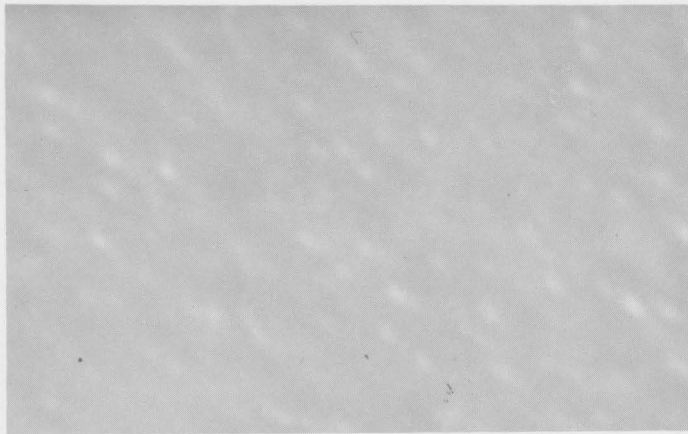
3.3 Experimental Results

3.3.1 Electron Microscopy

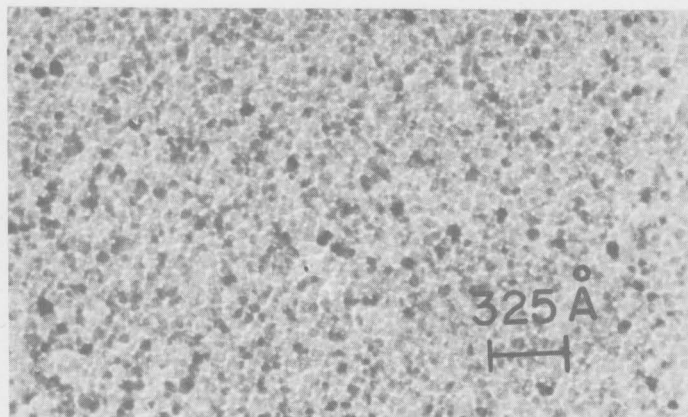
Figure 3-1 illustrates the results obtained from electron microscopy experiments on films sputtered in a reactive partial pressure of 1.5×10^{-5} torr oxygen and 1.5×10^{-5} torr nitrogen. The average resistivity and TCR for these films sputtered onto a carbon parting layer was $728 \mu\text{-cm} \pm 10\%$ and $-136 \text{ ppm}/^\circ\text{C} \pm 10\%$. Figures 3-1 a, 3-1 b, and 3-1 c show an electron diffraction pattern, a dark field micrograph, and a bright field micrograph for a film which had been heated at 500°C for ten minutes in the electron microscope. The electron diffraction pattern contains rings corresponding to metallic Ta_4O^{29} (Table 3-2), rings corresponding to inter-planar spacing d equal to 3.35 \AA and 2.17 \AA which are attributed to $\text{Ta}_2\text{O}_5^{30}$, and a ring corresponding to $d = 2.66 \text{ \AA}$ which could be due to either TaN^{31} ($d = 2.66 \text{ \AA}$) or $\beta\text{-Ta}^5$ ($d = 2.67 \text{ \AA}$). Since reactive sputtering of Ta in nitrogen inhibits¹⁴ the formation of $\beta\text{-Ta}$, it is assumed that the phase which is detected in the film is TaN rather than $\beta\text{-Ta}$. With the exception of the rings corresponding to crystalline Ta_2O_5 , there was no change in the electron diffraction pattern during heat treatment; however, the diffraction pattern obtained from non heat treated films did not contain the Ta_2O_5 rings, but instead showed



(a)



(b)



(c)

Figure 3-1

Electron microscope results for a heat treated Ta film reactively sputtered in a partial pressure of 1.5×10^{-5} torr oxygen and 1.5×10^{-5} torr nitrogen: (a) electron diffraction pattern; (b) dark field micrograph obtained from the Ta_4O_{11} 011 diffraction ring; and (c) bright field micrograph.

Table 3-2

COMPARISON OF ELECTRON DIFFRACTION PATTERN OF FIGURE 3-1 WITH
THE STANDARD Ta_4O ELECTRON DIFFRACTION PATTERN

h k l	Measured d-spacing (\AA)	Standard d-spacing (\AA)
011	2.26	2.29
200	1.81	1.80
002	1.57	1.59
211	1.42	1.42
112	1.31	1.33
220, 202	1.19	1.19
222	0.98	0.97
123	0.88	0.87

evidence of a diffuse ring which disappeared after the film had been heat treated at 500°C for ten minutes. The dark field micrograph of Fig. 3-1 b was obtained from the 011 metallic Ta_4O diffraction ring. Thus, the spots on the micrograph correspond to islands of metallic Ta_4O . The magnification of all micrographs is 310,000. The average island size for heat treated films is measured to be about 70\AA . The bright field micrograph of Fig. 3-1 c also illustrates the island structure. The inter-island gap regions are estimated to be about 35\AA . These regions are assumed to consist of the crystalline Ta_2O_5 . The corresponding dimensions for non heat treated films (micrographs not shown) are 40\AA for the islands and 20\AA for the gaps. As will be discussed in section 3.4.1, the gap material for non heat treated films is amorphous Ta_2O_5 . This structure is summarized in Table 3-3.

Table 3-3

SUMMARY OF THE STRUCTURE OF SELECTED TANTALUM FILMS REACTIVELY SPUTTERED IN
OXYGEN PLUS NITROGEN

Reactive Partial Pressure	Average Island Size Non Heat Treated Film (Å)	Average Gap Size Non Heat Treated Film (Å)	Average Island Size Heat Treated Film (Å)	Average Gap Size Heat Treated Film (Å)	Island Material	Gap Material
1.5 x 10 ⁻⁵ torr N ₂ plus 1.5 x 10 ⁻⁵ torr O ₂	40	20	70	35	Ta ₄ O + TaN	Ta ₂ O ₅
5 x 10 ⁻⁶ torr N ₂ plus 5 x 10 ⁻⁶ torr O ₂	70	35	100	50	Ta(O,N)	Ta ₂ O ₅
1 x 10 ⁻⁶ torr N ₂ plus 1 x 10 ⁻⁶ torr O ₂	300	200	400	300	Ta(O,N)	Ta ₂ O ₅
1 x 10 ⁻⁵ torr N ₂ plus 3 x 10 ⁻⁵ torr O ₂	35	20	50	35	Ta ₄ O	Ta ₂ O ₅
7 x 10 ⁻⁶ torr N ₂ plus 4.3 x 10 ⁻⁵ torr O ₂	Continuous, polycrystalline Ta ₂ O ₅					

For films sputtered in a reactive partial pressure of 5×10^{-6} torr oxygen and 5×10^{-6} torr nitrogen, the average resistivity and TCR for films deposited onto a carbon parting layer is $405 \mu\Omega\text{-cm} \pm 10\%$ and $-50 \text{ ppm}/^\circ\text{C} \pm 10\%$. The electron diffraction pattern of non heat treated films (not shown) corresponds to BCC Ta³² of lattice constant $a_0 = 3.34 \text{ \AA}$. The calculated and measured inter-planar spacings for this structure are compared in Table 3-4.

Table 3-4

ANALYSIS OF TANTALUM ELECTRON DIFFRACTION PATTERN BASED ON A
BCC LATTICE WITH $a_0 = 3.34 \text{ \AA}$

h k l	Measured d-spacing (\AA)	Calculated d-spacing (\AA)
110	2.38	2.37
200	1.66	1.67
211	1.38	1.38
220	1.20	1.19
310	1.07	1.06
222	0.91	0.96

In addition to these tantalum rings, the diffraction pattern for non heat treated films appears to contain a diffuse ring. After heat treatment of the films at 500°C for fifteen minutes, rings corresponding to inter-planar spacings of 2.59 \AA and 1.85 \AA were observed. These are attributed to Ta_2O_5 ³⁰. Heat treatment

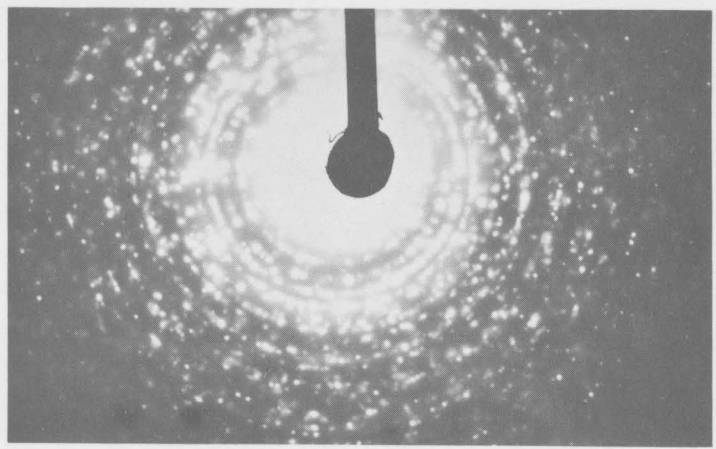
does not produce any change in the Ta diffraction pattern. Dark field and bright field micrographs illustrate that the films possess an island structure. For non heat treated films, the island and gap regions are estimated to be 70 \AA and 35 \AA respectively. For heat treated films the corresponding dimensions are 100 \AA and 50 \AA .

For films sputtered in a reactive partial pressure of 1×10^{-6} torr oxygen and 1×10^{-6} torr nitrogen, the average resistivity and TCR for films sputtered onto a carbon parting layer is $390 \mu\Omega\text{-cm} \pm 10\%$ and $-50 \text{ ppm}/^\circ\text{C} \pm 10\%$. Electron diffraction patterns indicate that the films are composed of BCC Ta of lattice constant $a_0 = 3.31 \text{ \AA}$. For non heat treated films the diffraction pattern appears to contain an additional diffuse ring which disappears during heat treatment. After the films had been heat treated at 500°C for fifteen minutes, rings corresponding to inter-planar spacings of 2.59 \AA and 1.85 \AA appeared. These are attributed to Ta_2O_5 ³⁰. Heat treatment does not produce any change in the BCC Ta diffraction pattern. Dark field and bright field micrographs illustrate that the films possess an island structure. The island and gap regions are very irregular in shape, with numerous protrusions occurring between islands. For non heat treated films, the island regions and gap regions are estimated to be 300 \AA and 200 \AA respectively. For heat treated films the corresponding dimensions are 400 \AA and 300 \AA . From Table 3-3 it may be seen that as the total reactive partial pressure increases, for equal partial pressures of reactive oxygen and nitrogen, the

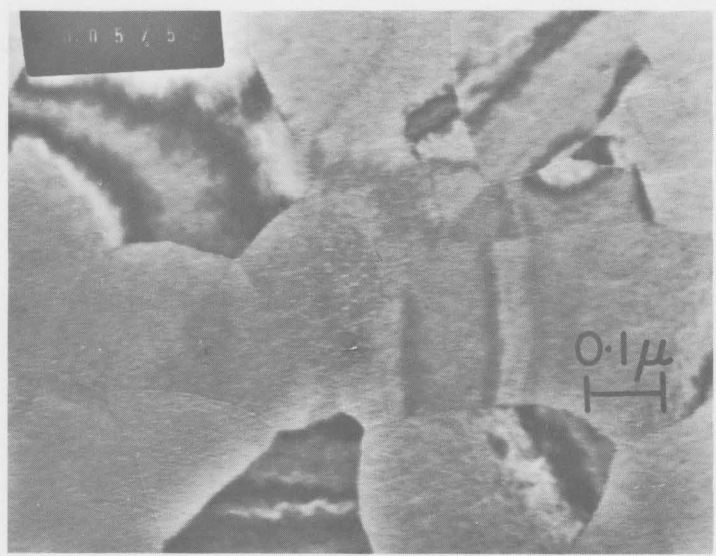
dimensions of both the islands and gaps decrease.

The average resistivity and TCR for films reactively sputtered in partial pressures of 1×10^{-5} torr nitrogen and 3×10^{-5} torr oxygen and deposited on a carbon parting layer are $580 \mu\Omega\text{-cm} \pm 10\%$ and $-190 \text{ ppm}/^\circ\text{C} \pm 10\%$. Electron diffraction experiments show that the films are composed of Ta_4O_{29} . Electron diffraction patterns obtained from films which have been heat treated at 500°C for fifteen minutes also contain rings corresponding to inter-planar spacings of 3.35 \AA and 2.17 \AA . These rings are attributed to Ta_2O_5 . Electron diffraction patterns of non heat treated films do not contain these rings but instead appear to contain a diffuse ring which disappears during heat treatment. Bright and dark field micrographs show the films to consist of islands of about 35 \AA surrounded by gap regions of about 20 \AA for non heat treated films. For heat treated films the corresponding dimensions are 50 \AA and 35 \AA respectively.

Figure 3-2 illustrates an electron diffraction pattern and a bright field micrograph for a heat treated film reactively sputtered in a partial pressure of 4.3×10^{-5} torr oxygen and 7×10^{-6} torr nitrogen. The electron diffraction pattern corresponds to Ta_2O_5 . This film does not possess an island structure but is a continuous, polycrystalline film, having an average grain size of about $1,500 \text{ \AA}$. Although the large TCR of $-2 \times 10^3 \text{ ppm}/^\circ\text{C}$ for this film renders it relatively useless as a device, this film will be significant in the interpretation of radiation damage experiments.



(a)



(b)

Figure 3-2

Electron microscope results for Ta films reactively sputtered in a partial pressure of 7×10^{-6} torr nitrogen and 4.3×10^{-5} torr oxygen: (a) electron diffraction pattern, and (b) bright field micrograph.

3.3.2 Electrical Conductivity and TCR of Non Heat Treated Films

The room temperature resistivity and TCR of non heat treated films as a function of total reactive partial pressure is given in Fig. 3-3. It should be noted that the TCR is negative for all reactive partial pressures investigated. The significance of this will become apparent when the structure of the films is discussed. Table 3-5 a gives the film resistivity and the film TCR corresponding to different reactive oxygen partial pressures, the reactive nitrogen partial pressure being kept constant. Under these conditions, both the resistivity and the magnitude of the TCR increases with an increasing reactive oxygen partial pressure. Table 3-5 b gives the film resistivity and the film TCR corresponding to different reactive nitrogen partial pressures, the reactive oxygen partial pressure being kept constant. Under these conditions the resistivity increases and the magnitude of the TCR decreases with an increase in the reactive nitrogen partial pressure. Table 3-5 c gives the film resistivity and the film TCR for different reactive oxygen and nitrogen partial pressures, the total reactive partial pressure being kept constant. This table illustrates that, for a fixed total reactive partial pressure of 4.0×10^{-5} torr, the film resistivity is $690 \mu\text{-cm} \pm 15\%$ as a ratio of nitrogen to oxygen reactive partial pressures varies from 3:1 to 1:12. The TCR varies by a factor of three over this range of reactive partial pressures.

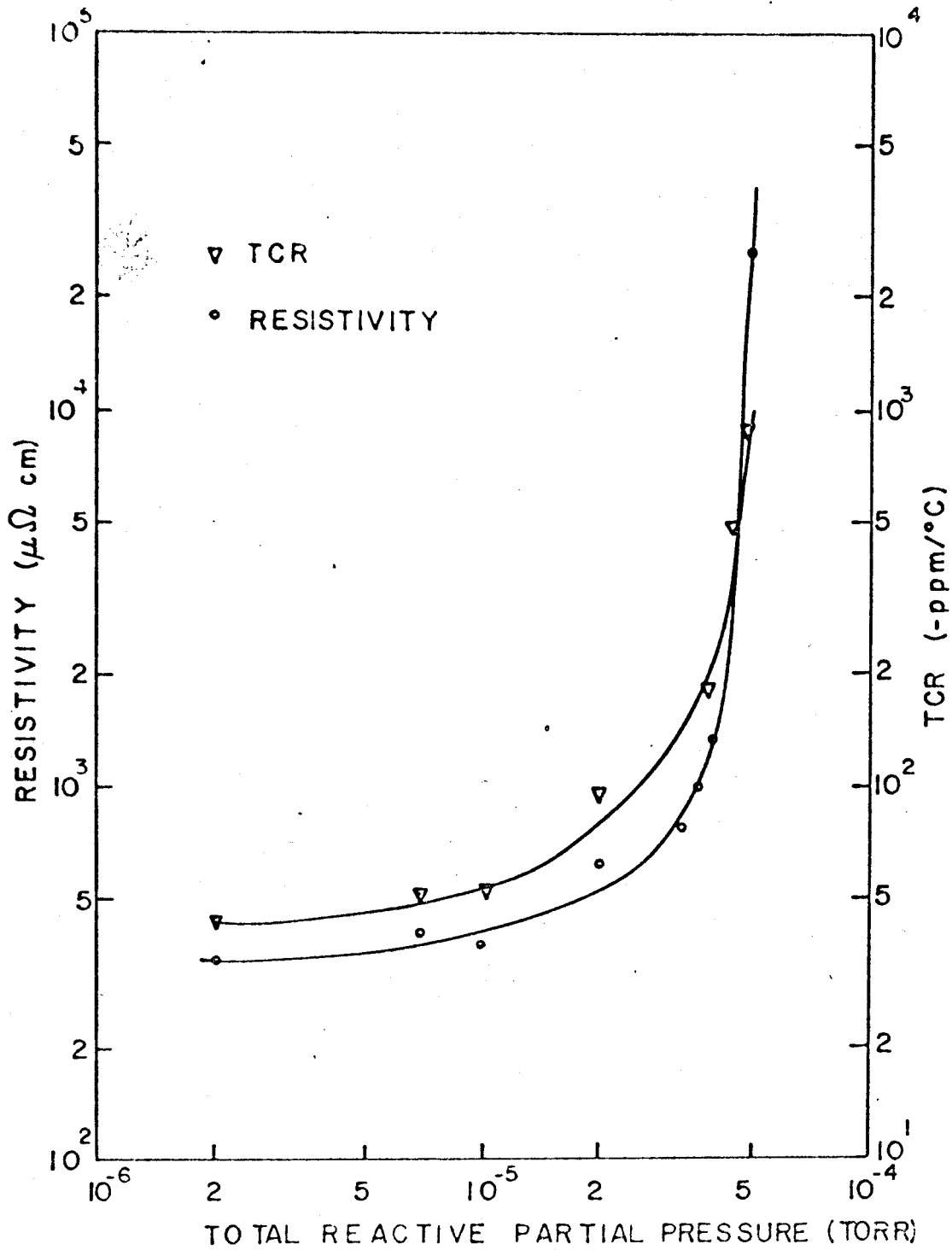


Figure 3-3

Room temperature resistivity and TCR of sputtered tantalum films as a function of total reactive partial pressure of oxygen plus nitrogen.

Table 3-5 a

ROOM TEMPERATURE RESISTIVITY AND TCR OF NON HEAT TREATED FILMS AS A FUNCTION OF REACTIVE OXYGEN PARTIAL PRESSURE, THE REACTIVE NITROGEN PARTIAL PRESSURE BEING CONSTANT

Reactive Partial Pressure x 10 ⁻⁵ torr		TCR ppm/°C	Resistivity μΩ-cm
Nitrogen	Oxygen		
0.7	0	- 50	400
0.7	0.6	- 70	500
0.7	2.6	-150	1,000

Table 3-5 b

ROOM TEMPERATURE RESISTIVITY AND TCR OF NON HEAT TREATED FILMS AS A FUNCTION OF REACTIVE NITROGEN PARTIAL PRESSURE, THE REACTIVE OXYGEN PARTIAL PRESSURE BEING CONSTANT

Reactive Partial Pressure x 10 ⁻⁵ torr		TCR ppm/°C	Resistivity μΩ-cm
Nitrogen	Oxygen		
1.0	1.0	-150	240
2.0	1.0	-100	330
3.0	1.0	- 60	800

Table 3-5 c

ROOM TEMPERATURE RESISTIVITY AND TCR OF NON HEAT TREATED
FILMS AS A FUNCTION OF REACTIVE OXYGEN AND
REACTIVE NITROGEN PARTIAL PRESSURES, THE TOTAL REACTIVE
PARTIAL PRESSURE BEING CONSTANT

Reactive Partial Pressure $\times 10^{-5}$ torr		TCR	Resistivity
Nitrogen	Oxygen	ppm/ $^{\circ}$ C	$\mu\Omega$ -cm
3.0	1.0	- 60	800
2.0	2.0	- 97	700
1.0	3.0	-170	630
0.3	3.7	-168	630

Figure 3-4 is an Arrhenius plot of the conductance of a resistor from substrate 9 as a function of reciprocal temperature. This temperature cycling does not produce any permanent change in the room temperature conductance of the film. The conductance has two components, corresponding to activation energies of 7.0×10^{-4} ev and 3.4×10^{-5} ev. In Fig. 3-5, the conductance of a film is plotted as a function of the square of the absolute temperature. As will be discussed in section 3.4.3, a comparison of Figures 3-4 and 3-5 will provide a basis for comments on the electrical conduction mechanisms which occur in the thin films.

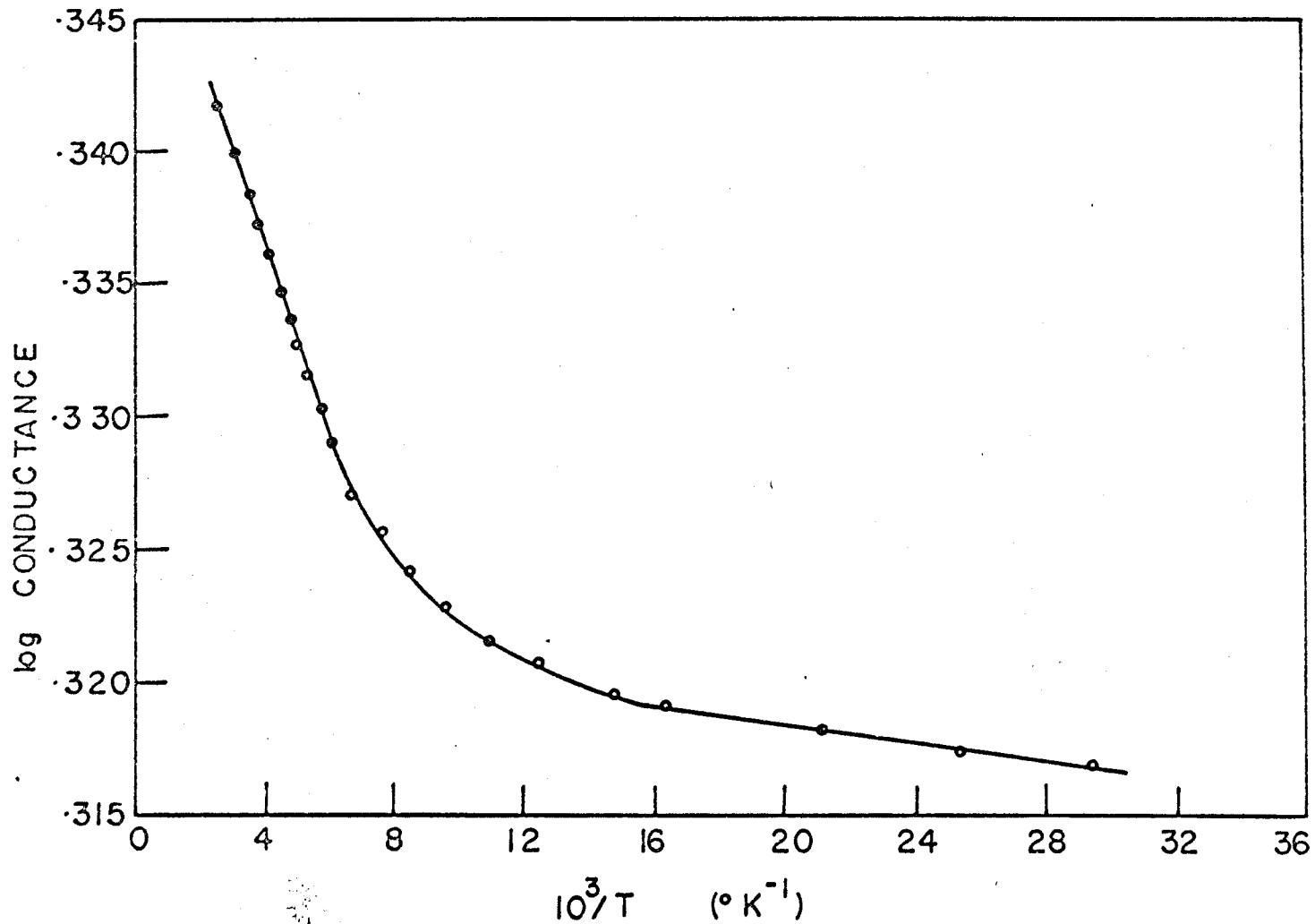


Figure 3-4

Arrhenius plot of film conductance, for a film sputtered in a total reactive partial pressure of 4.0×10^{-5} torr.

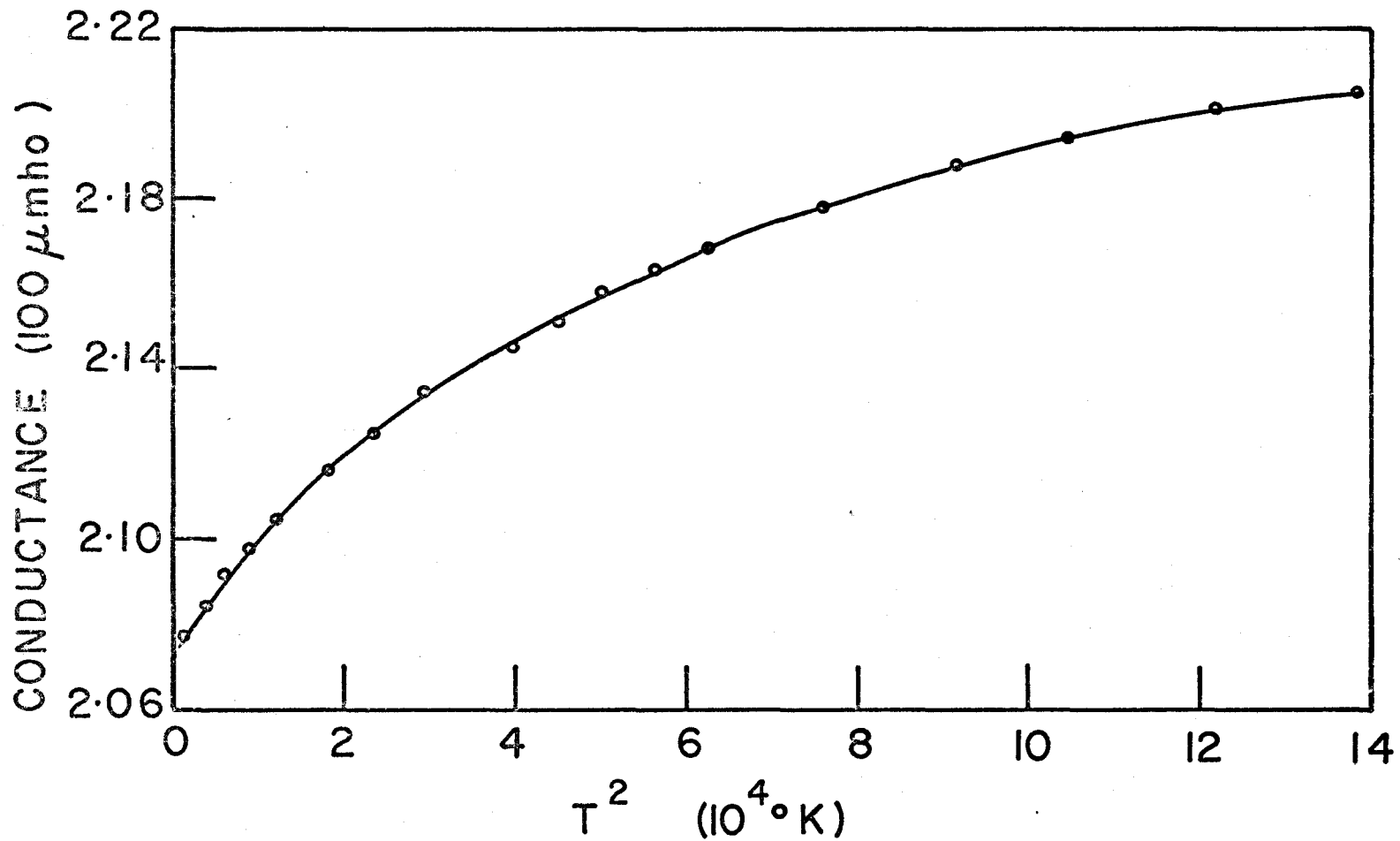


Figure 3-5

Film conductance plotted as a function of the square of the absolute temperature, for a film sputtered in a total reactive partial pressure of 4.0×10^{-5} torr.

3.3.3 Effects of Heat Treatment on the Electrical Properties of the Devices

After having received the standard heat treatment, the resistivity of the films increases typically by 10% to 15% with respect to the non heat treated films. The TCR becomes more negative by the same amount.

Information concerning the structure of the films may be obtained from a study of the heat treatment kinetics. To obtain this information, films which had not received any previous heat treatment were given a series of standard fifteen-minute heat treatments at 500°C in air at atmospheric pressure. Figure 3-6 illustrates the resulting conductance measured at 30°C, as a function of the square root of the heat treatment time for a resistor from substrate 8. The thermal activation energy for the conductance change during heat treatment was measured by performing a series of five-minute isochronal heat treatment cycles in an air ambient at atmospheric pressure. The resulting Arrhenius plot is shown in Fig. 3-7. The measured thermal activation energy is 1.3 ev. This isochronal heat treatment procedure was then repeated in vacuum of 10^{-6} torr for different resistors from the same substrate. The measured thermal activation energy for this process is 2.7 ev. The magnitude of the conductance change produced by heating films at 500°C for fifteen minutes under vacuum is reduced by a factor of sixty relative to the conductance change produced by heating different resistors from the same substrate at 500°C in air for fifteen minutes.

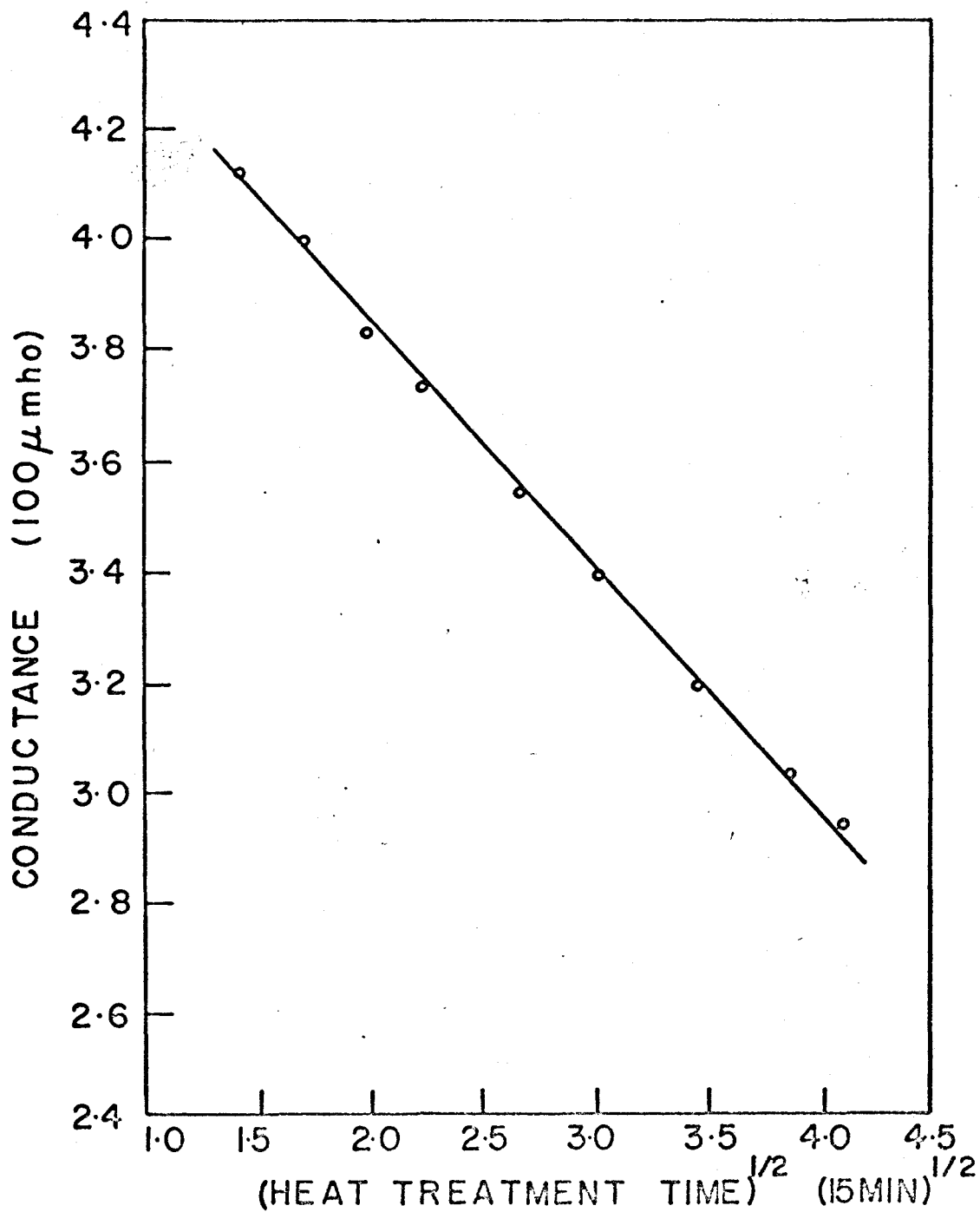


Figure 3-6

Room temperature conductance as a function of the square root of the heat treatment time, for a film heat treated at 500°C in an air ambient at atmospheric pressure. The film was sputtered in a total reactive partial pressure of 4×10^{-5} torr.

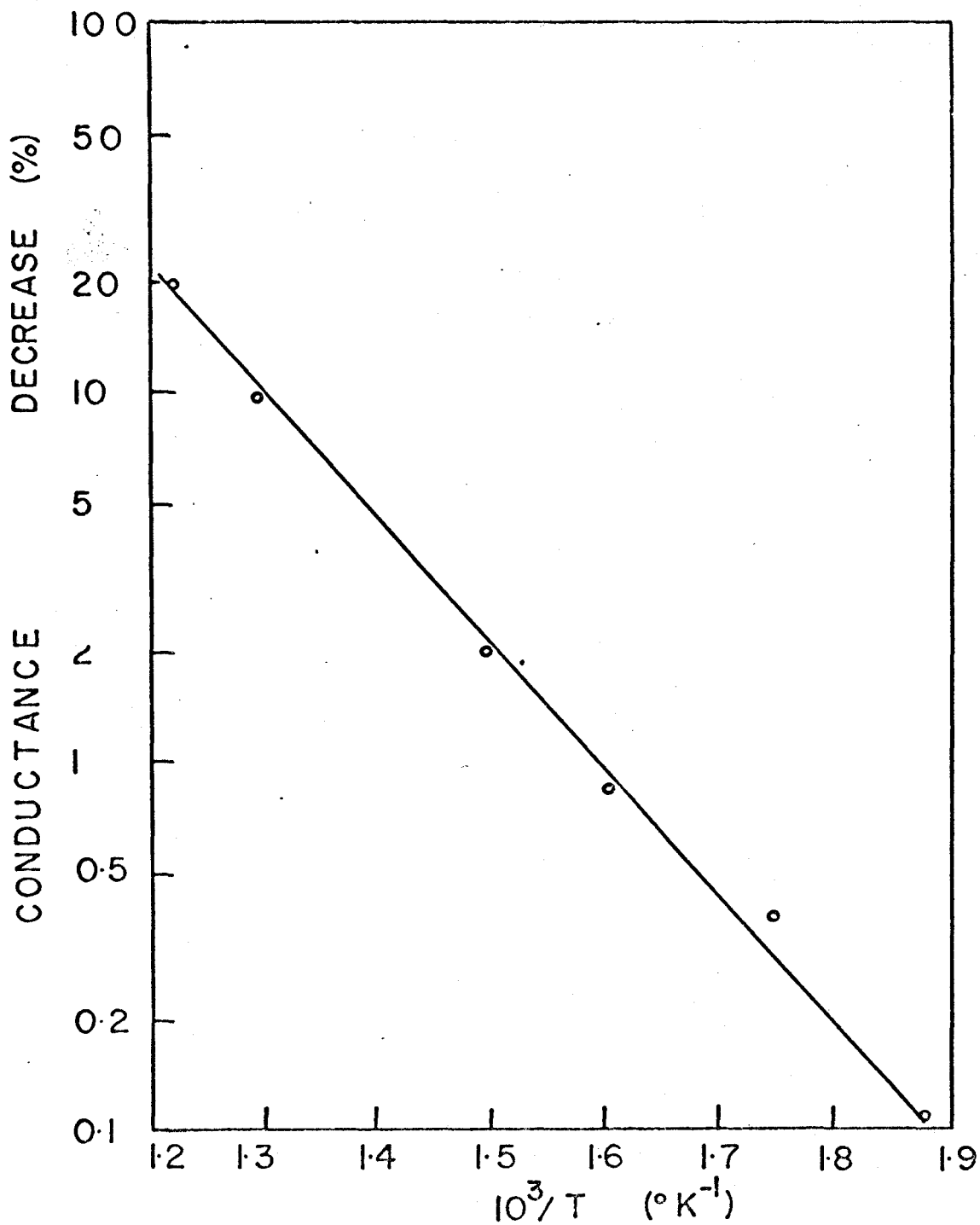


Figure 3-7

Arrhenius plot of the conductance change occurring in a film which was heat treated in air at atmospheric pressure. The film was sputtered in a total reactive partial pressure of 4×10^{-5} torr.

3.4 Discussion

3.4.1 Film Structure

Since the average resistivity and TCR of the films deposited on a carbon parting layer for observation in the electron microscope is the same as those values obtained for films deposited directly onto the substrate, it is assumed that the structure of these two types of film is similar. This conclusion has also been reached by Calbick and Schwartz ³³.

Electron diffraction patterns obtained from heat treated films sputtered in a "total" reactive partial pressure of 2×10^{-6} torr, 1×10^{-5} torr, 3×10^{-5} torr, and 4×10^{-5} torr show that these films consist of metallic Ta or metallic Ta_4O (depending on the reactive partial pressure) plus Ta_2O_5 . The fact that the time (10 minutes to 15 minutes) and temperature ($500^\circ C$) for crystallization of the amorphous material in non heat treated films (as shown by the disappearance of diffuse rings in the diffraction patterns and the appearance of rings corresponding to crystalline Ta_2O_5) agrees with those values ³⁴ for crystallization of amorphous Ta_2O_5 indicates that the non heat treated films contain amorphous Ta_2O_5 . Further evidence for assuming the amorphous material to be Ta_2O_5 is the fact that, when the heat treatment temperature was reduced by $50^\circ C$, no crystallization occurred ³⁵. Pawell and Campbell ³⁶ and Calvert and Draper ³⁷ have found Ta_2O_5 films crystallized in air to be crystallographically identical to Ta_2O_5 films crystallized in vacuum. Thus, it is suggested that the crystallization process which is observed to occur in the present films during

in situ heating in the electron microscope also occurs in the films during heat treatment in air.

The electron micrographs are consistent with a film structure consisting of metallic islands largely surrounded by Ta_2O_5 . For non heat treated films the inter-island Ta_2O_5 is amorphous, while for heat treated films this oxide is crystalline. Due to the fineness of the microstructure, it is expected that there would be some metallic contact between islands. As it is difficult to obtain well-focused micrographs at the high magnification used, these interconnecting metallic filaments may not be visible in the micrographs.

The structure of these films (metallic islands largely surrounded by an insulating inter-island region) is similar to that usually associated with cermet (ceramic + metal) films³⁸, formed by co-depositing a metallic material plus an insulating material. This structure is consistent with the fact that the films possess a negative TCR³⁹. This cermet structure has not been previously reported in reactively sputtered Ta films. For Ta films reactively sputtered in low partial pressures of oxygen only^{5,6}, it has been found that the films consisted of a uniform structure of Ta plus oxygen in solid solution. For reactive oxygen partial pressures in excess of about 3×10^{-5} torr, the films consisted of a uniform layer of amorphous Ta_2O_5 ⁴⁰. There was no evidence of either an island formation or of the presence of sub-oxides. Similarly, for Ta films reactively sputtered in nitrogen only^{5,6}, there has been no discrete island structure reported. However, Coyne and Tauber⁴¹ observed an island structure for Ta films sputtered in pure nitrogen, although they were

not able to identify the material present in the inter-island regions.

An estimate of the dopant concentration within the islands of BCC tantalum can be obtained from the measured lattice parameter. Gebhardt and Seghezzi⁴² have found a linear relationship between the lattice parameter of bulk Ta and the oxygen dopant concentration. According to their measurements, a lattice parameter of 3.31 \AA corresponds to a dopant concentration of 2 atomic per cent. Since the lattice expansion produced by a given concentration of nitrogen agrees to within 0.005 \AA ⁴³ of the lattice expansion produced by the same concentration of oxygen, it is estimated that the total dopant concentration ($\text{O}_2 + \text{N}_2$) within the islands for a reactive partial pressure of 1×10^{-6} torr oxygen and 1×10^{-6} torr nitrogen is 2 atomic per cent. Similarly, the total dopant concentration within the islands is estimated to be 9 atomic per cent for films sputtered in a reactive partial pressure of 5×10^{-6} torr oxygen and 5×10^{-6} torr nitrogen.

3.4.2 Effects of Heat Treatment on Film Structure

The observed kinetics for the conductance change of the films during heat treatment in an air ambient at atmospheric pressure may be used to obtain information concerning the mechanisms which affect the film properties during a standard heat treatment cycle. The conductance decrease was found to be proportional to the square root of the heat treatment time. It was also found that the mechanism which produced this conductance change had a thermal activation energy of 1.3 ev. Steidel

and Gerstenberg⁴⁴ have found that the thermal oxidation rate of thin films of BCC Ta, Ta₂N, and porous β -Ta (100 Å grains with 80 Å voids) is proportional to the square root of time and has a thermal activation energy of 1.4 ev. This oxidation produced a surface layer of Ta₂O₅. The agreement of the present experimental observations with these results suggests that the conductance change which occurs during heat treatment in air is due to the formation of a surface layer of Ta₂O₅ on the resistor film, thus reducing the volume of metallic tantalum.

There may be an additional process occurring during heat treatment, but it cannot be resolved by the above method since the conductance change due to this process is much less than the conductance change resulting from surface oxidation of the films. This possibility of the occurrence of a competing mechanism was investigated by repeating the heat treatment procedure in a vacuum of 10⁻⁶ torr. The conductance change produced by heat treatment in vacuum at 500°C is a factor of sixty less than that produced by heat treatment in air at 500°C. The measured thermal activation energy for the conductance change which occurs during heat treatment in vacuum is 2.7 ev. Thus, there is a mechanism, in addition to surface oxidation, which operates to produce a conductance decrease during heat treatment of the films. Since the heat treatment temperature is much too low for degassing of the metallic islands to occur⁴⁵, it is proposed that this competing mechanism is a crystallization

of the gap material and a growth of the islands, in agreement with the results obtained by electron microscopy. In addition, some of the oxygen within the gap regions may dissolve within the metallic islands ³⁷.

3.4.3 Electrical Conduction Mechanisms

Before discussing the electrical conduction mechanisms operative in the Ta-Ta₂O₅-Ta micro-structure of the thin films, it may be worthwhile to briefly consider the conduction mechanisms which have been found to occur experimentally in bulk Ta-Ta₂O₅ diodes. Conduction between bulk Ta and an anodized Ta₂O₅ surface oxide has been found to be limited by Schottky emission rather than by a Poole-Frenkle mechanism ⁴⁶. Standley and Maissel ⁴⁷ have studied electrical conduction in Ta-Ta₂O₅ thin film diodes prepared by anodizing a sputtered Ta film. These experimental results were consistent with a Schottky mechanism, although for oxide thicknesses of the order of 100 Å or less there was evidence of a tunneling mechanism. The experimental thermal activation energy for Schottky emission was 1 ev. This is in agreement with the 1.1 ev potential barrier which has been found to exist at Ta-Ta₂O₅ interfaces ⁴⁸.

In the case of the present thin films, the experimental conductance-temperature curves of Figures 3-4 and 3-5 will form the basis of the discussion. Henrickson et al ⁴⁹ have found that in co-sputtered Ta-Al₂O₃ cermet films a "bulk" tunneling mechanism between metallic grains will account for the observed temperature dependence of the conductivity. Although the tunneling probability is temperature independent, the tunneling current will

increase slightly with temperature due to the increase in carrier flux incident upon the barrier. If this mechanism were operative in the present case, the conductance $g(T)$ should vary with temperature according to the law ⁵⁰

$$\frac{g(T)}{g(0)} = 1 + 3.4 \times 10^{-6} T^2 \quad (3-1)$$

where $g(0)$ is the film conductance at 0°K . Since equation (3-1) is simply the first two terms of a series expansion, the validity of the equation is subject to the condition $T \ll 10^3^\circ\text{K}$. The graph of $g(T)$ vs T^2 shown in Fig. 3-5 is definitely nonlinear up to the maximum measured temperature of 400°K . Thus, it appears that this tunneling mechanism is not responsible for the observed results.

The Arrhenius plot of Fig. 3-4 suggests that the film conductance has two components, having activation energies of 7.0×10^{-4} ev and 3.4×10^{-5} ev. The small magnitude of the measured activation energy for the conduction mechanism precludes the possibility of a Schottky limited mechanism. Since the calculated image force lowering of the metal-insulator potential barrier is only 3×10^{-2} ev ⁵¹, the activation energy for a Schottky limited mechanism would be essentially given by the Ta-Ta₂O₅ potential barrier of 1.1 ev ⁴⁸. Since this value exceeds the experimentally obtained value by several orders of magnitude, it is concluded that conduction does not occur by means of a Schottky mechanism.

For a film possessing an island structure, Neugebauer and Webb ⁵² have proposed a model which suggests that, due to an activated tunneling mechanism, the conductance should vary with temperature according to the law

$$g = g_0 \exp(-E/kT) \quad (3-2)$$

where E is a thermal activation energy and g_0 is proportional to the temperature-independent tunneling probability. Neugebauer and Webb suggest that the thermal activation is due to the fact that the individual islands are not at a fixed potential, and thus thermal energy must be supplied to the carriers in order for them to be activated over the barrier associated with the electrostatic work which is required to transfer carriers between islands. According to this theory, the activation energy for conduction in a discontinuous film of island size 35 \AA separated by a 20 \AA gap of Ta_2O_5 is calculated to be 5.9×10^{-3} ev. The discrepancy between the calculated activation energy of 5.9×10^{-3} ev and the experimental value of 7.0×10^{-4} ev might be accounted for by the facts that: 1) the islands are not spherical as required by the model of Neugebauer and Webb, and 2) there is a distribution in the size of the islands and the inter-island gaps. This distribution in island and gap dimensions might also account for the apparent presence of two activation energies, but, in view of the fact that the factor of twenty difference in the measured activation energies is inconsistent with the electron microscopy results, this mechanism is rejected. It has been suggested by Hill⁵³ that the higher temperature component which appears on an Arrhenius plot of the conductance of a thin film may be due to the change in tunneling probability with temperature resulting from the change in the carrier distribution function with temperature. If this mechanism were responsible for the observed second component at temperatures

in excess of 200°K , the conductance should vary with temperature according to equation (3-1). According to this model, the slope of the curve on an Arrhenius plot, $d(\ln g)/d(1/T)$, would be 1.1×10^{-3} K at 200°K . According to the thermally activated tunneling model of Neugebauer and Webb, the slope of the Arrhenius plot is calculated to be 11°K . The experimentally observed slope is 1.5°K . Since the mechanism proposed by Hill will have a slope on an Arrhenius plot which is approximately three orders of magnitude smaller than the experimentally observed slope, this mechanism is unlikely to account for the change in slope which is observed at 200°K . 53

As a tentative explanation, it is postulated that the device conductance is the result of a competition between metallic island conduction of positive TCR and gap tunneling conduction of negative TCR. At high temperatures, gap conduction will dominate, producing a net negative TCR, whereas at sufficiently low temperatures, metallic conduction via connected islands will dominate, producing a net positive TCR. In some intermediate temperature range the rate of change of conductance with temperature for the gap mechanism will be partially cancelled by that for the island mechanism, producing a net device conductance which is relatively independent of temperature. It is proposed that, for the present devices, this relatively temperature independent conduction region occurs in the range of 60°K to less than 30°K , producing the apparent second component on the Arrhenius plot in Figure 3-4. At low enough

temperatures the conductance should show an increase. The data in Figure 3-4 does not indicate such an increase because this low temperature range was not accessible with the present experimental apparatus.

3.4.4 Effect of Simultaneous Doping with Oxygen and Nitrogen

It has been shown in section 3.3.2 that an increase in the reactive nitrogen partial pressure, for a fixed reactive oxygen partial pressure, will reduce the magnitude of the film TCR. Similarly, an increase in the reactive oxygen partial pressure will increase the magnitude of the film TCR. It was also shown that for a fixed total reactive partial pressure, the larger the reactive nitrogen partial pressure, the smaller the magnitude of the film TCR. The shape of the curves of resistivity and TCR as a function of total reactive partial pressure (Fig. 3-3) are qualitatively similar to those of the resistivity and TCR of Ta films as a function of reactive oxygen partial pressure, rather than of reactive nitrogen partial pressure⁶. This suggests that the role of nitrogen in determining film properties is secondary to that of oxygen, i.e., the film properties are determined principally by the reactive oxygen but are perturbed by the reactive nitrogen.

The effectiveness of this dual dopant scheme from a device point of view may be shown by considering Table 3-6 which lists the maximum resistivity obtained for a maximum allowable TCR of ± 100 ppm/ $^{\circ}$ C. It is seen that the present dopant scheme will permit the deposition of a film having a

resistivity a factor of three greater than obtainable with a single dopant of either nitrogen or oxygen. This table also illustrates the fact that for an arbitrarily selected film resistivity of $700 \mu\Omega\text{-cm}$, the dual dopant scheme produces a film having a TCR that is much closer to zero than is attainable by reactive sputtering in oxygen only. A resistivity of $700 \mu\Omega\text{-cm}$ cannot generally be attained by reactive sputtering in nitrogen only.

Table 3-6

COMPARISON OF Ta(O,N) FILM RESISTIVITY AND TCR WITH PREVIOUSLY PUBLISHED RESULTS

Reference	Dopant	Resistivity for -100 ppm/ $^{\circ}\text{C}$ TCR ($\mu\Omega\text{-cm}$)	TCR for 700 $\mu\Omega\text{-cm}$ resistivity (ppm/ $^{\circ}\text{C}$)
This work	O,N	700	-100
Gerstenberg	O	200	-400
and Calbick ⁶	N	250	-
McLean et al ⁵⁴	O	230	-400
	N	250	-

In order to discuss these results, it is first necessary to consider the manner in which the Ta-O-N components can interact when deposited onto a substrate. The possible reactions are:

- 1) formation of a Ta(O,N) solid solution;
- 2) limited oxygen-nitrogen replacement⁵⁵;
- 3) ternary oxy-nitride compound formation⁵⁵.

The electron diffraction results indicate that for the case of a relatively low total reactive partial pressure (1×10^{-5} torr or 2×10^{-6} torr), the metallic islands consist of a Ta(O,N) solid solution. For a relatively high total reactive partial pressure (3×10^{-5} torr) the metallic islands consist of a Ta₄O-TaN mixture. There was no indication of the formation of a tantalum oxy-nitride compound. These results indicate that as the nitrogen reactive partial pressure increases, the tantalum nitride content of the metallic islands increases.

The bonding of a tantalum nitride compound is relatively metallic, while that of a tantalum oxide compound is relatively ionic⁵⁵. On this basis, the nitride will have a greater positive TCR than the oxide. Thus, for a fixed oxygen content, the TCR of the metallic islands will become more positive as the reactive nitrogen partial pressure increases. Since the measured TCR of the film may be considered to consist of a TCR component due to the islands and a TCR component due to the gaps, the film TCR will become more positive (a smaller negative value) as the reactive nitrogen partial pressure increases for a fixed reactive oxygen partial pressure. Similarly, for a fixed nitrogen content within an island, an increase in the reactive oxygen partial pressure will cause the island component of the TCR to become less positive. This would account for the

fact that the film TCR becomes more negative with increasing reactive oxygen partial pressure.

This model will account for the observation that, for a fixed total reactive partial pressure, the film TCR becomes less negative as the reactive nitrogen partial pressure increases. The increase in the reactive nitrogen partial pressure makes the island contribution to the film TCR more positive, causing a film TCR which is less negative than a film having the same total reactive partial pressure, but with a smaller reactive nitrogen component.

Even though this model will explain the observed changes in TCR with reactive partial pressure, this hypothesis must be considered to be very tentative since relative magnitudes of conductance cannot be given to the individual components whose TCR's are being considered.

3.5 Summary

Tantalum thin film resistors have been reactively sputtered in oxygen and nitrogen simultaneously. Electron microscopy has been used to demonstrate that the structure of non heat treated resistors consists of metallic islands largely surrounded by amorphous Ta_2O_5 . The dopant concentration in the islands has been measured by electron diffraction. Heat treatment of these films in air enhances the island structure, as well as producing a stabilizing surface oxide. This procedure also produces a crystallization of the inter-island Ta_2O_5 .

The discontinuous films have TCR values ranging from -50 ppm/°C to -900 ppm/°C. The corresponding resistivities ranges from 400 $\mu\Omega$ -cm to $3 \times 10^4 \mu\Omega$ -cm. The dual dopant scheme of nitrogen and oxygen produces a higher resistivity film for a given TCR than has been previously reported for a dopant of either nitrogen or oxygen. The temperature dependence of the film conductance may be accounted for by an activated tunneling process occurring in the inter-island gaps and a metallic conduction process occurring concurrently within island regions of the film.

IV

LOW FLUENCE, ROOM TEMPERATURE RADIATION DAMAGE

4.1 General

This chapter considers the effects of radiation damage on the conductance of reactively sputtered Ta thin film resistors for a film temperature of 286°K and fluences up to 10^{16} p/cm². These data are considered for a range of reactive partial pressures for air heat treated, vacuum heat treated, and non heat treated films. The data obtained during irradiation experiments are presented in the form of the percent conductance change, $\Delta g/g_0$, where g_0 is the conductance of the unirradiated film, as a function of fluence, ϕ . These curves will be referred to as σ - ϕ curves, where σ is defined as $\Delta g/g_0$. The radiation-produced conductance change at a fluence of 10^{16} p/cm² is investigated as a function of beam energy. From these results a basic model is postulated to explain the radiation-produced conductance change.

4.2 Experimental Results

4.2.1 Conductance Changes as a Function of Fluence

Figure 4-1 shows the σ - ϕ curve for an air heat treated film sputtered in a reactive partial pressure of 2×10^{-5} torr nitrogen and 2×10^{-5} torr oxygen. The percentage conductance

increase is a linear function of fluence, up to the measured fluence of 10^{16} p/cm². The slope of this curve is 1.0%/10¹⁶ p/cm². The slope is independent of beam current density over the measured range of 0.1 μ amp/cm² to 15 μ amp/cm². After irradiation, the measured conductance of the film was independent of time, the conductance changing by less than 0.01% in a period of 36 hours. Figure 4-1 also shows the σ - ϕ curve for a vacuum heat treated film sputtered in a reactive partial pressure of 2×10^{-5} torr nitrogen and 2×10^{-5} torr oxygen. The conductance increase is a linear function of fluence, up to the measured fluence of 10^{16} p/cm². The slope of this curve is 0.4%/10¹⁶ p/cm². Figure 4-2 shows the σ - ϕ curve for a non-heat treated film sputtered in a reactive partial pressure of 2×10^{-5} torr nitrogen and 2×10^{-5} torr oxygen. In this case, the conductance increases with fluence, but in a non-linear fashion.

Figure 4-3 shows the slope of the σ - ϕ curves for air heat treated films as a function of total reactive partial pressure for equal reactive oxygen and nitrogen partial pressures. Each point is an average of three or four individual experimental values. The average value has a confidence limit of 10%. The deviation from the mean for the conductance of the non irradiated resistors on a given substrate is also typically 10%. This figure illustrates a difference in the rate of conductance change during irradiation with total reactive partial pressure for films sputtered in a relatively high total reactive partial pressure and for those sputtered in a relatively low total

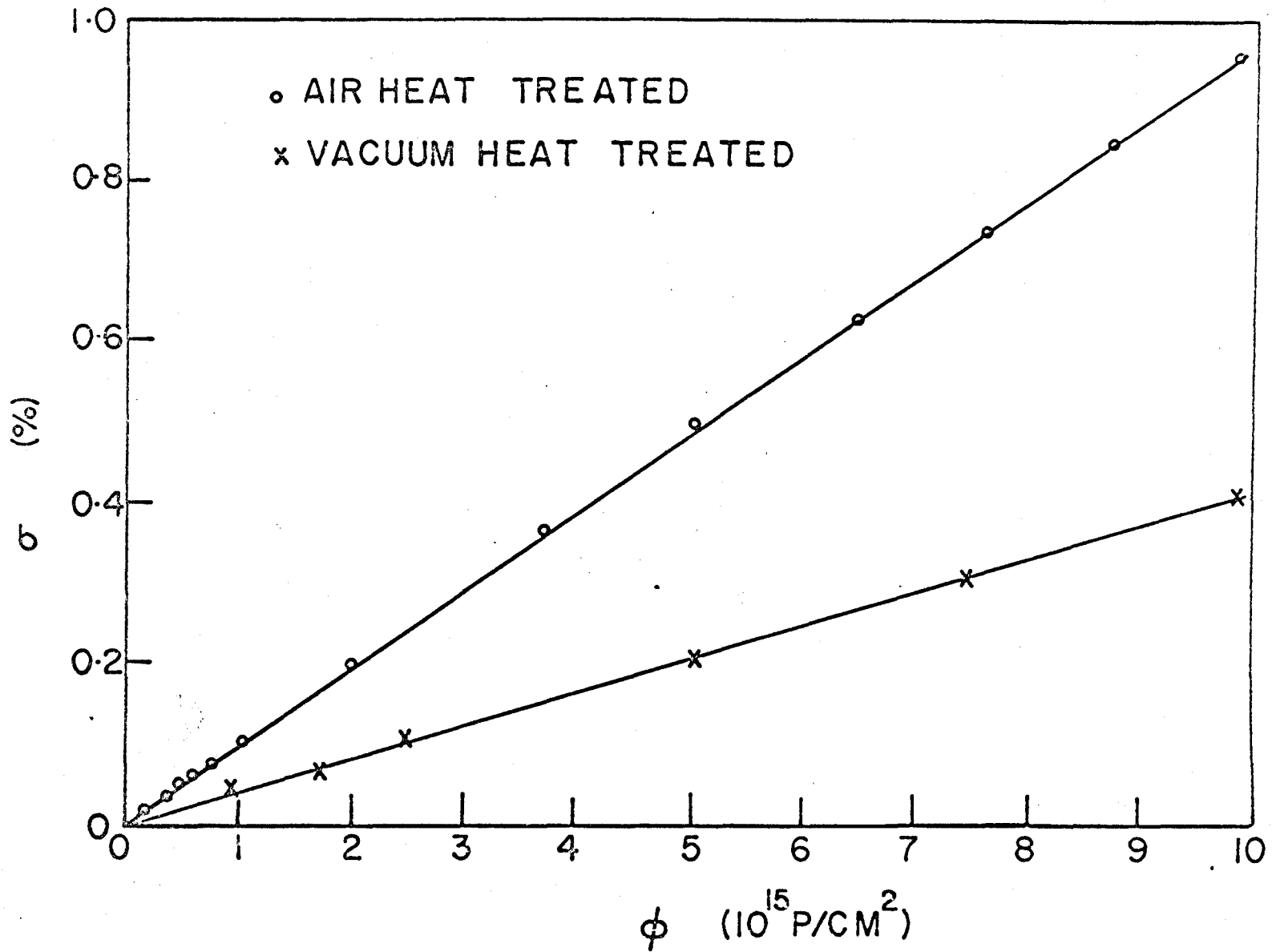


Figure 4-1

σ - ϕ curves for room temperature irradiation of films sputtered in a reactive partial pressure of 2×10^{-5} torr nitrogen and 2×10^{-5} torr oxygen. Heat treatment was carried out at 500°C , either in an air ambient or in a vacuum of 10^{-6} torr.

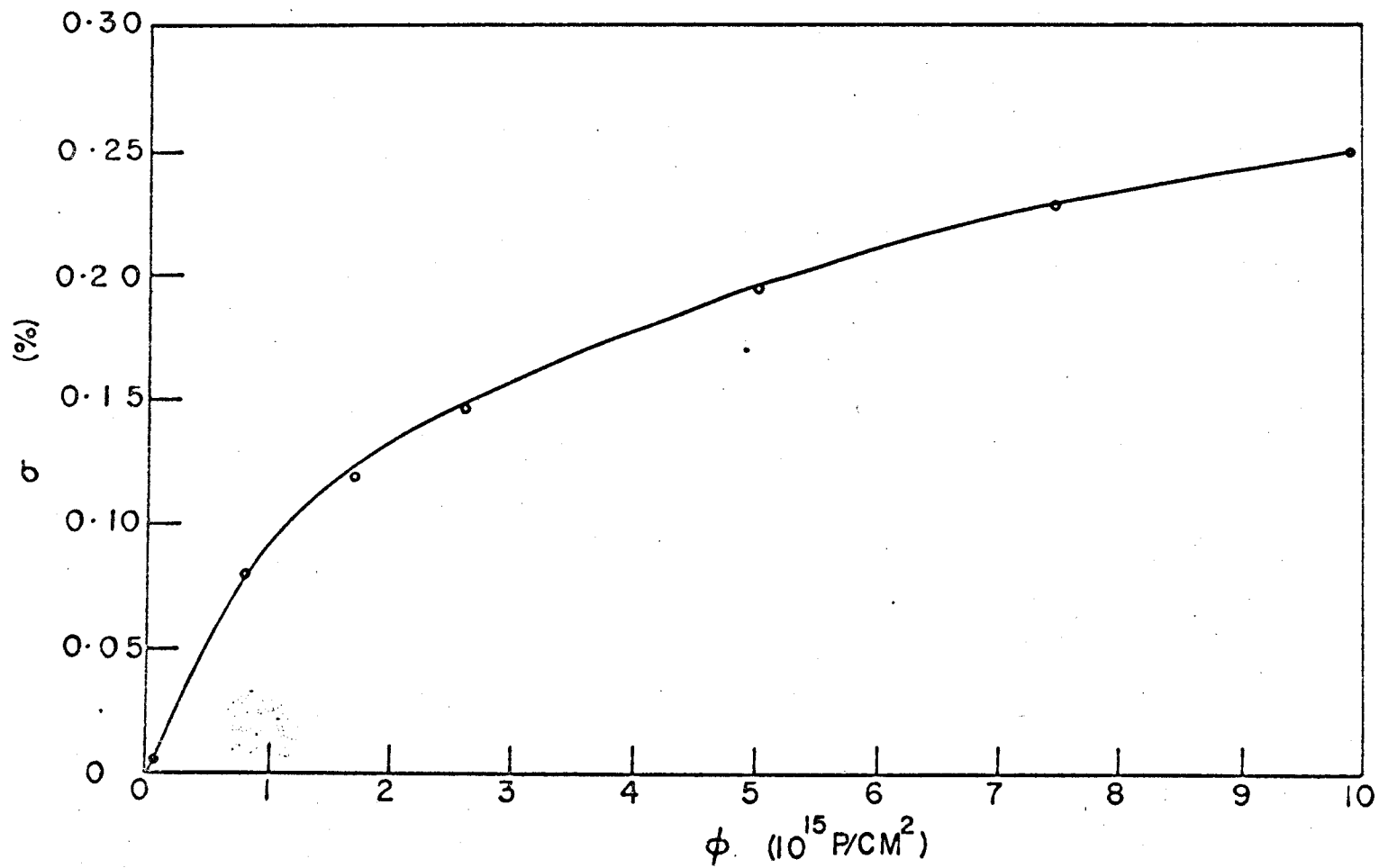


Figure 4-2

σ - ϕ curve for room temperature irradiation of a non heat treated film sputtered in a reactive partial pressure of 2×10^{-5} torr nitrogen and 2×10^{-5} torr oxygen.

reactive partial pressure: for the former films the slope of the $\sigma - \phi$ curves decreases with increasing total reactive partial pressure, whereas for the latter films the slope of the $\sigma - \phi$ curves increases with increasing total reactive partial pressure. Figure 4-4 shows the slope of the $\sigma - \phi$ curves for air heat treated films as a function of reactive oxygen partial pressure, the reactive nitrogen partial pressure being kept constant at 7×10^{-6} torr. The shape of this curve is qualitatively similar to that illustrating the slope of the $\sigma - \phi$ curves as a function of total reactive partial pressure.

Table 4-1 shows the slope of the $\sigma - \phi$ curves for air heat treated films as a function of reactive nitrogen partial pressure, the reactive oxygen partial pressure being kept constant at 1×10^{-5} torr. For reactive nitrogen partial pressures in the range of 7×10^{-6} torr to 2×10^{-5} torr, the slopes of the $\sigma - \phi$ curves are the same within experimental error. For a reactive nitrogen partial pressure of greater than 2×10^{-5} torr the slope of the $\sigma - \phi$ curve decreases. Table 4-2 shows the slope of the $\sigma - \phi$ curves for air heat treated films as a function of reactive oxygen and reactive nitrogen partial pressures, the total reactive partial pressure being kept constant at 4×10^{-5} torr. From this table it is seen that the slope of the $\sigma - \phi$ curve decreases as the reactive oxygen partial pressure increases relative to the reactive nitrogen partial pressure.

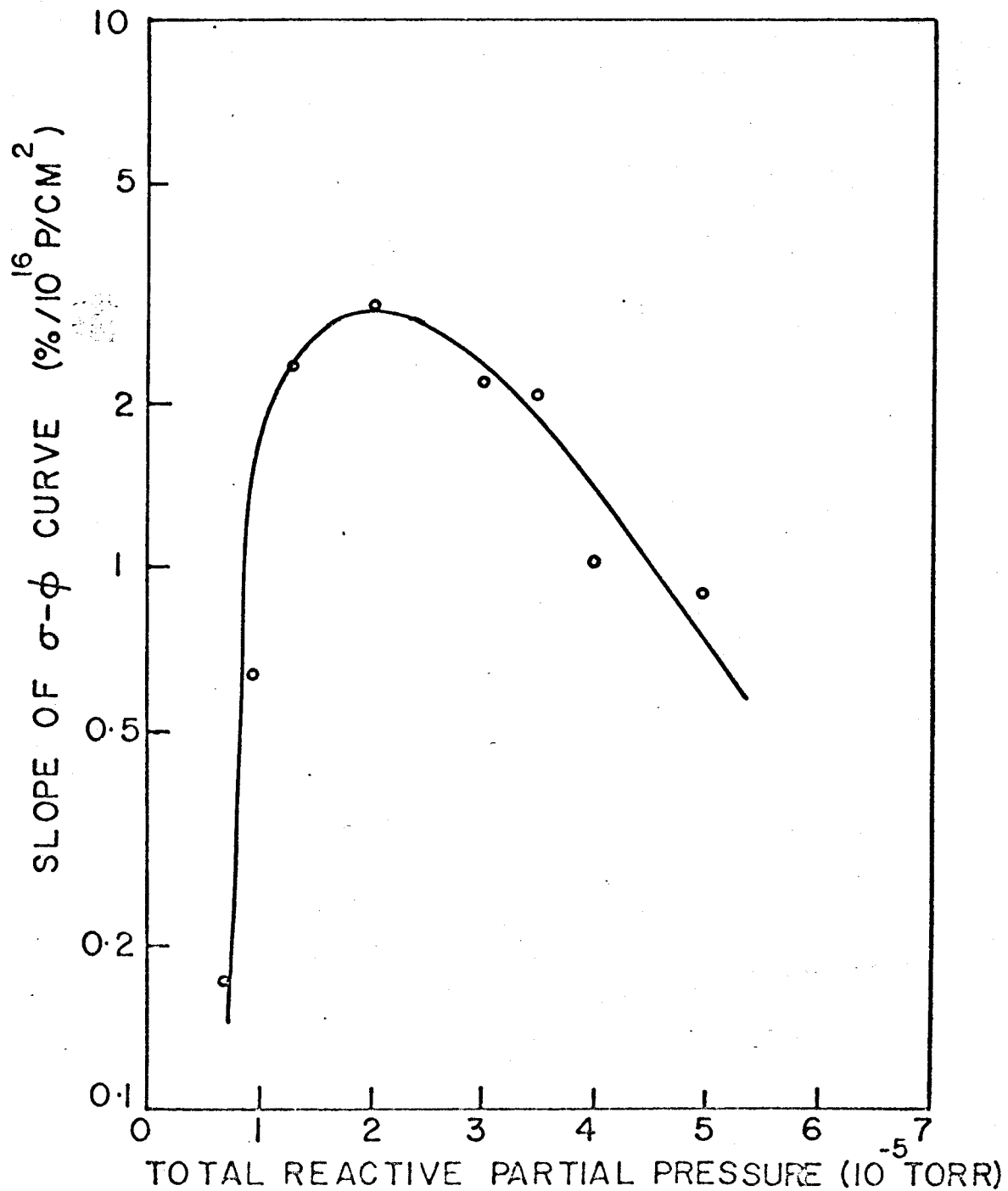


Figure 4-3

Slope of the σ - ϕ curves for room temperature irradiation of films heat treated in air at 500°C , as a function of the total reactive partial pressure, for equal oxygen and nitrogen reactive partial pressures.

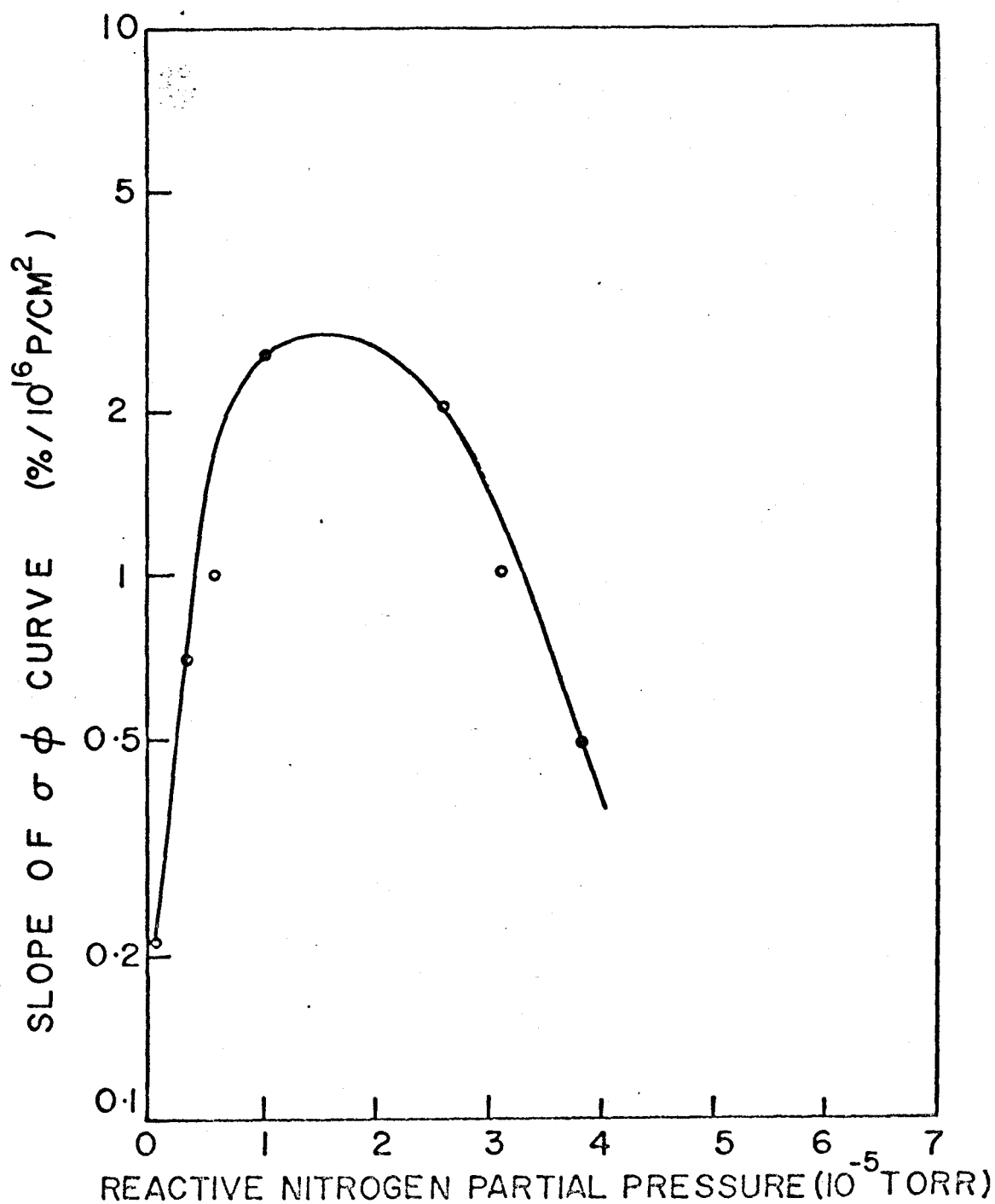


Figure 4-4

Slope of the $\sigma - \phi$ curves for room temperature irradiation of films heat treated in air at 500°C , as a function of reactive oxygen partial pressure, the reactive nitrogen partial pressure being kept constant at 7×10^{-6} torr.

Table 4-1

SLOPE OF THE $\sigma - \phi$ CURVES FOR FILMS HEAT TREATED IN AIR
AS A FUNCTION OF REACTIVE NITROGEN PARTIAL PRESSURE
THE REACTIVE OXYGEN PARTIAL PRESSURE BEING CONSTANT

Reactive Partial Pressure $\times 10^{-5}$ torr		Average Linear Slope $\%/10^{16}$ p/cm ² ($\pm 10\%$)
Nitrogen	Oxygen	
.7	1	2.5
1	1	2.5
2	1	3.0
3	1	1.4
4	1	0.9

Table 4-2

SLOPE OF THE $\sigma - \phi$ CURVES FOR FILMS HEAT TREATED IN AIR
AS A FUNCTION OF REACTIVE OXYGEN AND NITROGEN PARTIAL PRESSURES
THE TOTAL REACTIVE PARTIAL PRESSURE BEING CONSTANT AT 4×10^{-5} TORR

Reactive Partial Pressure $\times 10^{-5}$ torr		Average Linear Slope $\%/10^{16}$ p/cm ² ($\pm 10\%$)
Nitrogen	Oxygen	
3	1	1.4
2	2	1.0
1	3	0.8
.3	3.7	0.5

4.2.2 Conductance Change as a Function of Beam Energy

In order to investigate the effects of proton energy on the conductance change produced by radiation damage, films sputtered in a total reactive partial pressure of 3×10^{-5} torr were bombarded as a function of beam energy over the range 35 keV to 150 keV. Figure 4-5 shows the conductance increase at a fluence of 10^{16} p/cm² as a function of $\frac{1}{E} \ln 130E$, where E is the beam energy in units of 100 keV. This curve is linear for beam energies in the range of 150 keV to 50 keV. Below 50 keV the curve becomes nonlinear. The reason for this type of plot will be discussed in section 4.3.2.

4.2.3 Electron Microscopy

No evidence of defect clustering or of a radiation-produced change in either the physical or crystal structure of the films was detected by means of electron microscope examination of films which had been irradiated by 150 keV protons. Figure 4-6 illustrates a bright field micrograph of magnification 310,000 in addition to an electron diffraction pattern for a film of total reactive partial pressure 1×10^{-5} torr after the film had been irradiated to a fluence of 10^{16} p/cm².

4.3 Discussion

4.3.1 Conductance Change as a Function of Fluence

In Chapter III it was shown that the films consist of connected metallic islands largely surrounded by Ta₂O₅. Electrical conduction through the films at room temperature was

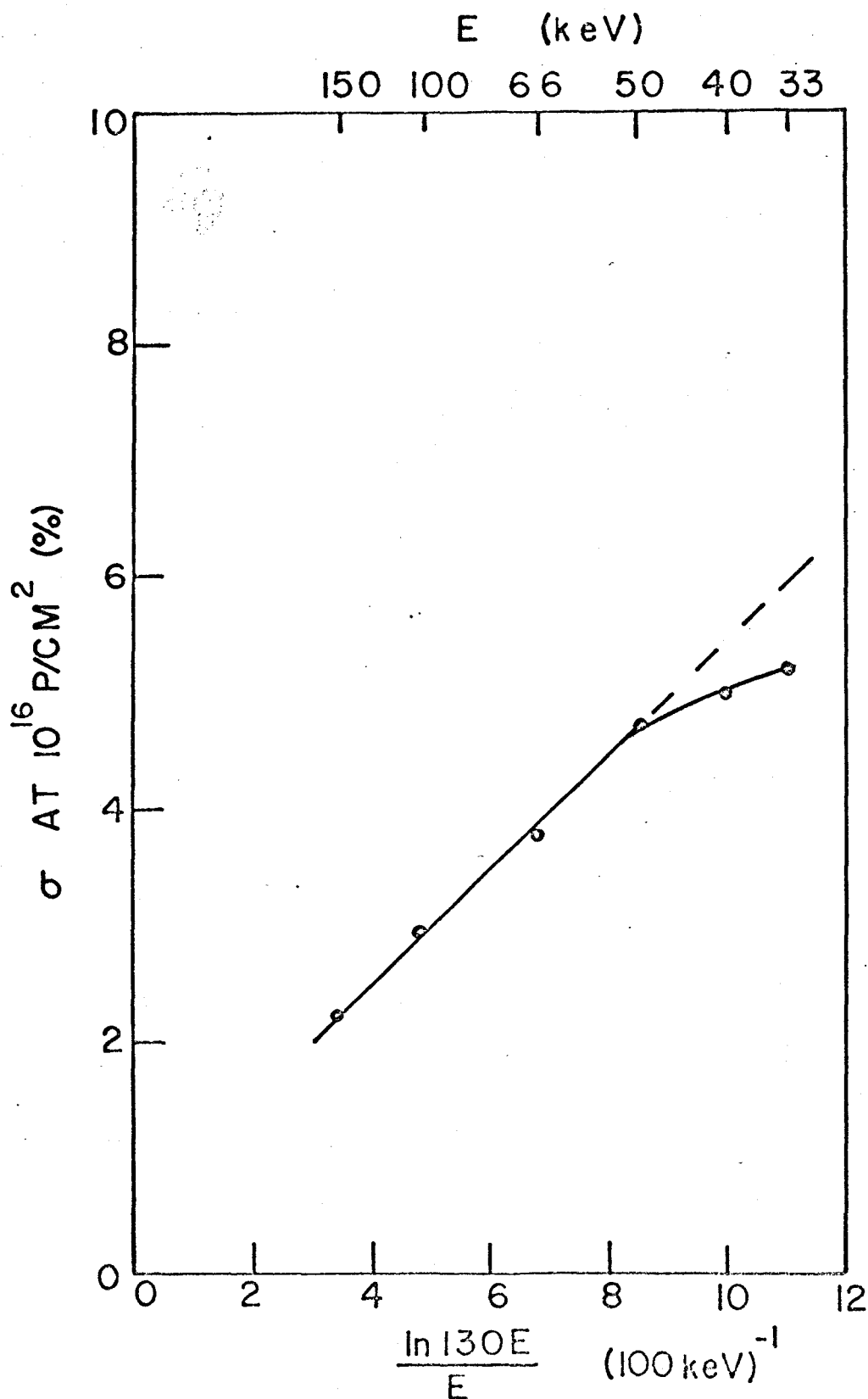
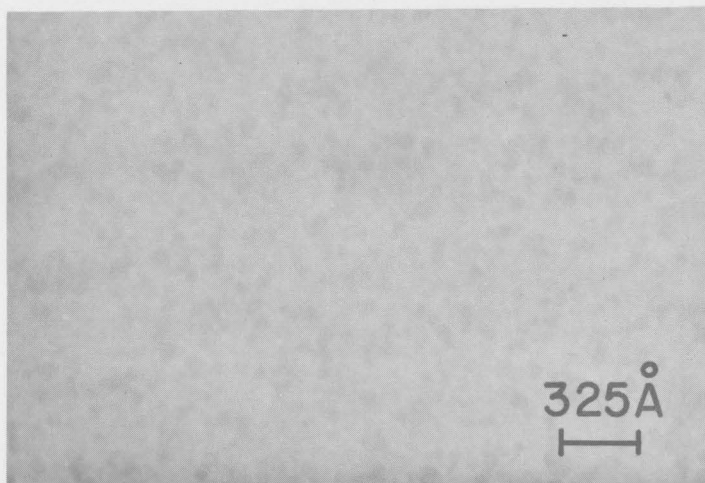
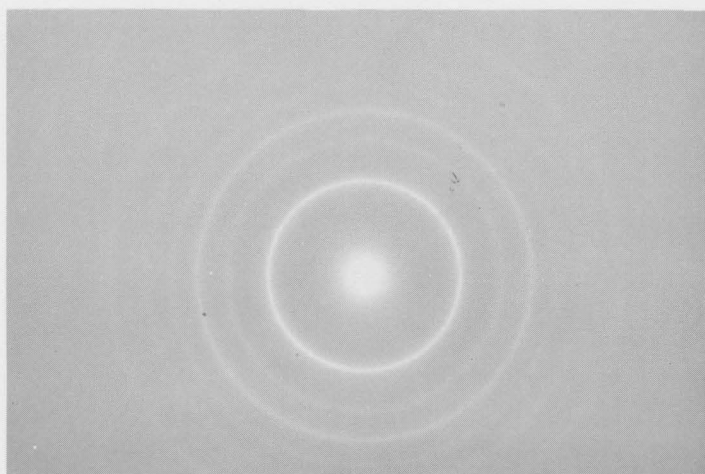


Figure 4-5

Conductance increase at a fluence of 10^{16} p/cm² as a function of $\frac{1}{E} \ln 130E$, where E is the beam energy. These films were sputtered in a reactive partial pressure of 1.5×10^{-5} torr nitrogen and 1.5×10^{-5} torr oxygen.



(a)



(b)

Figure 4-6

Electron microscope results for a film sputtered in a reactive partial pressure of 5×10^{-6} torr nitrogen and 5×10^{-6} torr oxygen after irradiation to 10^{16} p/cm²: (a) bright field micrograph, and (b) electron diffraction pattern.

shown to be consistent with a tunneling mechanism through the inter-island gaps. Penley⁵⁶ has shown that the presence of electronic trapping levels within an insulating oxide of a metal-oxide-metal structure will enhance the tunneling current through the oxide. As shown in Appendix A, the enhanced conductance for a spatial distribution of trapping levels within the oxide may be written as

$$\sigma = \frac{1}{g} \int C(x) g^t(x) dx \quad (4-1)$$

where g is the initial conductance of the barrier before enhancement, $g^t(x)$ is the enhanced conductance due to the presence of one trapping level at position x in the tunneling direction, and $C(x)$ is the concentration of initially unoccupied trapping levels in the oxide. Irradiation of the films will produce defect levels within the oxide, some of which are expected to act as trapping levels, i.e., during irradiation $C = C(x, \phi)$ is a function of fluence. Averaged over the inter-island regions of a film, the concentration of trapping levels within the gaps will be relatively independent of position x . Thus, from equation (4-1), σ is expected to increase linearly with $C(\phi)$, the concentration of initially unoccupied radiation-produced trapping levels, i.e.,

$$\sigma = \delta' C(\phi) \quad (4-2)$$

where $\delta' = \frac{1}{g} \int g^t(x) dx$ is the percent conductance increase per unit defect concentration of unoccupied trapping levels.

Based solely on geometrical considerations, the rate of enhancement of the film conductance with fluence (the slope of the σ - ϕ curves) should increase as the tunneling distance decreases⁵⁷. On this basis, the slope of the σ - ϕ curves would

be expected to increase as the total reactive partial pressure increases, since the gap size decreases as the total reactive partial pressure increases (Chapter 3). The experimental results for total reactive partial pressures greater than 2×10^{-5} torr are in opposition to this expectation (Fig. 4-3). Thus, some additional mechanism must be operative. A possible model will now be considered.

The concentration of initially unoccupied trapping levels is given by

$$C = N_d - N_T \quad (4-3)$$

where N_d is the concentration of radiation-produced trapping levels and N_T is the concentration of carriers from the conduction band which have been thermally trapped. Under equilibrium conditions, the trapped carrier concentration is given by ⁵⁸

$$N_T = P\sigma_c n v (N_d - N_T) \quad (4-4)$$

where P is the probability of thermal ejection of a carrier from the trapping level, σ_c is the capture cross-section for the level, and n is the concentration of free carriers having velocity v . The concentration of radiation-produced defect levels is given by (see Appendix B)

$$N_d = \nu \sigma_d N_a \int f(\phi) d\phi \quad (4-5)$$

where σ_d is the displacement cross-section, ν is the average number of secondary knock-ons per primary knock-on, ϕ is the fluence, $f(\phi)$ is a function of magnitude equal to or less than

unity which accounts for a nonlinear production of stable radiation-produced defects with increasing fluence, N_a is the concentration of atoms within the target. Combining equations (4-2), (4-3), (4-4), and (4-5), the value of σ is given by

$$\sigma = S' \sigma_d \nu N_a (1 + P \sigma_c n v)^{-1} \int f(\phi) d\phi \quad (4-6)$$

The experimental results will be discussed on the basis of this model.

The amorphous oxide present in non heat treated films will possess a large number of intrinsic defects which might act as trapping sites for radiation-produced defects. In this case, $f(\phi)$ will not be equal to unity, resulting in nonlinear $\sigma - \phi$ curves, as shown by equation (4-6). The crystalline oxide of heat treated films will not possess as large an intrinsic defect concentration as an amorphous oxide and, thus, the $\sigma - \phi$ curves for heat treated films will be linear for larger values of fluence than for non heat treated films. This model will be discussed further in Chapter VI.

Heat treatment of Ta_2O_5 in vacuum will produce a greater concentration of oxygen vacancies within the oxide than for Ta_2O_5 heat treated in air³⁷. Since these oxygen vacancies act as donor defects⁵⁹, the equilibrium free carrier concentration within the oxide will be greater for vacuum heat treated films than for air heat treated films. Therefore, according to expression (4-6), the slope of the $\sigma - \phi$ curves will be less for vacuum heat treated films than for air heat treated films. This

is in agreement with the experimental observations.

Heat treatment of the Ta-Ta₂O₅ interface is known to produce non-stoichiometric oxygen vacancies within the oxide⁵⁹. Since this oxygen depletion occurs by a diffusion mechanism, the smaller the gap regions of the films, the greater will be the average non-stoichiometric oxygen vacancy concentration. Thus, for air heat treated films, the free carrier concentration n increases as the gap dimensions decrease and, therefore, according to expression (4-6), the slope of the $\sigma - \phi$ curves decreases as the gap dimensions decrease. As shown in Chapter 3, the size of the gap regions decreases as the total reactive partial pressure increases, accounting for the observed decrease in the slope of the $\sigma - \phi$ curves with increasing total reactive partial pressure, for total reactive partial pressures in excess of 2×10^{-5} torr.

A comparison of Fig. 4-3 and Fig. 4-4 shows a qualitative similarity in the manner in which the slope of the $\sigma - \phi$ curves vary with total reactive partial pressure for equal reactive partial pressures of oxygen and nitrogen, and in the manner in which the slope varies as a function of reactive oxygen partial pressure for a fixed reactive nitrogen partial pressure. Table 4-1 shows that the slope of the $\sigma - \phi$ curves for a fixed reactive oxygen partial pressure is approximately independent of the reactive nitrogen partial pressure, for reactive nitrogen partial pressures of 2×10^{-5} torr or less. These observations connote that, for total reactive partial

pressures of less than 2×10^{-5} torr, the observed decrease in the slope of the $\sigma - \phi$ curves with decreasing total reactive partial pressure, for equal reactive partial pressures of oxygen and nitrogen, is due to a decrease in the reactive oxygen partial pressure, rather than being due to a decrease in the reactive nitrogen partial pressure. Reasons for this will be discussed in detail in section 6.3.1.

Although the radiation-produced conductance increase is attributed to an enhanced tunneling mechanism, the observed conductance increase could possibly be due to other causes. Some of these will now be considered briefly.

The increase in conductance of the films as a result of irradiation might possibly be due to hydrogen ion implantation of the films. According to the LSS theory⁶⁰, the mean projected range of 150 keV protons in the films is calculated to be 4,000 Å. On the basis of wide angle Rutherford scattering, the hydrogen ion concentration in the films is calculated to 10^{18} ions/cm³. In section 4.3.2 it will be shown experimentally that this implantation is not responsible for the observed results.

In Chapter III it was shown that heat treatment of a film in air at 500°C produces a layer of Ta₂O₅ on the surface of the film, in addition to producing a crystallization of the inter-island Ta₂O₅. Consideration of the following mechanisms suggests that radiation effects within this surface oxide are not the dominant mechanisms responsible for the linear $\sigma - \phi$ curves.

1) Sputtering of the Surface Oxide

Chemisorption of a gas on a metallic surface has been shown^{61,62} to reduce the conductance of the metal by the formation of electronic bonds between the gas atoms and the conduction electrons within the metal. A surface oxide may reduce the film conductance in an analogous fashion. Removal of this oxide by sputtering would result in an increase in film conductance. A sputtering coefficient of 3×10^{-3} atoms/proton for 150 keV protons incident on Ta_2O_5 was obtained by using the sputtering theory of Sigmund⁶³ to extrapolate the experimental sputtering coefficient obtained by Nghi and Kelly⁶⁴ for Kr on Ta_2O_5 . The maximum conductance increase due to sputtering at 10^{16} p/cm² is calculated to be $2 \times 10^{-4}\%$. The fact that the experimental conductance change is a factor of 5×10^3 greater than the calculated maximum conductance change due to sputtering suggests that sputtering is not responsible for the observed σ - ϕ curves.

2) Increased Electronic Conductivity of the Surface Oxide due to Radiation-Produced Defect Levels

Although it has been shown that the electronic conductivity of metallic oxide films does increase on irradiation⁶⁵, no quantitative data is available for radiation enhanced conductivity in Ta_2O_5 , and, thus, it is not possible to calculate the enhanced conductivity of the surface oxide. However, a consideration of the σ - ϕ results for vacuum heat treated films suggests that this effect is not the dominant mechanism

responsible for the $\sigma - \phi$ results. As will be discussed in section 4.3.2, the rate of damage production with energy is proportional to $\frac{1}{E} \ln 130E$ for beam energies in the range 50 keV to 150 keV. On this basis, the maximum deviation in damage concentration from the average, as a function of depth through the oxide, is calculated to be 3%. As discussed in Chapter 3, a film which has been vacuum heat treated will have a surface oxide which is at least a factor of 60 less in thickness than a film which has been air heat treated. If an enhanced conductivity of the surface oxide were the dominant mechanism responsible for the $\sigma - \phi$ results, the slope of the curves for vacuum heat treated films would be reduced by at least a factor of 60 relative to the films heat treated in air. Experimentally, the slope was reduced by a factor of two, indicating that enhanced conductivity of the surface oxide is not the dominant mechanism responsible for the $\sigma - \phi$ results.

The conductance increase produced by irradiation of the present discontinuous films is thus attributed to radiation-produced defects within the inter-island oxide regions. In previous investigations⁹⁻¹³ of radiation damage in thin films (discussed in Chapter I), the films possessed a continuous structure and would not be expected to exhibit a conductance increase due to the mechanism proposed here.

4.3.2 Conductance Change as a Function of Beam Energy

Strictly speaking, the displacement cross-section for Ta_2O_5 should be calculated by weighting the individual cross-sections for tantalum and oxygen by the atomic fraction present in the target. However, since the relative contribution of oxygen defects and tantalum defects to the observed conductance increase is not known, the "correct" procedure will be approximated by assuming an average monatomic target $_{27}M^{62}$. Then the damage concentration produced in the linear portion of the $\sigma - \phi$ curve may be approximated by equation (4-6) with $f(\phi)$ equal to unity.

For proton energies in excess of 4 keV, the proton-tantalum collisions are calculated⁸ to be of the Rutherford type. Similarly, for proton energies in excess of 1 keV the proton-oxygen collisions are expected to be of the Rutherford type. If the proton energy exceeds these minimum values, the conductance increase σ (equation (4-6)) is given by⁸

$$\sigma = \delta' N_a (1 + P \sigma_c n v)^{-1} \phi \beta \frac{1}{E} \ln \frac{4M_1 M_2 E}{(M_1 + M_2)^2 E_d} \quad (4-7)$$

where M_1 and M_2 are the masses of the incident and target atoms, E_d is the displacement threshold energy, and E is the instantaneous proton energy in the film. In equation (4-6) the effective Rutherford damage cross-section σ_d is given by⁸

$$\beta \frac{1}{E} \ln \frac{4M_1 M_2 E}{(M_1 + M_2)^2 E_d}, \text{ where } \beta \text{ is a constant. Taking }^{66} E_d \text{ to be}$$

50 eV, the conductance increase at a fixed fluence should depend

linearly on $\frac{1}{E} \ln 130E$, where E is in units of 10^5 eV. As illustrated in Fig. 4-5, the $\sigma - \frac{1}{E} \ln 130E$ curve is linear for beam energies in the range 150 keV to 50 keV. Henceforth, this curve will be referred to as the $\sigma(E)$ curve. It should be noted that although the data of Fig. 4-5 are consistent with the Rutherford law, these data do not "prove" that the Rutherford law holds due to the small range of energy available in this experiment. Even though there is some uncertainty as to the numerical value of E_d , this uncertainty will have a relatively small effect on the results since the $\frac{1}{E}$ term is the dominant term in equation (4-7).

From equations (4-6) and (4-7) the ratio of the slope of the $\sigma - \phi$ curve to the slope of the $\sigma(E)$ curve is given by

$$\frac{\text{slope of } \sigma - \phi \text{ curve}}{\text{slope of } \sigma(E) \text{ curve}} = \frac{\ln 130 E}{E \phi} \quad (4-8)$$

For 150 keV proton irradiation, the slope of the $\sigma - \phi$ curve is $3\%/10^{16}$ p/cm². Thus, the calculated slope of the $\sigma(E)$ curve is 8.5×10^2 eV. The experimental value is 5.5×10^2 eV. The experimental slope being less than the calculated slope can be attributed to the fact that energy loss within the film has been neglected.

The $\sigma(E)$ results suggest that the $\sigma - \phi$ results are not caused by hydrogen ion implantation of the film or by protons back-scattered from the substrate. Since the mean projected range of the protons decreases⁶⁰, and the back-scattering coefficient increases⁶⁷, with decreasing proton energy, the $\sigma(E)$ curve would concave upward if either of these mechanisms controlled the conductance change produced by irradiation.

The nonlinearity in the $\sigma(E)$ curve at energies below 50 keV is attributed to the onset of screened coulomb collisions⁸ as the beam energy is degraded in passing through the film.

4.4 Summary

The effect of room temperature proton irradiation on Ta thin film resistors has been discussed for fluences up to 10^{16} p/cm². For films which had been previously heat treated, irradiation of the films caused a linear increase in conductance of the films. Several mechanisms were considered as being possible for producing the linear conductance increase: sputtering, hydrogen ion implantation, radiation-produced defect levels within the surface oxide layer, and an enhanced tunneling mechanism via radiation-produced defect levels within the inter-island crystalline oxide regions. All except the last mechanism were found to be incompatible with the observations. The rate of conductance change with fluence, considered as a function of total reactive partial pressure, was a maximum for a total reactive partial pressure of about 2×10^{-5} torr. The nonlinear conductance increase observed for non heat treated films may be accounted for by the fact that the radiation-produced defect concentration is a nonlinear function of fluence. The damage rate with fluence, as a function of proton energy, was also discussed. For beam energies in the range of 50 keV to 150 keV, the Rutherford damage law was followed.

LOW TEMPERATURE IRRADIATION AND ISOCHRONAL ANNEALING EXPERIMENTS

5.1 General

This chapter considers the effects of proton irradiation on the conductance of non heat treated, air heat treated, and vacuum heat treated films maintained at 30°K during bombardment. Low temperature σ - ϕ curves obtained for films sputtered in a reactive partial pressure of 2×10^{-5} torr nitrogen and 2×10^{-5} torr oxygen are compared with those curves presented in Chapter IV for identical films which were maintained at room temperature during irradiation to 10^{16} p/cm². In order to study radiation damage parameters of Ta₂O₅, σ - ϕ curves have been obtained for fluences up to 2×10^{18} p/cm² for air heat treated and non heat treated films sputtered in a reactive partial pressure of 1×10^{-5} torr nitrogen and 3×10^{-5} torr oxygen.

After irradiation to 10^{16} p/cm², isochronal annealing experiments were performed on films sputtered in a reactive partial pressure of 1×10^{-5} torr nitrogen and 3×10^{-5} torr oxygen. Electron microscopy shows these films to consist of islands of metallic Ta₄O largely surrounded by Ta₂O₅. Annealing experiments were also carried out on films which were sputtered in a reactive partial pressure of 1×10^{-6} torr nitrogen and 1×10^{-6} torr oxygen. These films consist of islands of Ta

largely surrounded by Ta_2O_5 . Films sputtered in a reactive partial pressure of 3×10^{-5} torr nitrogen and 1×10^{-6} torr oxygen were not investigated by means of electron microscopy, but, as discussed in Chapter III, the islands of this film are expected to consist of BCC Ta. This postulate was checked by comparing the annealing spectrum obtained from this film with the known annealing spectrum for BCC Ta. Annealing results for a continuous Ta_2O_5 film sputtered in a reactive partial pressure of 7×10^{-6} torr nitrogen and 4.3×10^{-5} torr oxygen are presented for comparison.

5.2 Experimental Results

5.2.1 Damage Results

Figure 5-1 illustrates σ - ϕ curves up to a fluence 10^{16} p/cm² for devices sputtered in a reactive partial pressure of 2×10^{-5} torr nitrogen and 2×10^{-5} torr oxygen. The σ - ϕ curves are linear over this fluence range for air heat treated, vacuum heat treated and non heat treated films. There is no significant difference in the results for air heat treated and vacuum heat treated films. The slope of the σ - ϕ curve for non heat treated films is about one-third that of the heat treated films. On cessation of irradiation, the films remained at 26°K for 1-1/2 hours. Any annealing which occurred during this period produced a conductance change of less than the experimental accuracy of 0.01%.

Figure 5-2 shows the σ - ϕ curve (marked X) extended to 5×10^{17} p/cm² for a non heat treated film which was sputtered

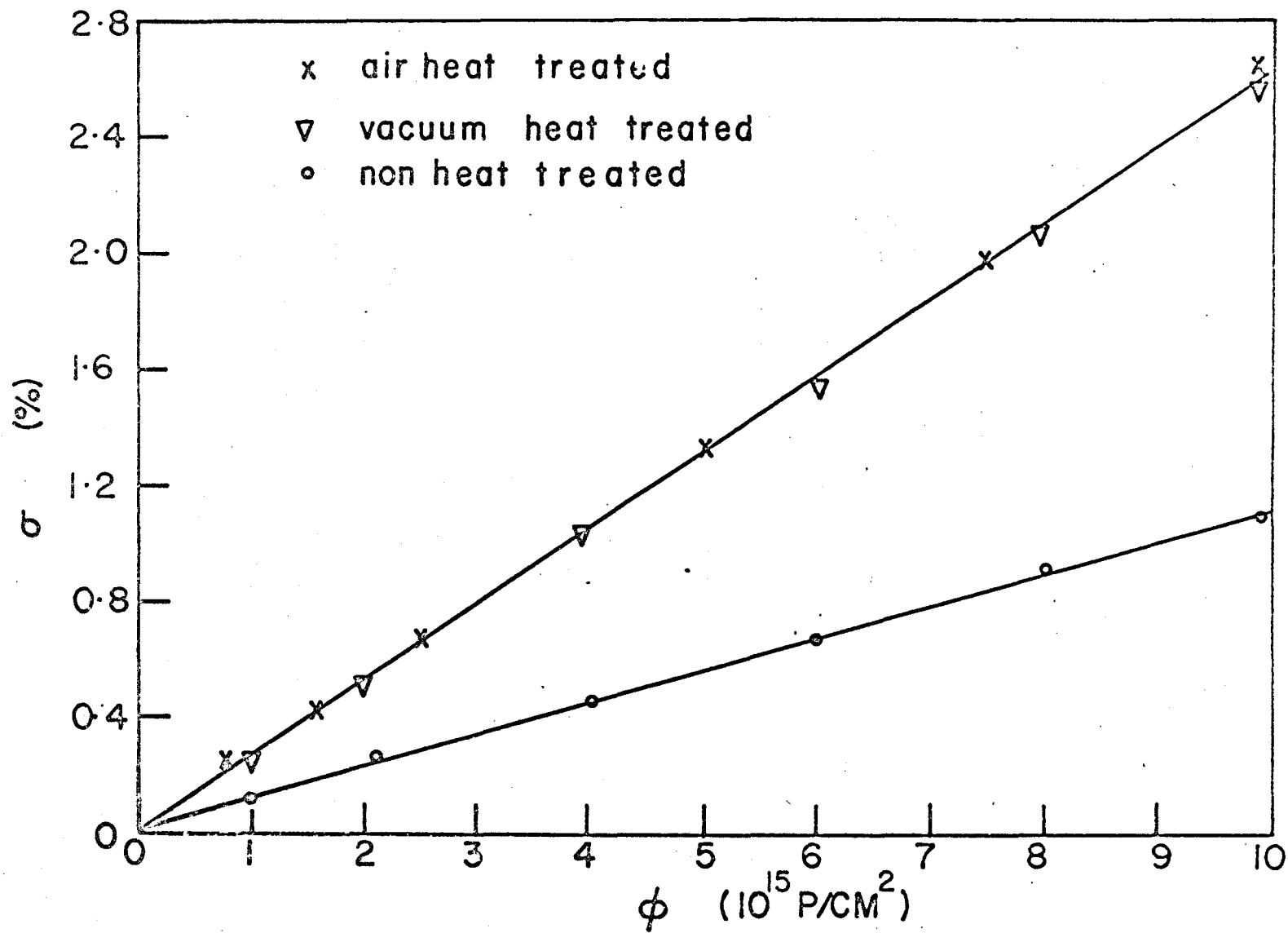


Figure 5-1

σ - ϕ curves for irradiation of non heat treated, vacuum heat treated, and air heat treated films to 10^{16} p/cm² at 30° K. These films were sputtered in a reactive partial pressure of 2×10^{-5} torr nitrogen and 2×10^{-5} torr oxygen.

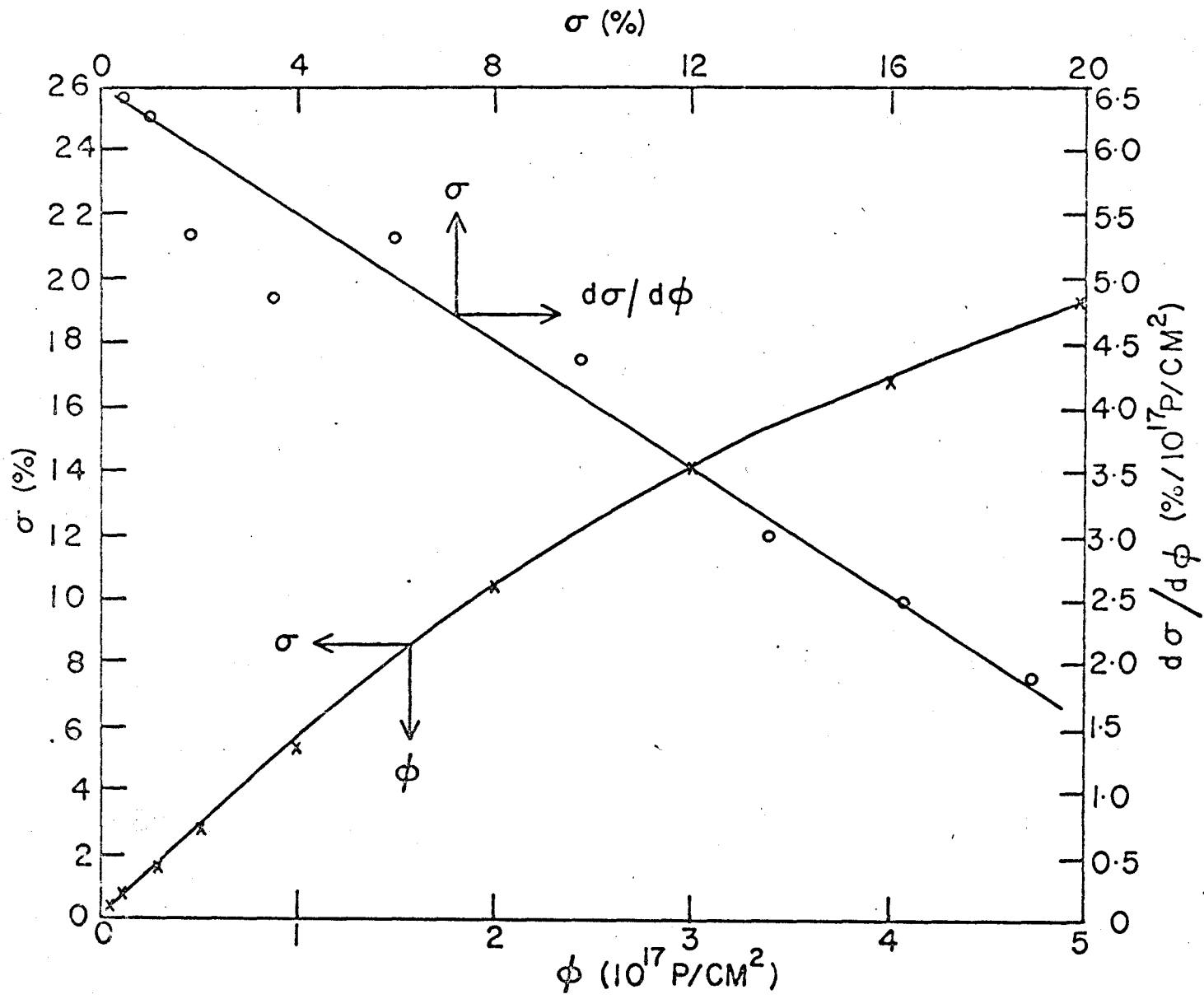


Figure 5-2

σ - ϕ curve (marked x), and rate of conductance increase $d\sigma/d\phi$ as a function of conductance increase σ (marked o), for 34°K irradiation of a non heat treated film sputtered in a reactive partial pressure of 1×10^{-5} torr nitrogen and 3×10^{-5} torr oxygen.

in a reactive partial pressure of 1×10^{-5} torr nitrogen and 3×10^{-5} torr oxygen. The film conductance increases continuously with fluence and appears to be approaching saturation. Figure 5-3 illustrates a similar curve (marked X) for an air heat treated film from the same substrate.

5.2.2 Annealing Results

In order to verify that the temperature cycling during annealing did not affect the electrical conductance of the films, an unirradiated film was cycled through the annealing process. This cycling process did not produce any measurable change in the film conductance, either at room temperature or at the base temperature.

Figure 5-4 illustrates an integral isochronal annealing curve for an air heat treated film sputtered in a total reactive partial pressure of 1×10^{-5} torr nitrogen and 3×10^{-5} torr oxygen after irradiation to 10^{16} p/cm². This curve was obtained using temperature increments of 5°K, each temperature level being maintained for ten minutes. All conductance measurements were made at 26°K. The corresponding differential annealing curve shown in Fig. 5-5 was obtained by plotting the slope of the integral curve between successive experimental points as a function of annealing temperature. The criterion used in drawing a curve through the points of the differential spectrum is that a recovery peak is considered to occur only if either 1) the difference in the rate of recovery between two successive experimental points forming a peak is much greater

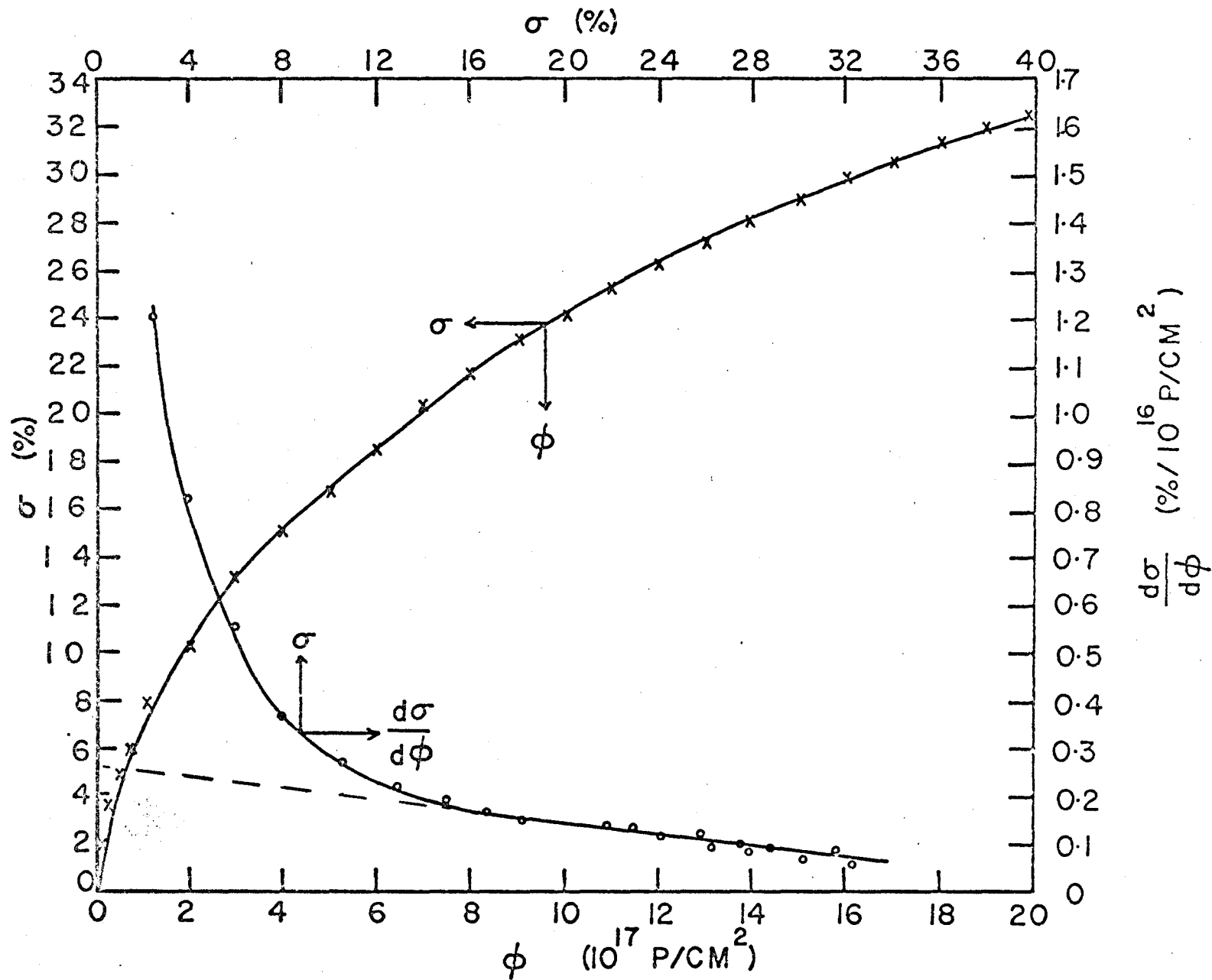


Figure 5-3 - σ - ϕ curve (marked x) for an air heat treated film irradiated at 34 K. The slope of the σ - ϕ curve ($d\sigma/d\phi$) is also shown as a function of σ (marked o). This film was sputtered in a reactive partial pressure of 1×10^{-5} torr nitrogen and 3×10^{-5} torr oxygen.

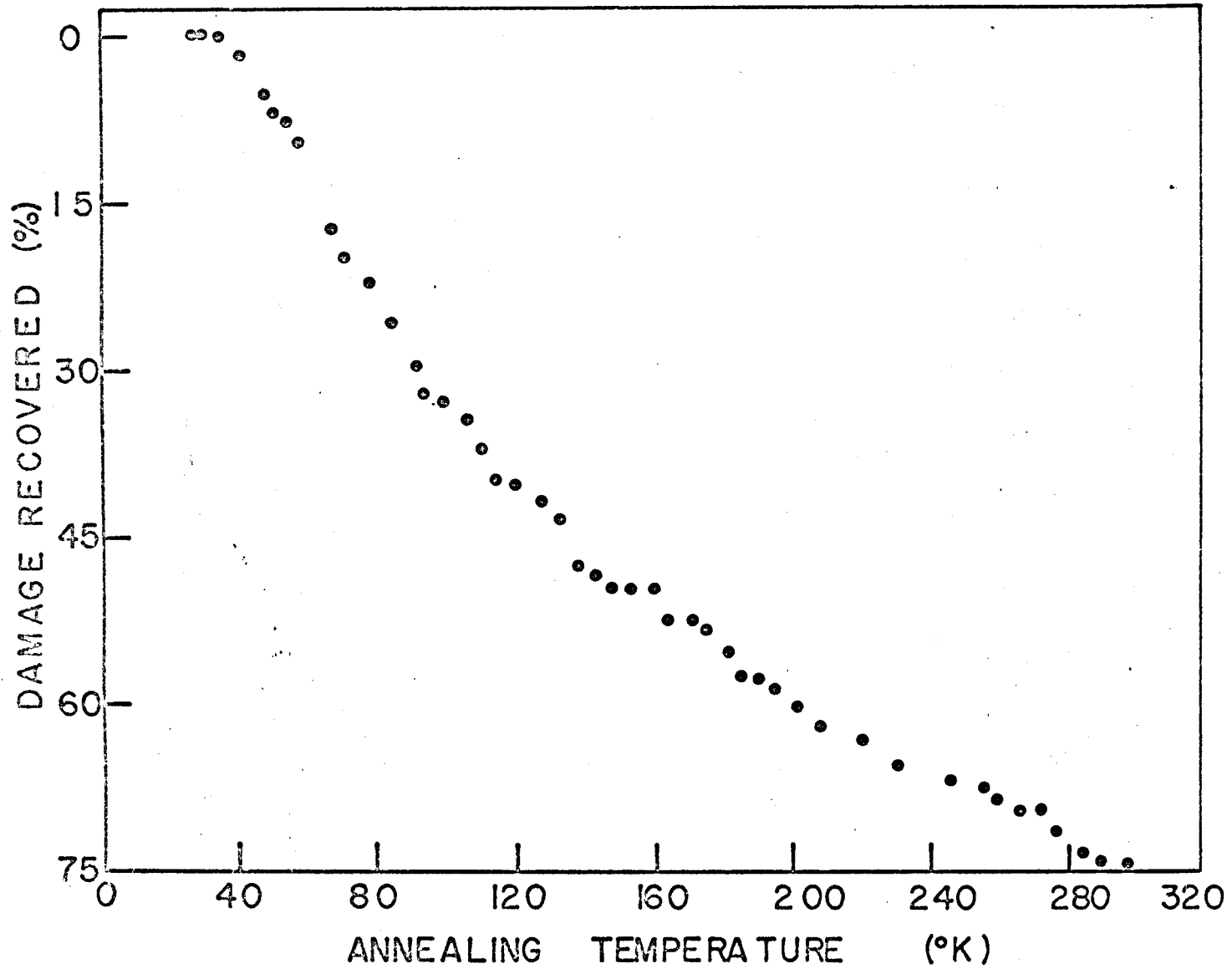


Figure 5-4

Integral isochronal annealing curve for an air heat treated film sputtered in a reactive partial pressure of 1×10^{-5} torr nitrogen and 3×10^{-5} torr oxygen.

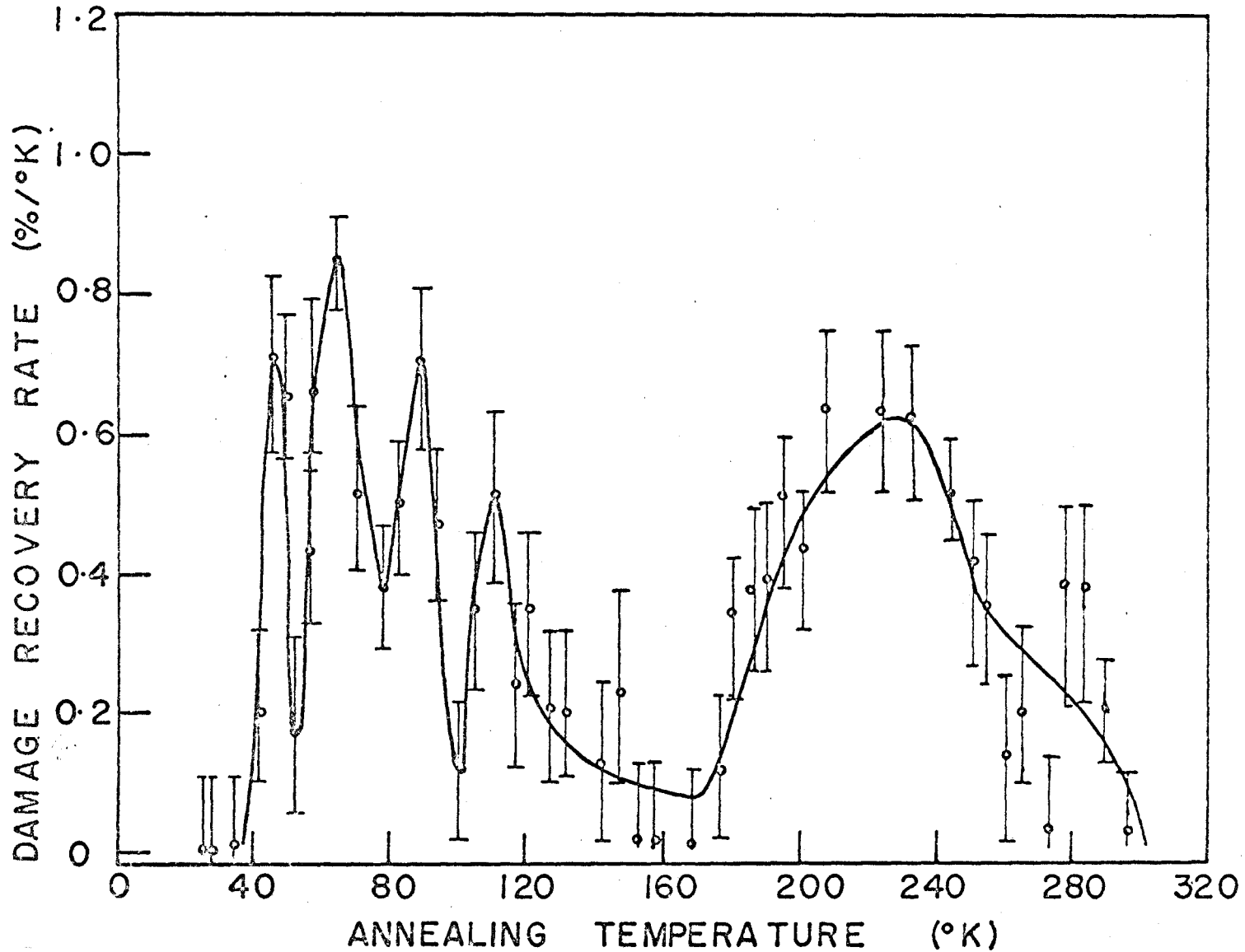


Figure 5-5

Differential isochronal annealing curve for an air heat treated film sputtered in a reactive partial pressure of 1×10^{-5} torr nitrogen and 3×10^{-5} torr oxygen.

than the experimental error, or 2) three or more points occur consecutively on the rising and falling edges of the peak. Figure 5-5 shows that the recovery of damage in an air heat treated film sputtered in a reactive partial pressure of 1×10^{-5} torr nitrogen and 3×10^{-5} torr oxygen occurs in two main stages extending from 34°K to 150°K and from 150°K to 300°K . These stages will be called Stage A and Stage B respectively. Stage A contains some substructure while Stage B consists primarily of a broad peak centered at about 230°K . The amount of damage which recovers in Stage A is approximately equal to that which recovers in Stage B. The annealing spectrum for vacuum heat treated films (not shown) from the same substrate is qualitatively similar to that obtained for air heat treated films, i.e., the spectrum is composed of Stage A which possesses some substructure and a broad, relatively structureless Stage B. The peak of Stage B occurs at 240°K .

Figure 5-6 shows a differential annealing curve for a non heat treated film from the same substrate after irradiation to 5×10^{17} p/cm². This annealing spectrum, which is qualitatively similar in shape to that obtained from non heat treated films after irradiation to 10^{16} p/cm², can be considered to consist of Stage A and Stage B. Neither stage possesses any substructure. Between these stages the differential annealing spectrum does not approach zero, indicating a possible overlap of stages.

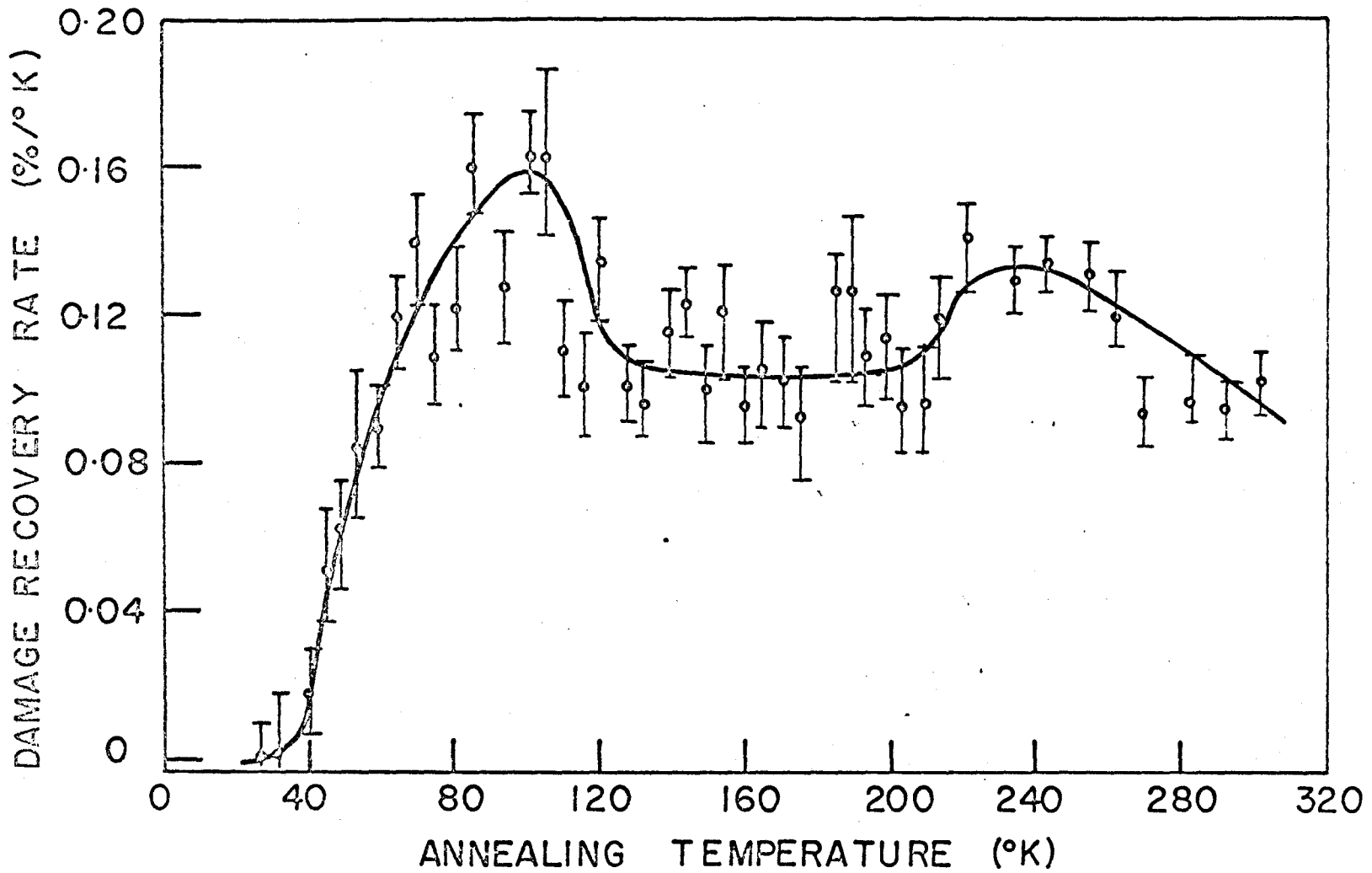


Figure 5-6

Differential isochronal annealing curve for a non heat treated film sputtered in a reactive partial pressure of 1×10^{-5} torr nitrogen and 3×10^{-5} torr oxygen.

Figure 5-7 illustrates the annealing results obtained for an air heat treated film sputtered in a reactive partial pressure of 1×10^{-6} torr nitrogen and 1×10^{-6} torr oxygen after irradiation to 10^{16} p/cm². Stage A recovery is clearly evident in the differential annealing spectrum. Although there is evidence of a small, narrow recovery peak centered at 200°K, Stage B recovery consists primarily of a large, broad peak centered at 280°K. Recovery in this broad peak is incomplete at 300°K. The amount of damage which recovers in Stage A is approximately equal to that which recovers in Stage B. The annealing spectrum suggests that negative annealing occurs at 170°K, i.e., annealing in this temperature region produces a conductance increase.

Figure 5-8 depicts a differential annealing curve for an air heat treated film sputtered in a reactive partial pressure of 7×10^{-6} torr nitrogen and 4.3×10^{-5} torr oxygen. In contrast to the films considered previously, the amount of annealing occurring during Stage A recovery greatly exceeds that occurring during Stage B recovery.

Figure 5-9 shows a differential annealing curve for an air heat treated film sputtered in a reactive partial pressure of 3×10^{-5} torr nitrogen and 1×10^{-6} torr oxygen. Stage A is well resolved, whereas the recovery corresponding to Stage B is incomplete at 300°K. A negative annealing peak is centered at 260°K.

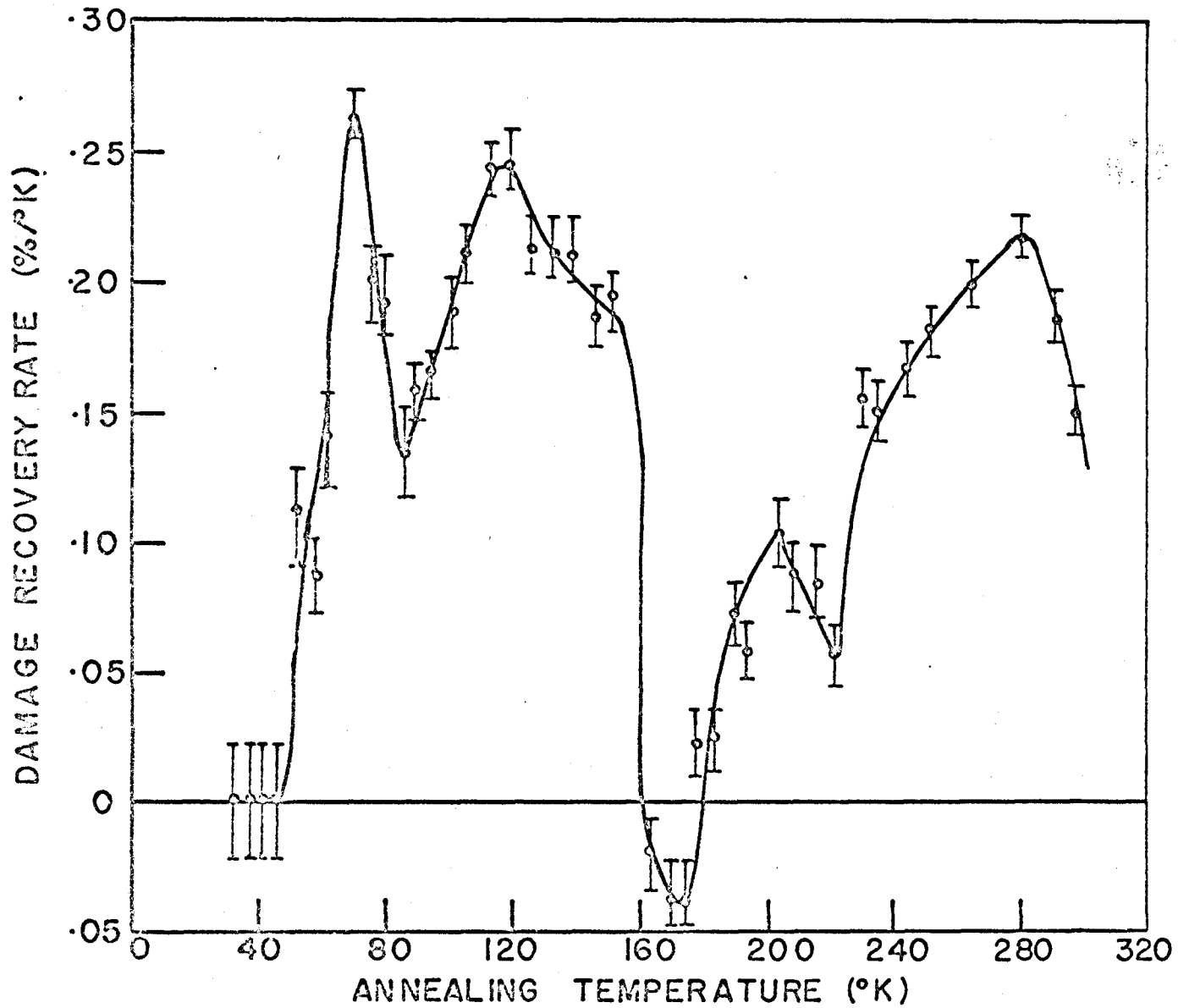


Figure 5-7

Differential isochronal annealing curve for an air heat treated film sputtered in a reactive partial pressure of 1×10^{-6} torr nitrogen and 1×10^{-6} torr oxygen.

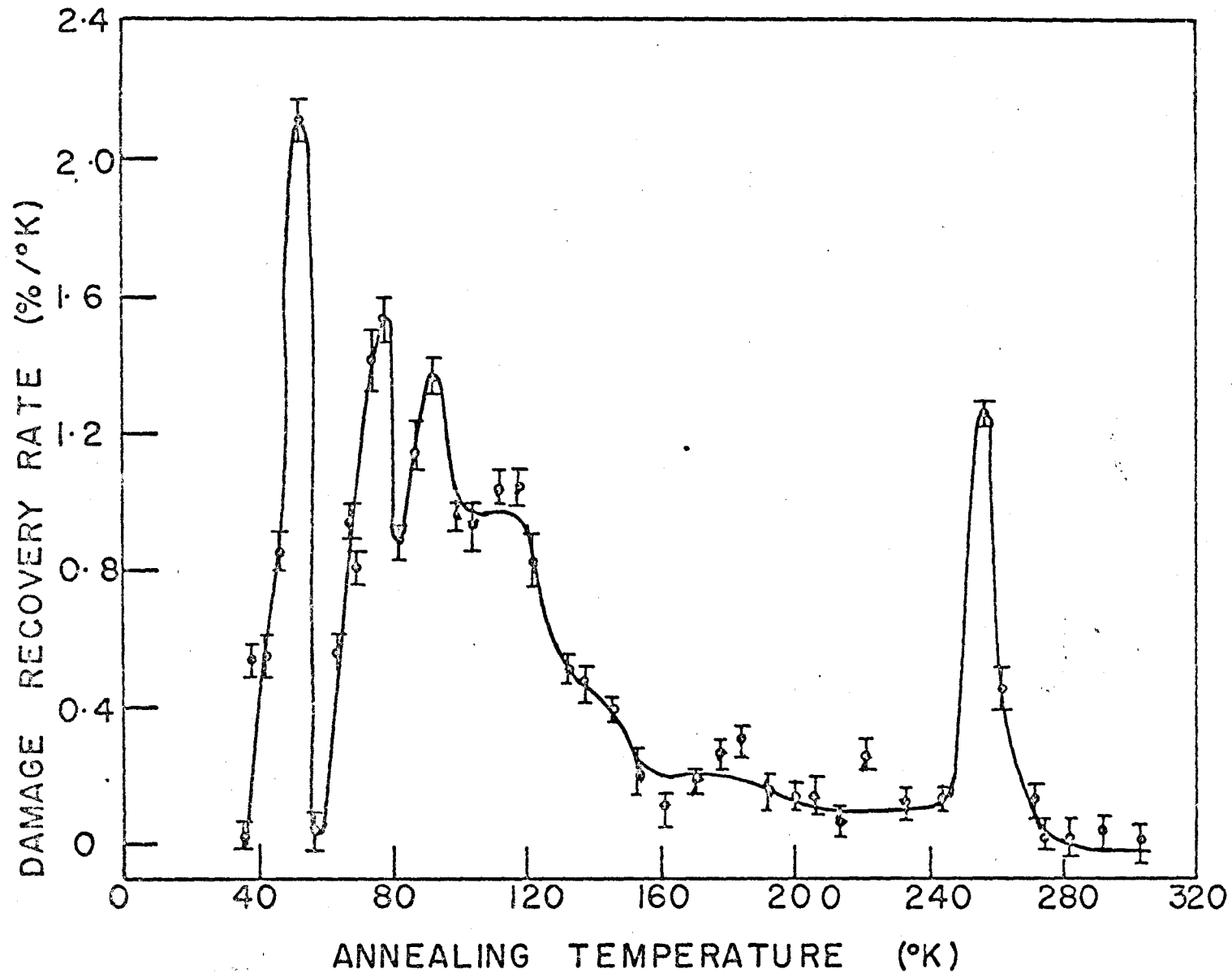


Figure 5-8

Differential isochronal annealing curve for a polycrystalline Ta_2O_5 film which was sputtered in a reactive partial pressure of 7×10^{-6} torr nitrogen and 4.3×10^{-5} torr oxygen.

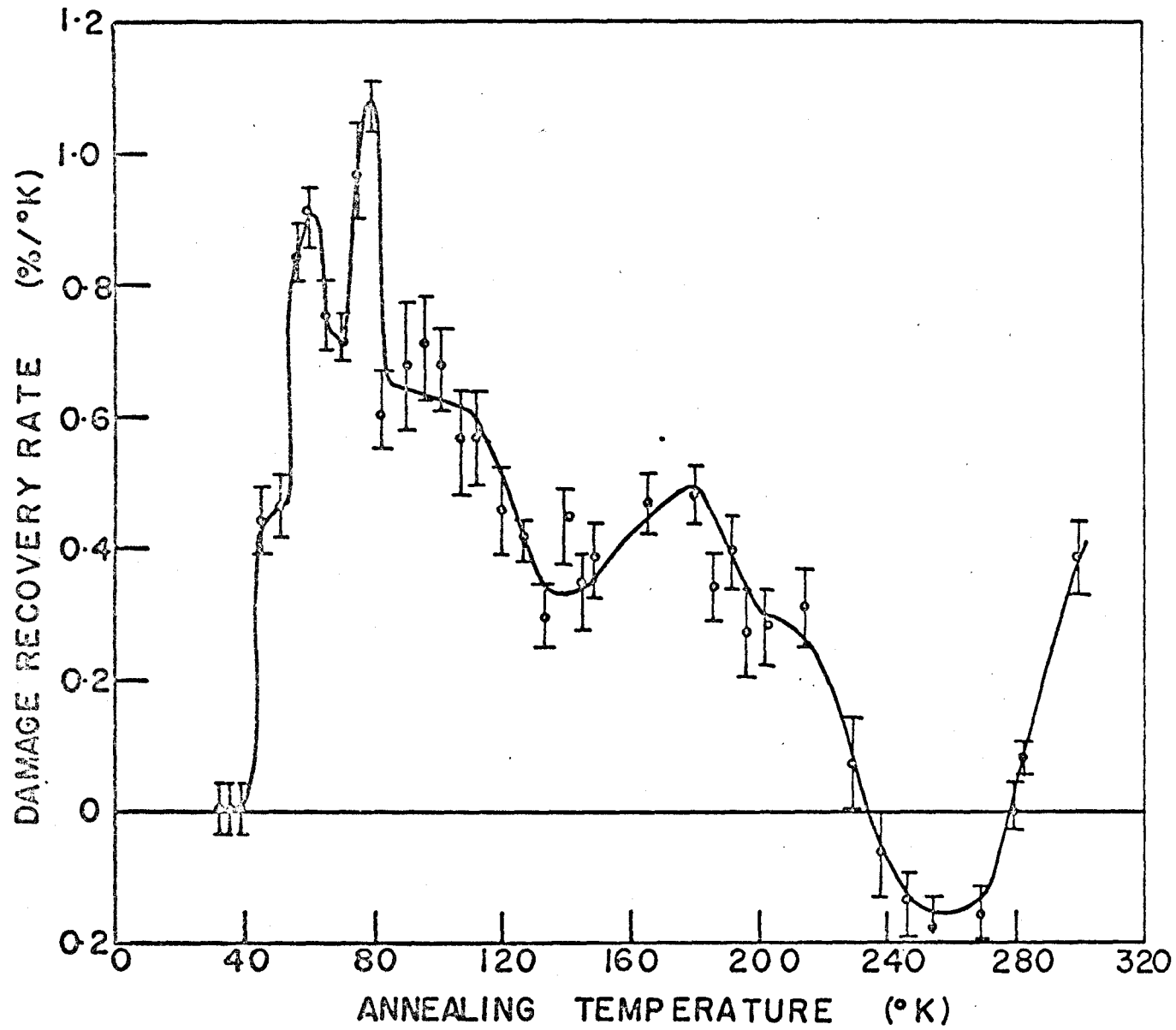


Figure 5-9

Differential isochronal annealing curve for an air heat treated film sputtered in a reactive partial pressure of 3×10^{-5} torr nitrogen and 1×10^{-6} torr oxygen.

5.3 Discussion

5.3.1 Damage Results

In Chapter IV the increase in conductance with fluence which occurs during room temperature irradiation of films for fluences up to 10^{16} p/cm² was attributed to an enhanced tunneling mechanism, the magnitude of which increases linearly with defect concentration. For air heat treated and vacuum heat treated films, the defect concentration is a linear function of fluence, resulting in linear σ - ϕ curves. The greater slope of the σ - ϕ curves for air heat treated films relative to vacuum heat treated films was attributed to a greater suppression of tunneling in the latter case as a result of a larger proportion of radiation-produced defects being filled thermally by carriers originating in ionized oxygen vacancy donors. At sufficiently low irradiation temperatures, these donors will not be ionized, suggesting that the slope of the σ - ϕ curves should be the same for air heat treated and vacuum heat treated films. The present low temperature experimental results show that this does occur, providing additional evidence for the proposed enhanced conduction model.

The nonlinearity which was discussed in Chapter IV for room temperature irradiations of 10^{16} p/cm² for non heat treated films was attributed to a nonlinear rate of defect production with fluence due to the trapping of mobile radiation-produced defects. The σ - ϕ curve for identical films is linear for irradiation to 10^{16} p/cm² at 30°K, indicating that radiation-

produced defects are not mobile at this temperature. The difference in slope of the σ - ϕ curves for heat treated and non heat treated films suggests that proton irradiation may introduce different defect levels in amorphous Ta_2O_5 and crystalline Ta_2O_5 .

For low temperature irradiation of films to fluences in excess of 10^{16} p/cm², the defect concentration may not be a linear function of fluence due to a combination of close-pair thermal annealing and spontaneous recombination⁸. If this is occurring, the σ - ϕ curve will be nonlinear and the rate of change of conductance with fluence will be given by (see Appendix B)

$$\frac{d\sigma}{d\phi} = \delta \nu \sigma_d \left(1 - \frac{m\sigma}{\delta}\right) \quad (5-1)$$

where σ_d is the primary displacement cross-section, ν is the number of displacements per primary knock-on, δ is the percent conductance increase per fractional defect concentration, and m is the number of unstable sites surrounding each defect. Figure 5-2 and Fig. 5-3 show the experimental results replotted with the slope of the σ - ϕ curve ($d\sigma/d\phi$) as a function of σ for non heat treated and air heat treated films respectively. A linear relation between $d\sigma/d\phi$ and σ indicates that spontaneous recombination and possibly close-pair thermal annealing do occur during irradiation.

The number of unstable sites surrounding each defect can be obtained from the measured value of 2.4×10^{-18} cm²

for $m\nu\sigma_d$, the slope of the $d\sigma/d\phi$ versus σ curve for non heat treated films. Assuming a random target, the effective Rutherford damage cross-section, $\nu\sigma_d$, is calculated⁸ to be $2 \times 10^{-19} \text{ cm}^2$. Thus, the value of m for amorphous Ta_2O_5 is calculated to be 12. For the crystalline oxide of air heat treated films, $\nu\sigma_d$ is expected to be equal to or less than⁸ the calculated value of $2 \times 10^{-19} \text{ cm}^2$. The experimental value of $7.3 \times 10^{-19} \text{ cm}^2$ for the slope of the linear portion of the $d\sigma/d\phi$ versus σ curve produces a value of m equal to or greater than 4 for crystalline Ta_2O_5 . These values of m for Ta_2O_5 are comparable with the value of 20 for SiO_2 ⁶⁸. The fact that the value of m is much less than the 300 to 500 usually obtained for metals⁸ suggests the possibility of electronic bond formation between defects and adjacent lattice atoms during the irradiation of nonmetals. The fact that the $d\sigma/d\phi$ versus σ curve is initially linear for non heat treated films consisting of amorphous Ta_2O_5 in the inter-island regions suggests that the nonlinearity which is initially observed for air heat treated films may be due to collision sequences (focused or not)⁶⁹ which are expected to occur over the very small ($\sim 50^\circ\text{A}$) distances involved in the crystalline Ta_2O_5 , provided this oxide has a sufficiently small defect concentration. As the fluence increases, the concentration of radiation-produced defects becomes sufficient to inhibit this additional mechanism. When this occurs, the $d\sigma/d\phi$ versus σ curve is expected to become linear.

5.3.2 Annealing Results

The fact that an annealing cycle did not produce any change in the conductance of unirradiated films indicates that any thermal stresses which may exist in the film due to the film-substrate interface³⁹ do not affect the defect structure of the films. Thus, conductance changes measured during the annealing of irradiated films are assumed to be due to radiation-produced defects and not due to mechanical effects within the films.

For air heat treated films sputtered in reactive partial pressures of 1×10^{-6} torr nitrogen and 1×10^{-6} torr oxygen, 1×10^{-5} torr nitrogen and 3×10^{-5} torr oxygen, and 7×10^{-6} torr nitrogen and 4.3×10^{-5} torr oxygen, the annealing spectra contain two main stages in the range of 34°K to 300°K . On the basis of Rutherford scattering, the number of primary tantalum defects is calculated⁸ to be 5.6 times the number of primary oxygen defects in the inter-island Ta_2O_5 . The two stages in the recovery spectra could result either by tantalum defects and oxygen defects recombining at their respective centers in different temperature ranges, or by tantalum defects recombining simultaneously with oxygen defects at one type of center in Stage A and at a different type of center in Stage B. The fact that, in films sputtered in reactive partial pressures of 7×10^{-6} torr nitrogen and 4.3×10^{-5} torr oxygen (continuous polycrystalline Ta_2O_5 films of grain size about $1,500 \text{ \AA}$) the percent damage annealed in Stage A greatly exceeds that of

Stage B, whereas for films sputtered in reactive partial pressures of 1×10^{-6} torr nitrogen and 1×10^{-6} torr oxygen as well as films sputtered in 1×10^{-5} torr nitrogen and 3×10^{-5} torr oxygen (films which possess an island structure of dimensions of the order of 100 \AA) approximately equal amounts of damage anneal in each stage, indicates that Stage A consists of close-pair or correlated annihilation of defects while Stage B is primarily due to long range uncorrelated migration of defects to sinks at the gap-island interface.

The order of the annealing process could not be determined accurately by isothermal annealing experiments due to the small conductance change occurring during annealing at any given temperature. However, assuming first order kinetics on the basis of close-pair recombination in Stage A, the activation energy is calculated to be 0.30 eV for a typical recovery peak centered at 110°K . The width of a single close-pair recovery peak at this temperature is calculated⁷⁰ to be 5°K . This value indicates that Stage A should be composed of a number of sub-stages. This is found to occur experimentally for heat treated films although, due to the large errors involved, it is difficult to state with certainty that sub-stages occur at the same temperatures for all the heat treated films studied. The lack of Stage A substructure for non heat treated films suggests that Stage A recovery for these films consists of a number of close-pair peaks which overlap, resulting in an apparent single broad peak. Such a process may be the result of the large

degree of disorder which exists in the amorphous oxide.

Assuming first order kinetics ⁷¹ for uncorrelated recombination of defects at the gap-island interface during Stage B annealing, the activation energy for the recovery peak situated at 230°K for films sputtered in a reactive partial pressure of 1×10^{-5} torr nitrogen and 3×10^{-5} torr oxygen is calculated ⁷² to be 0.73 eV for a pre-exponential frequency factor ⁷⁰ of 10^{15} sec^{-1} and for defect migration from the center of the gaps to the interface (20 Å). The width of a single recombination peak at this temperature is calculated ⁷⁰ to be 21°K. The observed peak will be due to a superposition of a number of such single peaks since the distance a defect must migrate for annihilation to occur at the interface depends on the initial location of the defect within the gap. For a lower limit of 3 Å (approximate inter-atomic distance) and an upper limit of 35 Å (gap size) for the migration distance, the corresponding temperature range for the location of these single peaks about 230°K is calculated to be 25°K. This suggests that a total peak width of about 46°K should be observed. Although this value is less than the observed width (about 70°K), these calculations illustrate that annihilation at the gap-island interface will produce a wide peak. The discrepancy between the calculated and observed widths may be due to:

- 1) an incorrect pre-exponential frequency factor;
- 2) the fact that the temperature of 230°K may not

correspond to 20 Å migration; and

- 3) the fact that the upper limit for the diffusion distance may exceed 35 Å since defects may not diffuse to the interface via the shortest possible path.

The proposed model will account for the observation that the main Stage B recovery peak occurs at a lower temperature for films sputtered in a reactive partial pressure of 1×10^{-5} torr nitrogen and 3×10^{-5} torr oxygen than for films sputtered in a reactive partial pressure of 1×10^{-6} torr nitrogen and 1×10^{-6} torr oxygen since the gap dimensions are smaller for the former films than for the latter. If the migration distances for defects produced at the center of the gaps and recombining at the interface are d_1 and d_2 for these films respectively then, for $d_1/d_2 \ll 1$, the peak annealing temperatures T_1 and T_2 are related by ⁷³

$$\ln (d_1/d_2)^2 = - \frac{E}{k} \left(\frac{1}{T_1} - \frac{1}{T_2} \right) \quad (5-2)$$

for a process having migration energy E . For the films being considered, electron microscopy shows that $d_1/d_2 \approx 0.1$. Then for $T_1 = 230^\circ\text{K}$ and $E = 0.73 \text{ eV}$, T_2 is calculated to be 279°K . This is in agreement with the observed peak temperature of 280°K for films reactively sputtered in 1×10^{-6} torr nitrogen and 1×10^{-6} torr oxygen.

The small, relatively narrow recovery peak which occurs at 200°K in Stage B for films sputtered in a reactive partial pressure of 1×10^{-6} torr nitrogen and 1×10^{-6} torr oxygen, as well as the recovery occurring between 150°K and 300°K for films sputtered in a reactive partial pressure of 7×10^{-6} torr nitrogen and 4.3×10^{-5} torr oxygen, may be due to a mechanism such as the release of radiation-produced defects from traps or to uncorrelated recombination of radiation-produced vacancies and interstitials. For films sputtered in 1×10^{-5} torr nitrogen and 3×10^{-5} torr oxygen, this secondary recovery peak may not be resolvable from the broad peak which is attributed to recombination at the gap-island interface.

For films sputtered in a reactive oxygen partial pressure of 1×10^{-6} torr, the annealing spectrum appears to contain negative recovery peaks at 170°K and 260°K. Burger et al ⁷⁴ have found that ten-minute isochronal annealing of bulk Ta irradiated to 7×10^{17} nvt has an annealing peak at 170°K. Doping the Ta with 0.1 atomic percent oxygen produced annealing peaks at 170°K and 250°K. Myhrra and DeFord ⁷⁵ have found that ten-minute isochronal anneals on bulk Ta irradiated with 2.2 MeV electrons produced an annealing peak at 167°K. Ten-minute isochronal annealing ⁷⁶ of both pure Ta and Ta doped with 0.1 atomic percent oxygen after irradiation with 3 MeV electrons has been found to produce recovery peaks at 170°K and 275°K. The correspondence of the negative annealing peak found in films reactively sputtered in 1×10^{-6} torr nitrogen and $1 \times$

10^{-6} torr oxygen (for which electron microscopy indicates the islands are composed of BCC Ta) with that peak found for bulk Ta strengthens the previously proposed (Chapter III) conduction model that tunneling through the oxide gaps acts in competition with metallic conduction via connected islands. The agreement of the 260°K negative recovery peak in films sputtered in a reactive partial pressure of 3×10^{-5} torr nitrogen and 1×10^{-6} torr oxygen with a corresponding recovery peak in bulk BCC Ta reinforces the argument presented in Chapter III that the crystal structure of the islands is largely determined by the amount of reactive oxygen in the sputtering system, rather than by the amount of reactive nitrogen. The apparent absence of a positive, broad Stage B recovery peak in this film may be due to the cancellation of this peak by the observed negative recovery peak. These negative peaks are not expected to be observed in films sputtered in a reactive partial pressure of 1×10^{-5} torr nitrogen and 3×10^{-5} torr oxygen since electron microscope examination shows that the metallic structure is not BCC Ta in these films.

5.4 Summary

Proton irradiation of reactively sputtered air heat treated and vacuum heat treated tantalum films at 30°K produces a linear increase in conductance with fluence, for fluences equal to or less than 10^{16} p/cm². The fact that the conductance increase is the same for both types of heat treated films suggests that the oxygen vacancy donors within the Ta₂O₅ inter-island

regions are not ionized at 30°K and, therefore, do not inhibit the enhanced tunneling mechanism by a thermal filling of radiation-produced defects by free carriers within the Ta₂O₅. Low temperature irradiation of non heat treated films consisting of amorphous Ta₂O₅ in the inter-island regions produces a linear increase in conductance with fluence, for fluences equal to or less than 10¹⁶ p/cm². Since radiation-produced defects are not expected to undergo any long range migration at 30°K, this observed linearity indicates that the nonlinear conductance increase with fluence which occurs for identical films during room temperature irradiation is due to a trapping of mobile radiation-produced defects during irradiation. For fluences greater than 10¹⁶ p/cm², the nonlinear conductance increase with fluence is attributed to a nonlinear increase in the defect concentration with fluence as a result of a combination of spontaneous recombination and close-pair thermal annealing. The number of unstable sites surrounding each defect was found to be equal to or greater than 4 for crystalline Ta₂O₅ and equal to 12 for amorphous Ta₂O₅.

Annealing of the damage proceeds in two stages: Stage A (34°K to 150°K) is attributed to close-pair or correlated recombination, and Stage B (150°K to about 300°K) is attributed to uncorrelated annihilation of defects at the gap-island interface. Negative annealing peaks at 160°K and 260°K indicate that metallic conduction occurs in the films consisting of islands of BCC Ta. The present experiments cannot directly demonstrate

metallic conduction in films consisting of islands of metallic
 Ta_4O .

VI

HIGH FLUENCE, ROOM TEMPERATURE RADIATION DAMAGE

6.1 General

This chapter considers σ - ϕ measurements obtained at room temperature for films irradiated to 2×10^{18} p/cm². The motivation for extending the results of Chapter IV to higher values of fluence is: 1) to investigate the effects of high fluence, room temperature proton irradiation on circuit properties of the thin film resistors; 2) to damage the films at a temperature where uncorrelated defect annihilation at gap-island interfaces is expected to occur during irradiation, thus attempting to verify the defect recovery model proposed in Chapter V; and 3) to investigate further the observation made in Chapter III, that the slope of the σ - ϕ curves decreases with decreasing total reactive partial pressure, for total reactive partial pressures less than 2×10^{-5} torr.

In order to attain these objectives, films possessing three distinct types of structure have been investigated:

- 1) films which were sputtered in a reactive partial pressure of 1.5×10^{-5} torr nitrogen and 1.5×10^{-5} torr oxygen and are composed of metallic Ta₄O islands largely surrounded by Ta₂O₅. These films were irradiated in order to investigate whether or

not the $\sigma - \phi$ curves obtained at room temperature are characteristic of those expected for the recombination of mobile defects at gap-island interfaces during irradiation;

- 2) polycrystalline Ta_2O_5 films sputtered in a reactive partial pressure of 7×10^{-6} torr nitrogen and 4.3×10^{-5} torr oxygen. Since these films do not possess any gap-island interfaces, the $\sigma - \phi$ curves resulting from high fluence irradiation of these films are not expected to be characteristic of curves which result from defect recombination at gap-island interfaces during irradiation; and
- 3) films sputtered in a reactive partial pressure of 3×10^{-6} torr nitrogen and 3×10^{-6} torr oxygen. These films were used to investigate the observed decrease in slope of the $\sigma - \phi$ curves with decreasing total reactive partial pressure, for total reactive partial pressures less than 2×10^{-5} torr.

6.2 Experimental Results

Figure 6-1 illustrates the conductance change σ at room temperature as a function of fluence for an air heat treated film sputtered in a reactive partial pressure at 3×10^{-6} torr nitrogen and 3×10^{-6} torr oxygen. The conductance initially increases with fluence for fluences up to 3×10^{16} p/cm². For greater values of fluence, the conductance decreases slightly

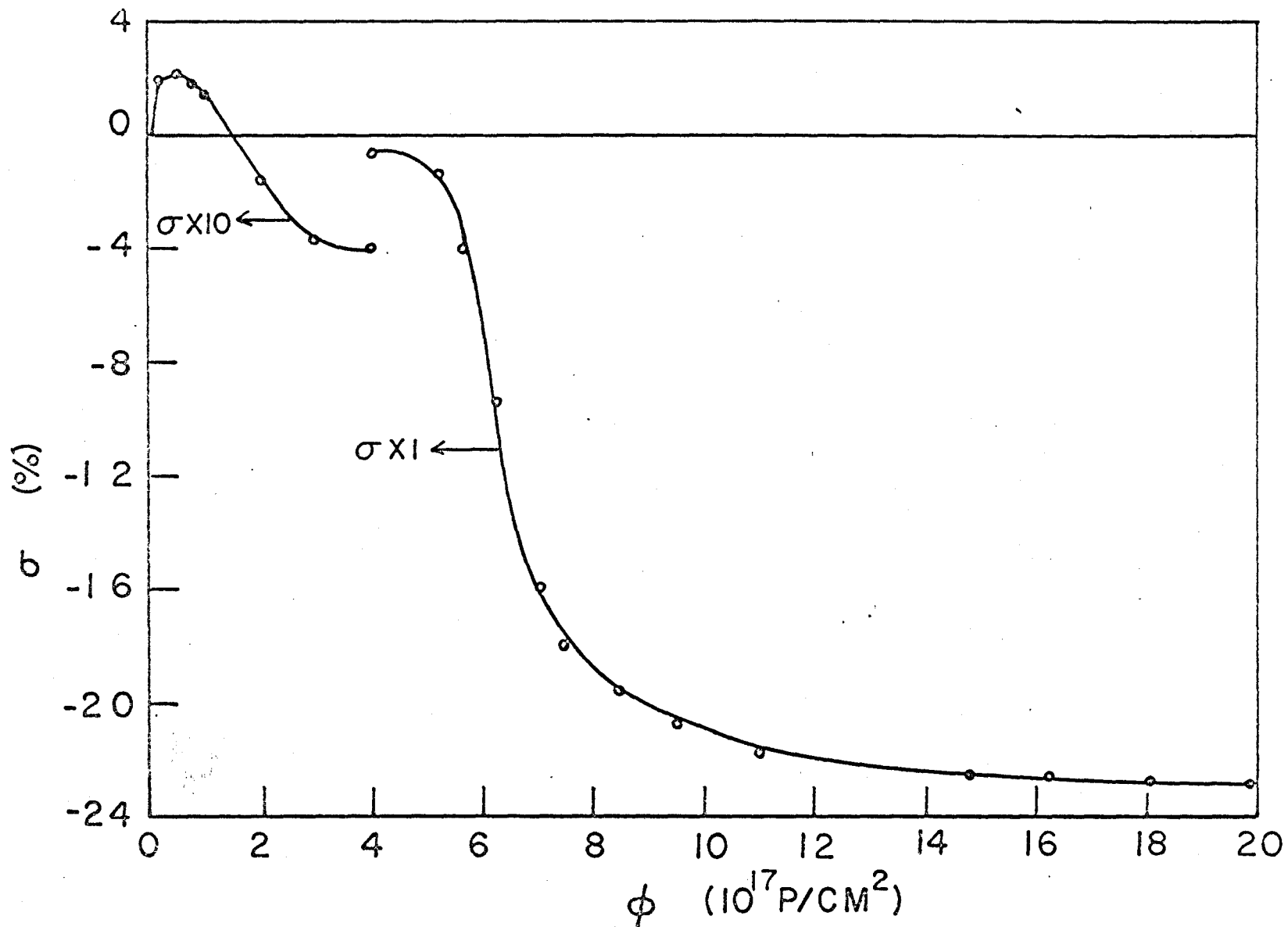


Figure 6-1

σ - ϕ curve for a 286°K irradiation of a film sputtered in a reactive partial pressure of 3×10^{-6} torr nitrogen and 3×10^{-6} torr oxygen. The experimental values of σ have been magnified by a factor of 10 for fluences equal to and less than 4×10^{17} p/cm².

with fluence until quasi-saturation occurs at 4×10^{17} p/cm². At 5.3×10^{17} p/cm² the conductance decreases drastically, approaching apparent saturation at 2×10^{18} p/cm². The small conductance increase at low fluences, followed by a small decrease in conductance preceding a large radiation-produced conductance decrease, is observed to occur for all films which were reactively sputtered in equal reactive partial pressures of oxygen and nitrogen, for total reactive partial pressures of less than 2×10^{-5} torr.

The σ - ϕ curve for an air heat treated film sputtered in a reactive partial pressure of 1.5×10^{-5} torr nitrogen and 1.5×10^{-5} torr oxygen is shown in Fig. 6-2. As discussed in Chapter IV, this curve is linear for fluences up to 10^{16} p/cm². For the range 10^{16} p/cm² to 7×10^{17} p/cm² the conductance increase is a nonlinear function of fluence. At 7×10^{17} p/cm², the conductance begins to decrease nonlinearly with increasing fluence, approaching apparent saturation at a conductance value less than the pre-irradiated value. This large conductance increase followed by a rapid decrease in conductance with fluence is characteristic of films sputtered in equal reactive partial pressures of oxygen and nitrogen, for total reactive partial pressures of 2×10^{-5} torr and greater. The σ - ϕ curve for films sputtered in a reactive partial pressure of 1×10^{-5} torr nitrogen and 3×10^{-5} torr oxygen also has this characteristic shape. Figure 6-2 also illustrates the σ - ϕ curve for a non heat treated resistor from the same substrate. The shape of this curve is qualitatively similar to that obtained for the air heat treated resistor. Figure 6-3

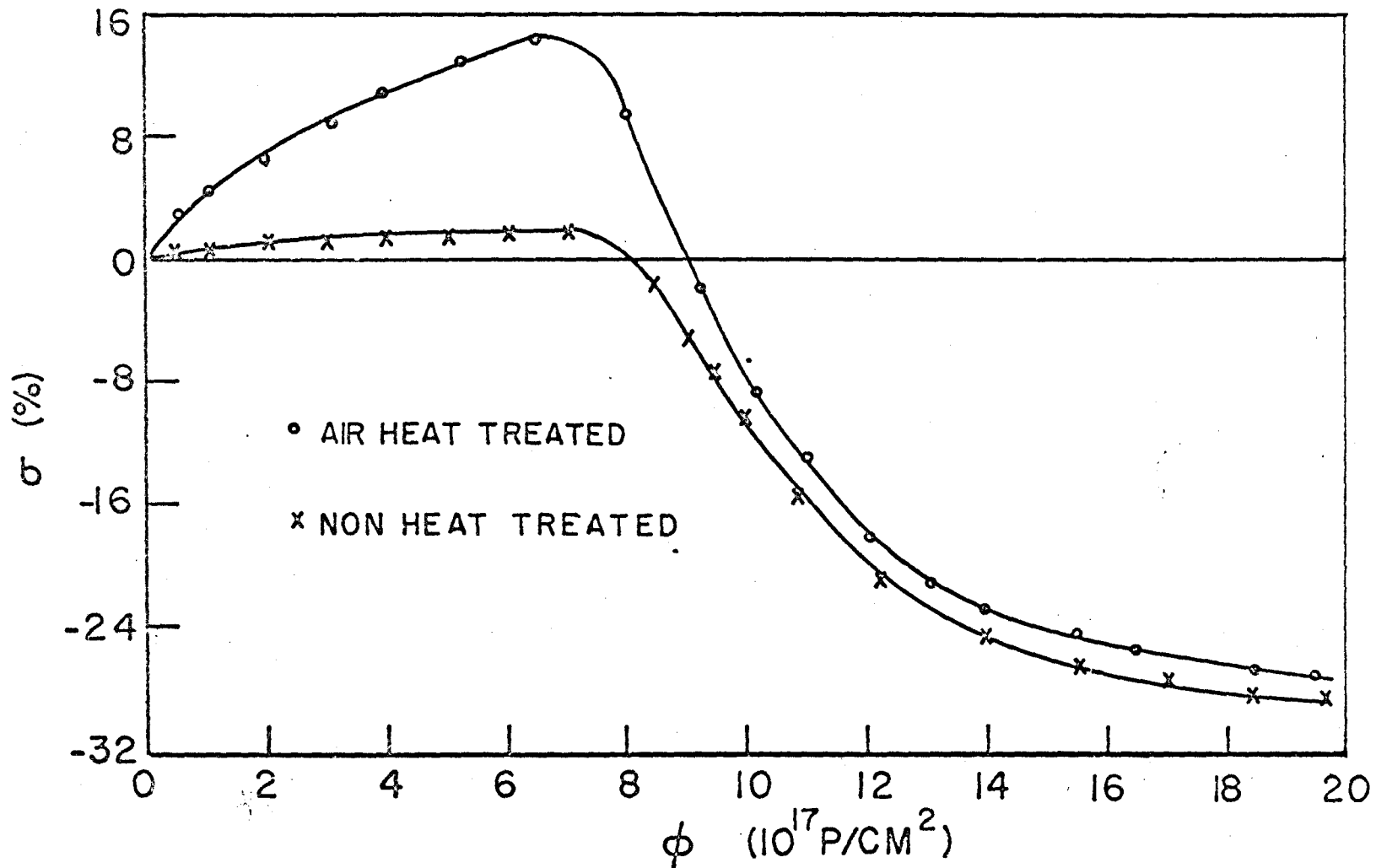


Figure 6-2

σ - ϕ curves for 286°K irradiation of air heat treated and non heat treated films sputtered in a reactive partial pressure of 1.5×10^{-5} torr nitrogen and 1.5×10^{-5} torr oxygen.

illustrates the magnitude of the total conductance decrease (the difference between the maximum enhanced conductance and the conductance decrease at apparent saturation) for air heat treated films as a function of total reactive partial pressure, for equal partial pressures of reactive oxygen and nitrogen. Figure 6-3 also shows the fluence at which this conductance decrease begins, as a function of total reactive partial pressure.

Figure 6-4 shows the σ - ϕ curve for an air heat treated film sputtered in a reactive partial pressure of 7×10^{-6} torr nitrogen and 4.3×10^{-5} torr oxygen. The conductance increases nonlinearly with fluence, approaching apparent saturation at 2×10^{18} p/cm². No radiation-produced conductance decrease is observed.

6.3 Discussion

6.3.1 Conductance Increase

6.3.1 a Films Sputtered in a Reactive Partial Pressure of 1.5×10^{-5} Torr Nitrogen and 1.5×10^{-5} Torr Oxygen

In Chapter V it was shown that, for discontinuous films, there is a broad annealing stage in the temperature range 150°K to 300°K. This recovery stage was attributed to the migration of radiation-produced defects to sinks at the gap-island interface. During the present experiments, performed at 286°K, radiation-produced defects may be free to diffuse to these sinks during irradiation. An order-of-magnitude estimate⁷⁷ of C_t , the effective sink concentration due to the interface, may be obtained from the ratio of the number of lattice sites at the

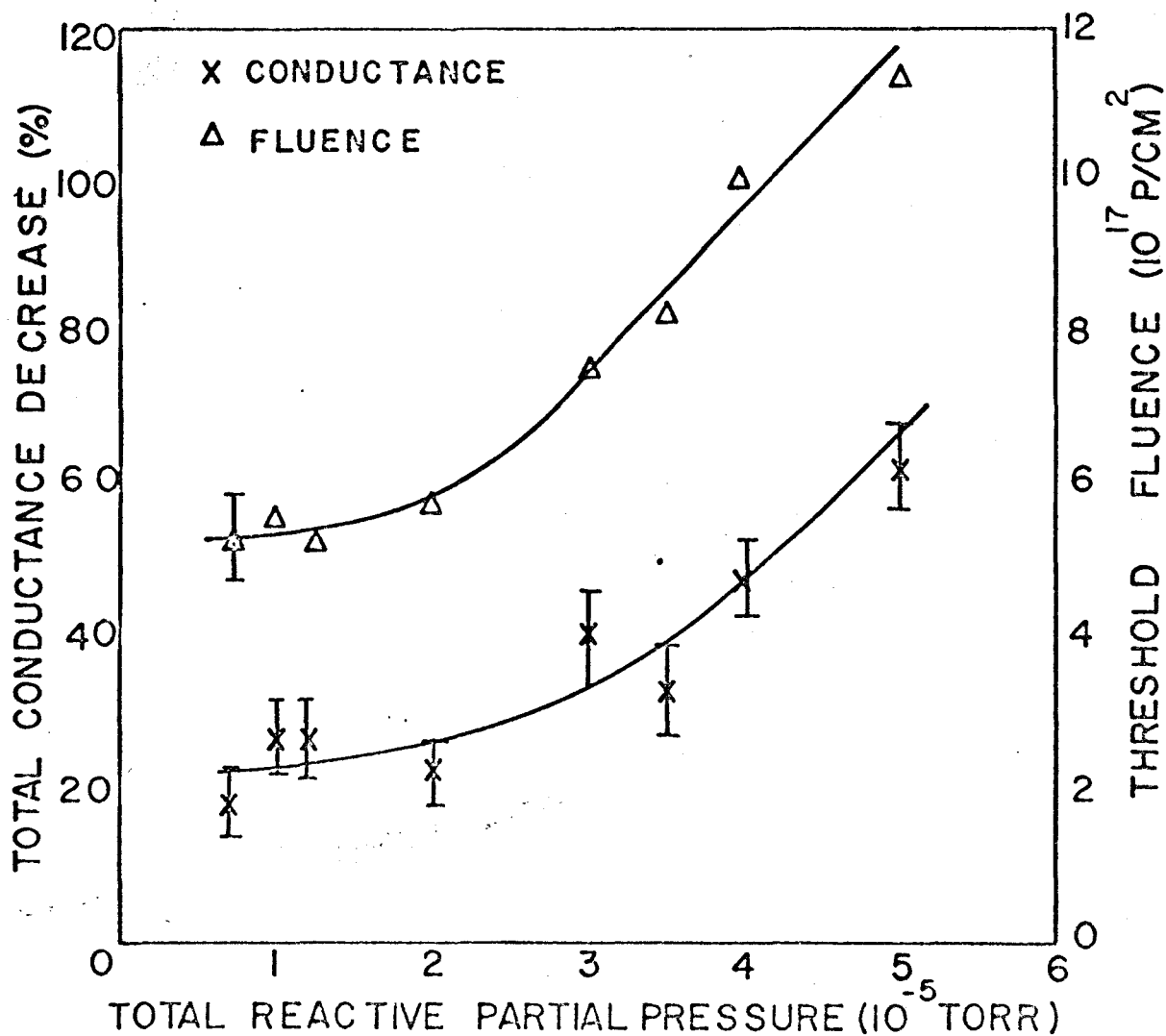


Figure 6-3

Curves illustrating the threshold fluence for the radiation-produced conductance decrease occurring at 286°K (marked x) and the magnitude of this decrease (marked Δ), as a function of total reactive partial pressure for equal partial pressures of reactive oxygen and nitrogen.

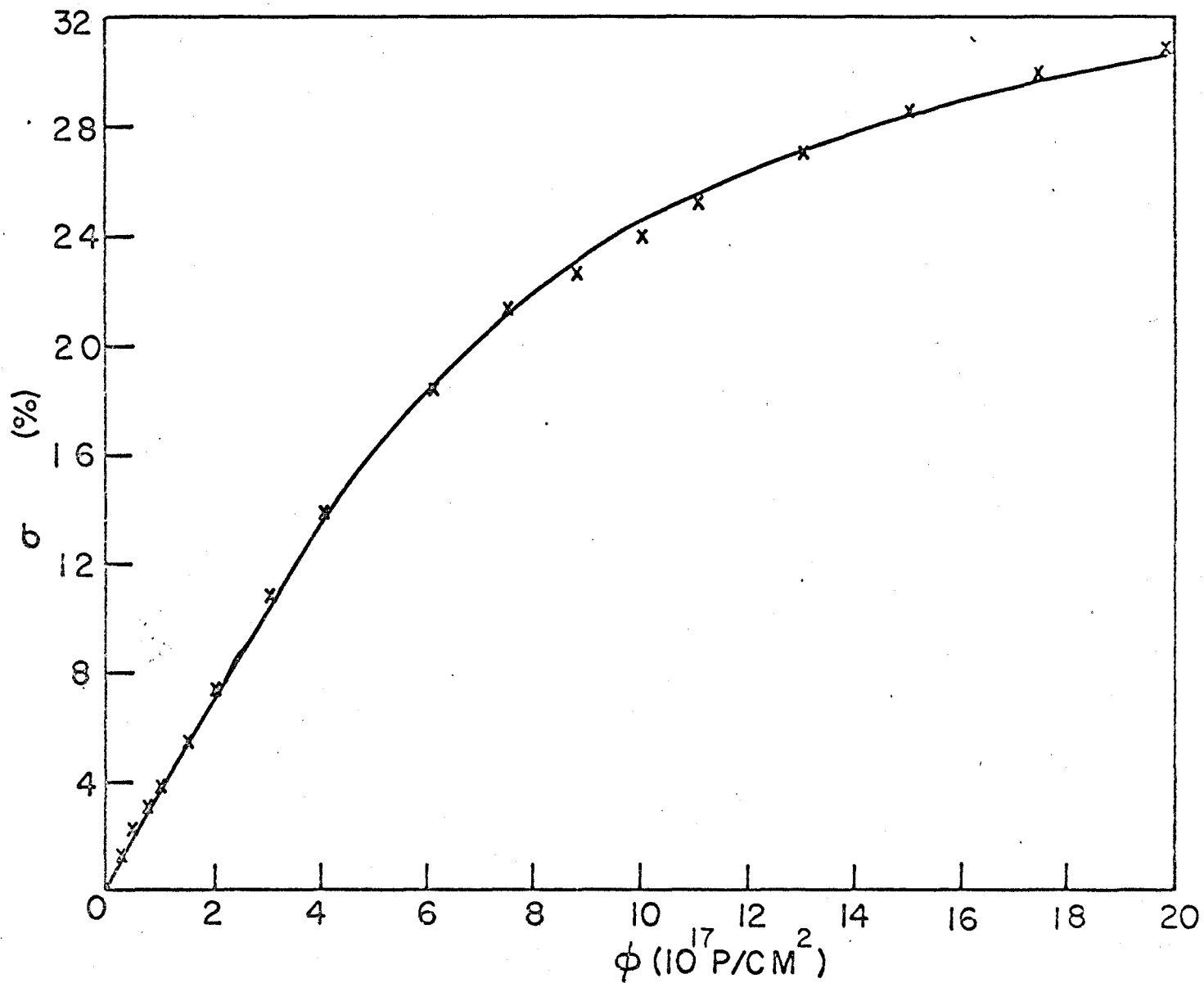


Figure 6-4

σ - ϕ curve for 286°K irradiation of a polycrystalline Ta₂O₅ film which was sputtered in a reactive partial pressure of 7×10^{-6} torr nitrogen and 4.3×10^{-5} torr oxygen.

interface to the number of lattice sites within the gap. For a cylindrical gap of radius r and length l ,

$$C_t \sim \frac{\frac{2r}{a_0} \frac{l}{a_0}}{r^2 l / a_0^3} = \frac{2a_0}{r} \quad (6-1)$$

where a_0 is the lattice constant. For 20 Å gaps, $C_t \sim 3 \times 10^{-1}$. Due to this large concentration of sinks, they are expected to behave as unsaturable traps. If defect migration to unsaturable traps occurs during irradiation, the defect concentration will be a nonlinear function of fluence. In this case, $d\phi/d\sigma$, the reciprocal slope of the σ - ϕ curve is given by ⁷⁸ (see Appendix B)

$$\frac{d\phi}{d\sigma} = \frac{1}{\delta \nu \sigma_d} \left(1 + \frac{\sigma}{\delta q_t C_t} \right) \quad (6-2)$$

where δ is the fractional conductance increase per fractional defect concentration as a result of enhanced tunneling, σ_d is the displacement cross-section, ν is the number of secondary knock-ons per primary knock-on, and q_t is the ratio of the capture cross-sections of unsaturable traps to vacancies (assuming interstitial migration). Figure 6-5 shows the σ - ϕ results for the non heat treated film of Fig. 6-2 replotted as $d\phi/d\sigma$ vs σ . As shown by equation (6-2), the resulting linear relationship demonstrates that the experimental results are consistent with defect migration to the interface during irradiation.

The intercept at $\sigma = 0$, given by $(\delta \nu \sigma_d)^{-1}$, is estimated to be 10^{-18} cm^2 . As discussed in Chapter V, $\nu \sigma_d$, the effective Rutherford damage cross-section is calculated to be $2 \times 10^{-19} \text{ cm}^2$.

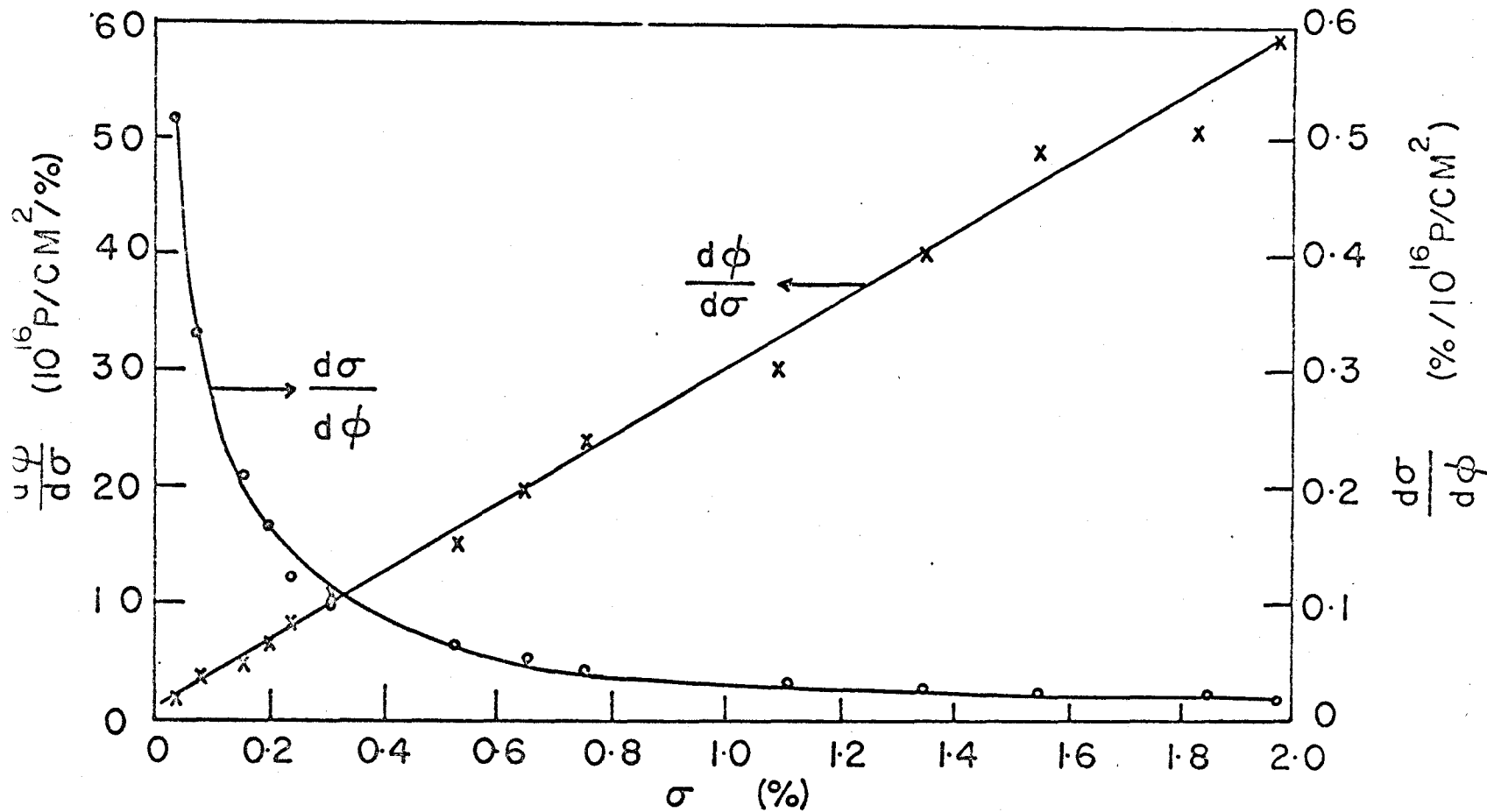


Figure 6-5

Graph showing the σ - ϕ curve for the non heat treated film of Fig. 6-2 (sputtered in a reactive partial pressure of 1.5×10^{-5} torr nitrogen and 1.5×10^{-5} torr oxygen) replotted as the slope of the σ - ϕ curve $d\sigma/d\phi$ (marked o), and the reciprocal slope of the σ - ϕ curve $d\phi/d\sigma$ (marked x), as a function of the conductance increase σ .

Thus, ξ is estimated to be 2.5 %/at-% defects. The slope of the $d\phi/d\sigma$ vs σ curve is given by $(\xi\nu\sigma_d)^{-1}(\xi q_t C_t)^{-1}$. Using a C_t value of 3×10^{-1} , q_t is calculated to be 0.046.

An alternate mechanism which might be responsible for the nonlinear increase in conductance with fluence is a combination of spontaneous recombination and close-pair thermal annealing. As was discussed in Chapter V, if this mechanism were responsible for the observed nonlinearity of the σ - ϕ curve, the slope of the σ - ϕ curve, $d\sigma/d\phi$, would be a linear function of σ . The curve $d\sigma/d\phi$ vs σ is shown in Fig. 6-5. The nonlinearity of this curve indicates that spontaneous recombination and close-pair annealing is not the dominant mechanism responsible for the nonlinearity of the conductance increase with fluence.

Figure 6-6 illustrates the reciprocal slope of the σ - ϕ curve ($d\phi/d\sigma$) as a function of σ for an air heat treated film which was sputtered in a reactive partial pressure of 1.5×10^{-5} torr nitrogen and 1.5×10^{-5} torr oxygen. The $d\phi/d\sigma$ vs σ curve is initially nonlinear, but it becomes linear for $\sigma > 3\%$. The linear portion of the $d\phi/d\sigma$ vs σ curve suggests that the nonlinearity of the σ - ϕ curve may be due to defect migration to unsaturable traps. Replotting the σ - ϕ curve as $d\sigma/d\phi$ vs σ produces a nonlinear curve over the complete range of experimental points (Fig. 6-6), illustrating that the nonlinearity of the conductance increase with fluence in air heat treated island-structure films is not due to spontaneous recombination

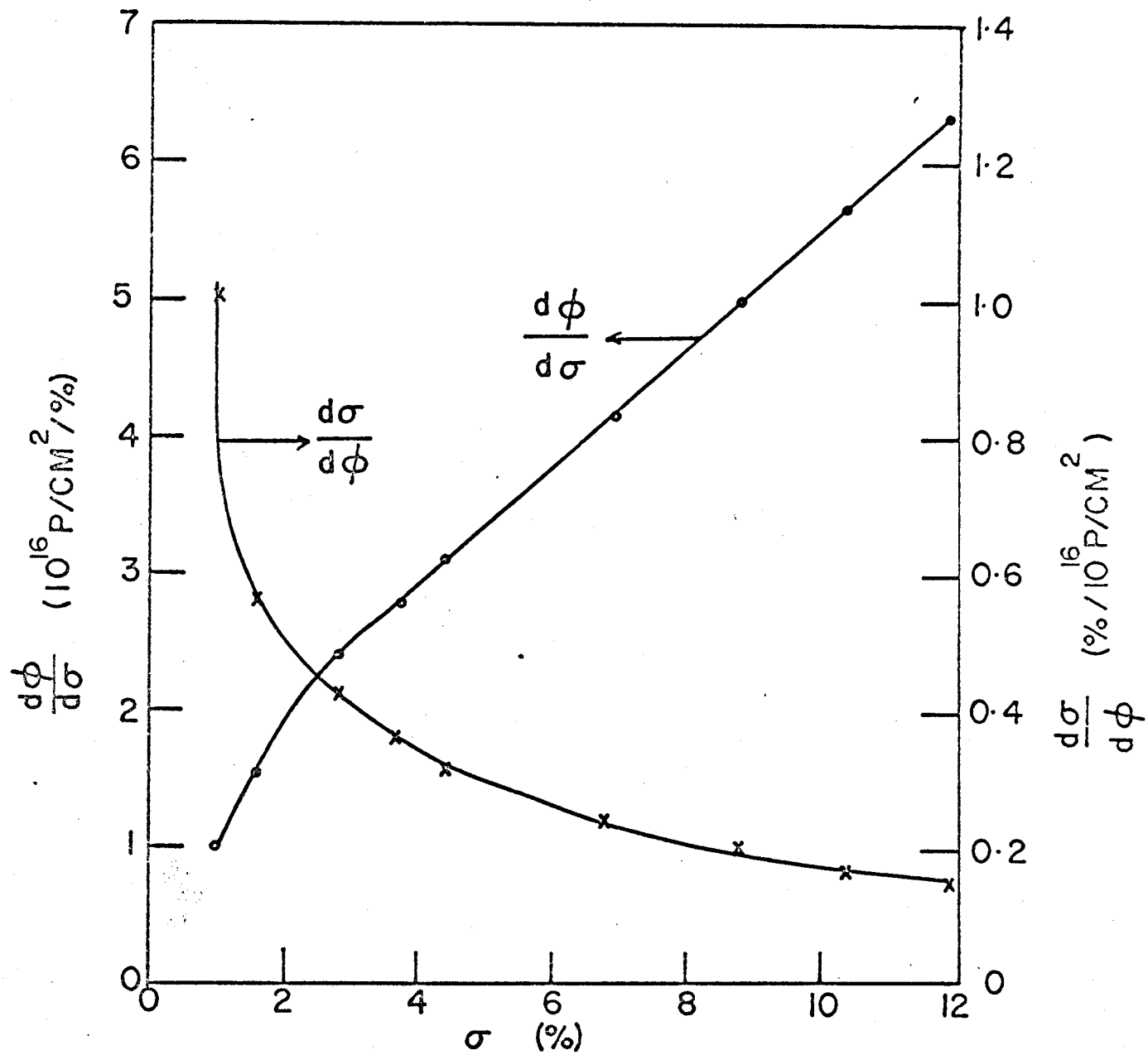


Figure 6-6

Graph showing the $\sigma - \phi$ curve for the air heat treated film of Fig. 6-2 (sputtered in a reactive partial pressure of 1.5×10^{-5} torr nitrogen and 1.5×10^{-5} torr oxygen) replotted as the slope of the $\sigma - \phi$ curve $d\sigma/d\phi$ (marked x), and the reciprocal slope of the $\sigma - \phi$ curve $d\phi/d\sigma$ (marked o), as a function of the conductance increase σ .

or close-pair thermal annealing. For values of σ less than 3% the nonlinearity of the $d\phi/d\sigma$ vs σ curve suggests that a mechanism in addition to defect diffusion to the gap-island interface may be occurring at low values of fluence in air heat treated films. As discussed in section 5.3.1 in connection with low temperature irradiation experiments, this additional mechanism may involve the propagation of collision sequences⁶⁹ in crystalline Ta_2O_5 .

6.3.1 b Films Sputtered in a Reactive Partial Pressure of 7×10^{-6} Torr Nitrogen and 4.3×10^{-5} Torr Oxygen

Figure 6-7 shows the σ - ϕ curve for a film sputtered in a reactive partial pressure of 7×10^{-6} torr nitrogen and 4.3×10^{-5} torr oxygen replotted as the reciprocal slope of the σ - ϕ curve ($d\phi/d\sigma$) as a function of σ . The nonlinearity of the $d\phi/d\sigma$ vs σ curve indicates that migration of defects to unsaturable traps during irradiation is not the dominant mechanism responsible for the nonlinearity of the conductance increase with fluence (the σ - ϕ curve). Since this film consists of 1,500 Å grains of Ta_2O_5 , rather than small (50-100 Å) regions of Ta_2O_5 , the lack of recombination at unsaturable traps in this film is consistent with the proposed model, i.e., in island-structure films, recombination of defects occurs at unsaturable centers at the gap-island interface during irradiation.

The absence of gap-island interfaces in this film suggests that the mechanism responsible for the nonlinearity

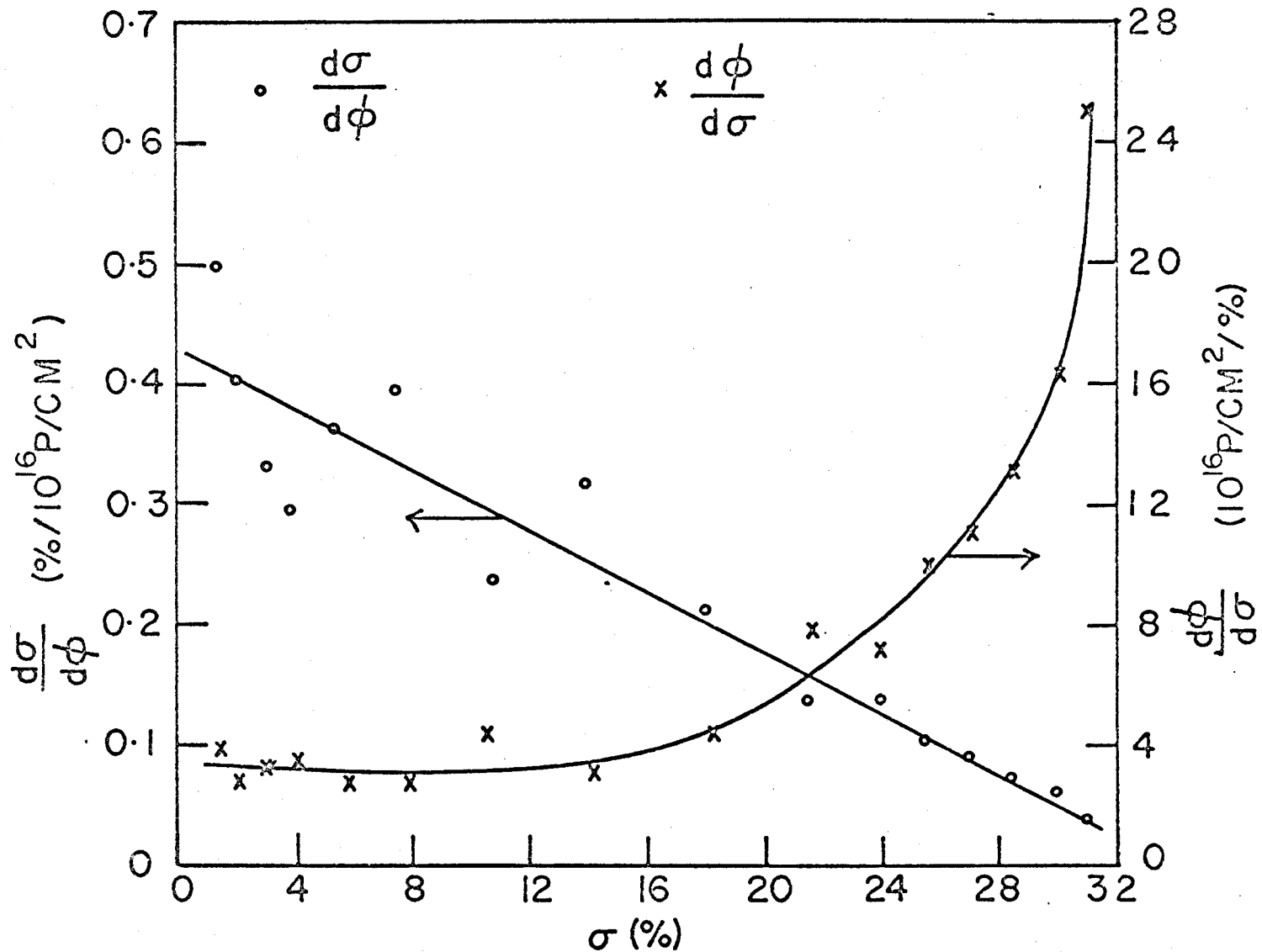


Figure 6-7

Graph showing the σ - ϕ curve for the air heat treated film of Fig. 6-3 (sputtered in a reactive partial pressure of 7×10^{-6} torr nitrogen and 4.3×10^{-5} torr oxygen) replotted as the slope of the σ - ϕ curve $d\sigma/d\phi$ (marked o), and the reciprocal slope of the σ - ϕ curve $d\phi/d\sigma$ (marked x), as a function of the conductance increase σ .

of the $\sigma - \phi$ curve may be a combination of spontaneous recombination and close-pair thermal annealing, since saturation of damage is expected to occur ultimately by this mechanism. The linearity of the $d\sigma/d\phi$ vs σ curve shown in Fig. 6-7 indicates that these mechanisms do occur. The slope of the $d\sigma/d\phi$ vs σ curve is $1.3 \times 10^{-18} \text{ cm}^2$, giving a value of m equal to 7 for Ta_2O_5 irradiated at room temperature. This value of m is greater than the value of 4 found for low temperature irradiations. This indicates that the size of the unstable zone is greater at room temperature than at low temperatures, possibly due to a greater amount of close-pair thermal recombination which is expected to occur at the higher temperature than at the lower temperature.

6.3.1 c Films Sputtered in a Reactive Partial Pressure of 3×10^{-6} Torr Nitrogen and 3×10^{-6} Torr Oxygen

This section will consider the conductance changes which occur for fluences less than $5.3 \times 10^{17} \text{ p/cm}^2$. The large conductance decrease occurring for fluences greater than $5.3 \times 10^{17} \text{ p/cm}^2$ will be considered in section 6.3.2.

As discussed in Chapter V, the radiation-produced change in the conductance of the films consists of two components: an increase in conductance due to enhanced tunneling and a concurrent decrease in conductance due to damage in the connected metallic islands. Thus, it is proposed that the observed initial increase in the $\sigma - \phi$ curve for films sputtered in a reactive partial pressure of 3×10^{-6} torr nitrogen and 3×10^{-6}

torr oxygen (Fig. 6-1) is due to the difference between the conductance increase due to enhanced tunneling and the conductance decrease due to metallic damage. At 3×10^{16} p/cm² the conductance increase due to the tunneling mechanism becomes smaller than the conductance decrease due to metallic damage, producing the observed decrease in the σ - ϕ curve up to 5.3×10^{17} p/cm².

This model is consistent with the data presented previously in Chapter IV where it was shown that the conductance increase at 10^{16} p/cm² decreases with decreasing total reactive partial pressures, for total reactive partial pressures of 1×10^{-5} torr or less. For these values of total reactive partial pressure, the islands are composed of BCC Ta, in contrast to larger values of total reactive partial pressures where the islands consist largely of Ta₄O. Using a value of resistivity increase of $5 \mu\Omega\text{-cm}$ per atomic-% defect concentration⁴² and assuming a value of $m = 500$ for BCC Ta⁸, the conductivity decrease at 10^{16} p/cm² due to damage within metallic regions of the film is calculated to be $8 \times 10^{-5} (\mu\Omega\text{-cm})^{-1}$, or 3% of the film conductivity. This is in order-of-magnitude agreement with the observed conductivity increase due to the enhanced tunneling mechanism, and may serve to reduce the net observed conductivity increase at 10^{16} p/cm².

Assuming dR , the increase in resistivity per unit defect concentration, to be approximately independent of the oxygen dopant concentration for BCC Ta, the radiation-produced

conductance decrease ($-\delta\sigma = dR/R^2$) per unit defect concentration increases as the dopant concentration within the islands, and thus R , the resistivity of the islands, decreases. This may account for the observation that the slope of the σ - ϕ curves for films consisting of BCC Ta islands decreases as total reactive partial pressure decreases, and thus the island dopant concentration decreases. The absence of any apparent effect of metallic damage on the σ - ϕ curves during irradiation to 2×10^{18} p/cm² for films sputtered in a total reactive partial pressure greater than 2×10^{-5} torr may be due to the large value of R possessed by the non BCC Ta islands of these films, i.e., metallic damage is expected to occur in these films, but the magnitude of the resulting conductance change is insufficient to significantly affect the conductance change which is attributed to the enhanced tunneling mechanism.

6.3.2 Conductance Decrease

For both heat treated and non heat treated films consisting of an island structure, the conductance abruptly decreases with fluence when a given threshold fluence is reached. As will be discussed in the following paragraphs, the suddenness of the onset of the conductance decrease for irradiation at room temperature, as well as the lack of a radiation-produced conductance decrease for irradiation at 30°K, suggests that this decrease may be due to a radiation-induced shift in the Fermi level of the inter-island Ta₂O₅, thereby increasing the height of the tunneling barrier and reducing the tunneling probability.

Before discussing the room temperature radiation-produced conductance decrease, it may be instructive to consider the significance of the fact that a similar conductance decrease is not observed for irradiation at 30°K. As discussed in Chapter V, only close-pair annihilation of defects occurs during these low temperature irradiations, and since one member of the stable vacancy-interstitial pairs will act as a donor while the other member acts as an acceptor⁷⁹, the concentration of radiation-produced donors will equal the concentration of radiation-produced acceptors. If these donor levels are higher in energy than the original Fermi level (which is determined by the non-stoichiometric oxygen vacancy concentration) and the acceptor levels lower in energy than the original Fermi level, the Fermi level will be independent of fluence. Thus, the radiation-produced conductance change is proportional to the concentration of radiation-produced defects via which enhanced tunneling can occur.

During room temperature irradiation, defects are mobile and probably annihilate at the gap-island interface. Since vacancies and interstitials are expected to have different values of mobility and different capture cross-sections at recombination centers, perfect compensation is not expected to occur during room temperature irradiation. This lack of compensation will result in a radiation-induced shift in the Fermi level. An excess of radiation-produced acceptor

levels[†] relative to radiation-produced donor levels would cause a lowering of the Fermi level, with a resultant increase in the tunneling barrier and a decrease in the magnitude of the conductance.

The energy difference between the Fermi level and the conduction band⁷⁹ and thus B, the height of the tunneling barrier is given by

$$B = kT \ln \frac{N_c}{V_o - bC(\phi)} \quad (6-3)$$

where N_c is the density of states in the conduction band, V_o is the oxygen vacancy donor concentration, and $bC(\phi)$ is the concentration of uncompensated radiation-produced acceptor levels which exist at a radiation-produced defect concentration $C(\phi)$. This equation is plotted in Fig. 6-8 for $N_c = V_o = 1$ and $bC(\phi)$ in relative units. From this Figure it may be seen that the height of the tunneling barrier will be independent of the concentration of uncompensated radiation-produced acceptors until this concentration approaches that of the non-stoichiometric oxygen vacancy donors. At this point the height of the tunneling barrier will suddenly increase with increasing fluence, accounting for the observed threshold fluence for the radiation-produced conductance decrease.

This threshold fluence will increase as the concentration of non-stoichiometric oxygen vacancy donors increases.

[†]In analogy with metals, the surviving defects may be oxygen vacancies and tantalum vacancies. Although oxygen vacancies are normally expected to act as donor defects and tantalum vacancies as acceptor defects, it cannot be intrinsically determined whether donor or acceptor defects should predominate in the present case since this "normal" situation does not necessarily apply to oxides for large defect concentrations⁸⁰ such as exist as a result of irradiation to fluences greater than 5×10^{17} p/cm.

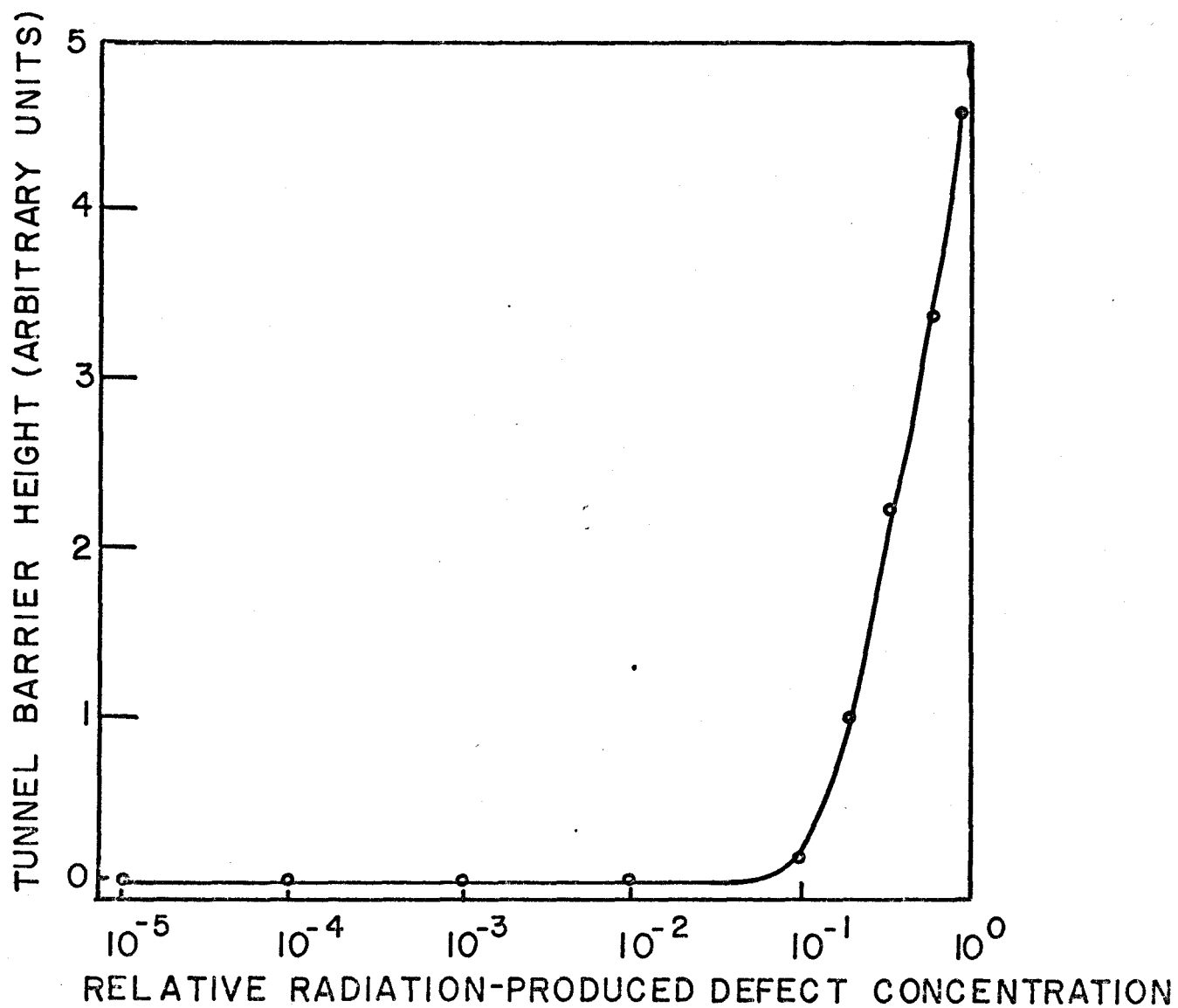


Figure 6-8

Graph of the function $\ln \{1/[1-bC(\phi)]\}$ as a function of $bC(\phi)$.

The observed increase in the threshold fluence with increasing total reactive partial pressure is in agreement with the model proposed in Chapter IV; i.e., as the dimensions of the oxide regions decrease with increasing total reactive partial pressure, the average non-stoichiometry of the oxide is inferred to increase due to oxygen removal by the metallic islands. The apparent saturation of the threshold fluence for films sputtered in total reactive partial pressures less than 2×10^{-5} torr suggests that the diffusion distance for oxygen atoms during the fifteen-minute heat treatment at 500°C is very much less than the gap size for these films so that the average non-stoichiometry becomes relatively independent of gap size and, thus, of total reactive partial pressure.

The observed increase in the total conductance decrease with increasing total reactive partial pressure is in agreement with the proposed model since, as the total reactive partial pressure increases the average non-stoichiometric oxygen vacancy concentration will increase, thus causing the tunneling barrier of unirradiated films to decrease. A given radiation-induced shift in the barrier height will have a greater effect on the conductance as the initial barrier height decreases and, thus, as the total reactive partial pressure increases.

For island-structure films which have been irradiated to between 1.5×10^{18} p/cm² and 2×10^{18} p/cm² at 30°K , about 20% of the damage recovers during isochronal annealing experiments carried out to a maximum temperature of 300°K ; i.e., a

large conductance decrease, analogous to that observed during room temperature irradiation of different resistors from the same substrate, does not occur. This suggests that, after low temperature irradiation, sufficient close-pair recombination occurs during the heating of the film that the defect concentration available for annihilation at gap-island interfaces is inadequate to produce a shift in the Fermi level.

As discussed in Chapter III, the measured film conductance consists of two components, that due to tunneling and that due to metallic conduction via connected metallic islands. Thus, the film conductance g may be approximated by ⁸¹ (see Appendix C)

$$g = g_t + g_m \quad (6-4)$$

where g_t and g_m are the components due to the tunneling mechanism and the metallic conduction mechanism respectively. To within a factor of e^{-1} , the tunneling probability is proportional to $\exp(-dB^{1/2})$, where d is the width of the gap. Assuming ⁸ $m = 500$ for the islands, damage within the islands will effectively saturate at a fluence of 1×10^{17} p/cm²; i.e., g_m will be constant in the fluence range where the radiation-produced conductance decrease occurs. Thus, from equation (6-4),

$$g = g_1 e^{-dB^{1/2}} + g_m \quad (6-5)$$

where g_t is given by the first term on the right hand side of the equation.

From equation (6-2), for a tunneling distance of $d = 2r$ in A, and for $\sigma = \delta C(\phi)$,

$$C(\phi) \approx \frac{3 \times 10^{-10} \sqrt{\phi}}{\sqrt{d}} \quad (6-6)$$

for $\phi \gg 5 \times 10^{16}$ p/cm². Substituting equation (6-6) into equation (6-3) and expanding $B^{1/2}$ by the binomial theorem, equation (6-5) gives

$$\frac{d\sigma}{d\phi} = \frac{dg}{d\phi} = A\phi^{-1/2} \exp(-\phi^{1/2}) \quad (6-7)$$

where A is a constant. According to equation (6-7), a plot of $\ln(\phi^{1/2} d\sigma/d\phi)$ vs $\phi^{1/2}$ should yield a straight line. The experimental points for a film sputtered in a reactive partial pressure of 1.5×10^{-5} torr nitrogen and 1.5×10^{-5} torr oxygen are plotted in this fashion in Fig. 6-9. The resultant linear relationship is in agreement with the proposed model.

The absence of a radiation-produced conductance decrease in films sputtered in a reactive partial pressure of 7×10^{-6} torr nitrogen and 4.3×10^{-5} torr oxygen is consistent with the proposed model. The annealing studies of Chapter V indicate that the absence of an island structure (and, thus, the lack of a large concentration of sinks) inhibits long range, uncorrelated defect annihilation; i.e., close-pair or correlated recombination occurs mainly. Room temperature irradiation of a continuous film is, therefore, expected to produce equal concentrations of stable donors and stable acceptors, and, thus, there is neither a radiation-produced shift in the Fermi level nor an associated conductance decrease.

6.4 Summary

This chapter has considered changes in film conductance during room temperature irradiation for fluences up to 2×10^{18} p/cm². Three different types of film structures were investigated:

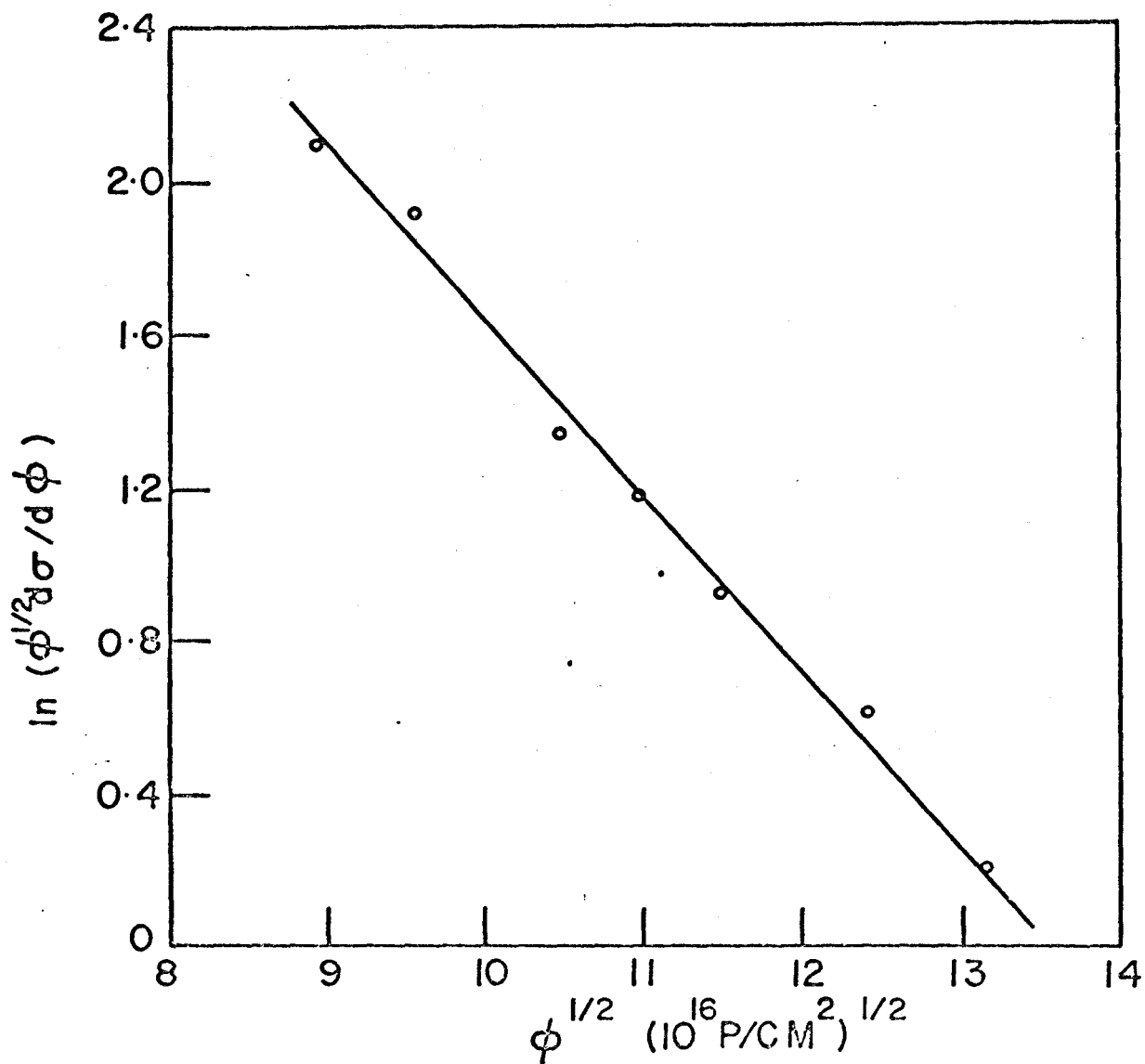


Figure 6-9

Graph of $\ln(\phi^{1/2} d\sigma/d\phi)$ as a function of $\phi^{1/2}$ for fluences in excess of the threshold value for the radiation-produced conductance decrease. This film was sputtered in a reactive partial pressure of 1.5×10^{-5} torr nitrogen and 1.5×10^{-5} torr oxygen.

- 1) films composed of Ta_4O islands largely surrounded by Ta_2O_5 ;
- 2) films composed of BCC Ta islands largely surrounded by Ta_2O_5 ; and
- 3) polycrystalline films of Ta_2O_5 .

For films composed of Ta_4O islands largely surrounded by Ta_2O_5 , the nonlinearity of the conductance increase with fluence is attributed to a nonlinear rate of defect production with fluence due to defect recombination at the gap-island interface during irradiation. The fact that the magnitude of the conductance increase for films consisting of BCC Ta islands is less than that for films consisting of Ta_4O islands is attributed to a greater relative effect of metallic damage in the former films than in the latter films as a result of the fact that the resistivity of BCC Ta is less than that of Ta_4O .

For fluences exceeding a threshold value, the conductance decreases to a value less than the pre-irradiation value. This decrease is attributed to a shift in the Fermi level of the Ta_2O_5 and, thus, an increase in the tunneling barrier, as a result of unequal concentrations of stable radiation-produced donors and acceptors. Unequal concentrations of stable donors and acceptors are postulated to result from unequal concentrations of donors and acceptors annihilating at the gap-island interfaces during irradiation.

The nonlinearity of the σ - ϕ curves for continuous, polycrystalline Ta_2O_5 films is attributed to a nonlinear rate of defect production with fluence as a result of the occurrence of spontaneous recombination and close-pair thermal annealing. The absence of σ - ϕ curves which are characteristic of defect

recombination at unsaturable traps is consistent with the absence of gap-island interfaces in the films as has been indicated by electron microscopy (Chapter III) and by annealing experiments (Chapter V). Similarly, the absence of a radiation-produced conductance decrease is compatible with equal concentrations of stable radiation-produced donors and acceptors - a situation which is postulated to occur in the absence of defect recombination at gap-island interfaces.

VII

EFFECTS OF RADIATION DAMAGE ON FILM TCR

7.1 General

This chapter concludes the investigation of radiation damage on reactively sputtered tantalum thin film resistors with a consideration of the changes in the film TCR which result from 150 keV proton irradiation at 286°K for fluences up to 2×10^{18} p/cm². In addition to the "useful" temperature range of 303°K to 403°K for resistor operation, TCR measurements were also performed over the range 33°K to 44°K in an attempt to obtain information about the processes which affect the film TCR. The use of this low temperature TCR range also permitted a measurement of the TCR recovery following film irradiation at 30°K.

7.2 Experimental Results

Figure 7-1 shows a plot of the percentage change in film conductance as a function of temperature for an air heat treated film sputtered in a reactive partial pressure of 2×10^{-5} torr nitrogen and 2×10^{-5} torr oxygen, both for an unirradiated film and for the same film after irradiation to 2×10^{18} p/cm². For the unirradiated film the conductance increases as a linear function of temperature over the range 30°C to 130°C. The TCR is -86 ppm/°C, where the TCR, α , is

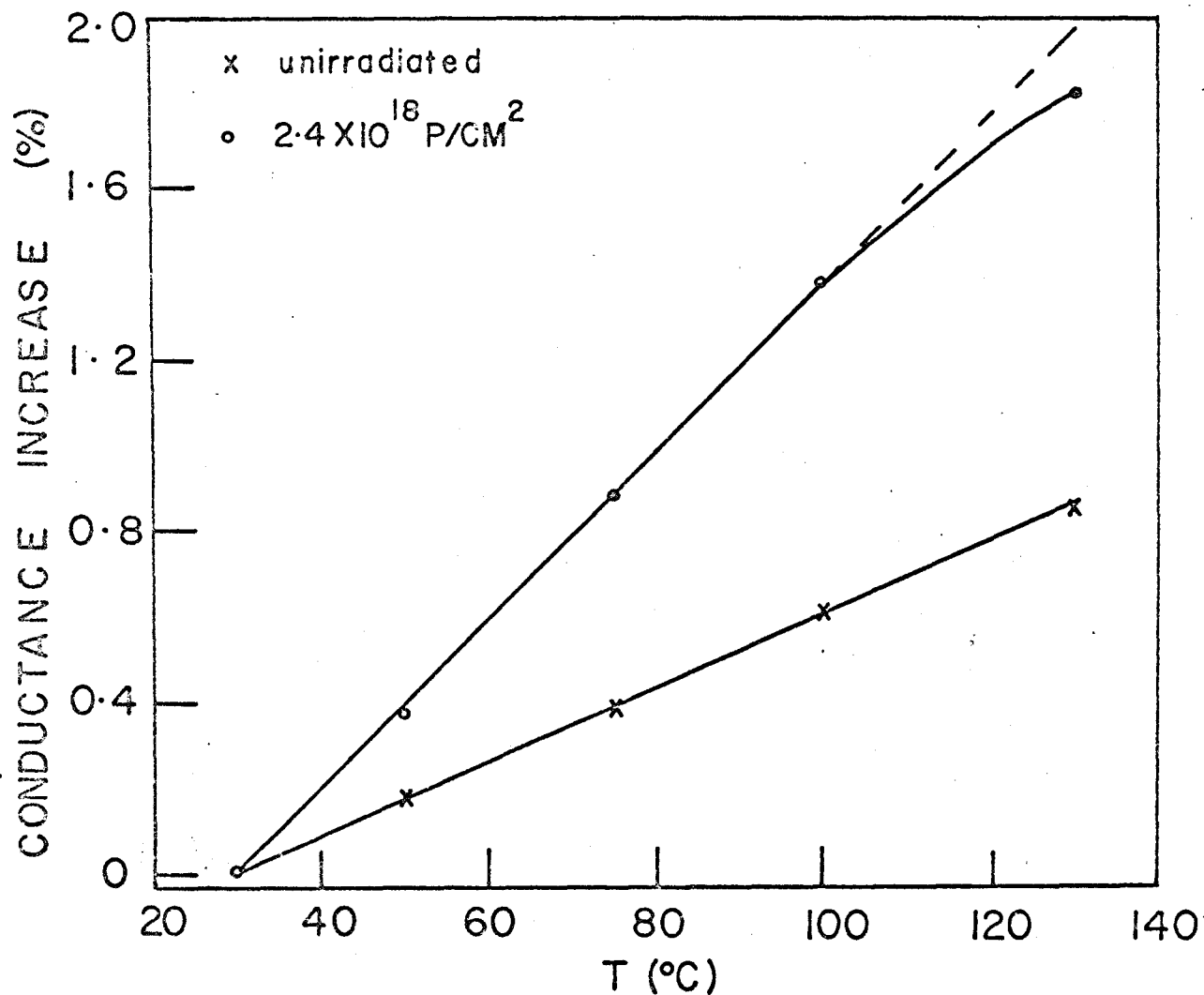


Figure 7-1

Curves showing the conductance increase as a function of temperature for a film sputtered in a reactive partial pressure of 2×10^{-5} torr nitrogen and 2×10^{-5} torr oxygen before irradiation (marked x), and after irradiation to 2.4×10^{18} p/cm² (marked o).

defined by

$$\alpha = - \frac{1}{g(30^{\circ}\text{C})} \frac{dg}{dT} \quad (7-1)$$

where $g(30^{\circ}\text{C})$ is the film conductance at 30°C . The value of $g(30^{\circ}\text{C})$ is unchanged by heating the unirradiated film to 130°C .

After irradiation to 2×10^{18} p/cm², the conductance increases as a linear function of temperature over the range 30°C to 100°C . From 100°C to 130°C the conductance increases, but as a nonlinear function of temperature. Considering the linear portion of the TCR curve for the irradiated film shown in Fig. 7-1, the TCR has increased to -196 ppm/ $^{\circ}\text{C}$ from -86 ppm/ $^{\circ}\text{C}$. After the film had been maintained at 130°C for thirty minutes, the difference between the conductance value obtained by extrapolating the linear portion of the conductance vs temperature curve for the irradiated film to 130°C , and the measured conductance value at 130°C , is $0.27 \mu\text{mhos}$. After completion of the TCR measurements, the conductance at 30°C had decreased by $0.28 \mu\text{mho}$. For all island-structure films investigated, the conductance decrease at room temperature following a post-irradiation TCR run was equal to the difference between the actual conductance at 130°C and the value obtained by extrapolating the linear portion of the post-irradiation TCR curve. This former quantity will be referred to as the post-irradiation TCR conductance decrease. Heating the films to 130°C does not produce any observable change in the slope of the linear portion

of the post-irradiation TCR curve.

Figure 7-2 shows the ratio of the post-irradiation TCR (30°C to 100°C) to the pre-irradiation TCR (30°C to 100°C) as a function of fluence for an air heat treated film sputtered in a reactive partial pressure of 2×10^{-5} torr nitrogen and 2×10^{-5} torr oxygen. This TCR ratio increases rapidly with fluence, for fluences less than 7×10^{17} p/cm². For larger fluences, the TCR ratio increases relatively slowly with fluence. This figure also shows the ratio of the post-irradiation TCR to pre-irradiation TCR for air heat treated films as a function of fluence for room temperature irradiation, where the TCR is measured over the range 33°K to 44°K . The unirradiated film has a TCR of -65 ppm/ $^{\circ}\text{C}$ over this temperature range. For fluences less than 6×10^{17} p/cm² this TCR ratio increases with fluence. For larger fluences this ratio decreases, becoming less than unity for fluences in excess of about 6×10^{17} p/cm².

Figure 7-3 shows the post-irradiation TCR conductance decrease measured at 30°C , as a function of fluence for an air heat treated film sputtered in a reactive partial pressure of 2×10^{-5} torr nitrogen and 2×10^{-5} torr oxygen. For fluences of 2.5×10^{17} p/cm² or less there is no change in the room temperature conductance following a post-irradiation TCR run. For larger fluences the post-irradiation TCR conductance decrease increases rapidly with fluence, reaching apparent saturation at 2.4×10^{18} p/cm². Figure 7-4 illustrates the post-irradiation TCR conductance decrease at 2×10^{18} p/cm² as a function of

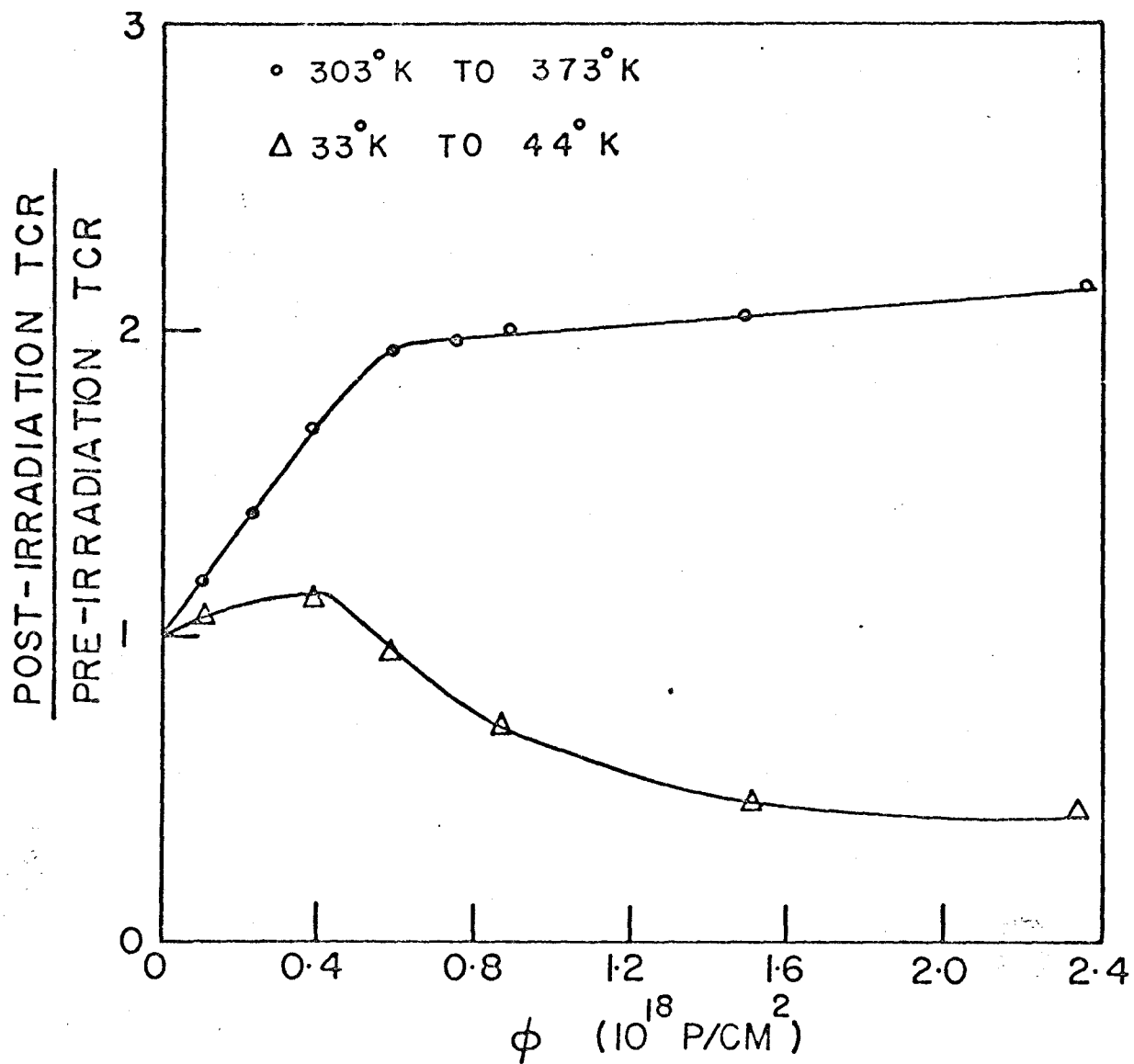


Figure 7-2

Curves showing the ratio (post-irradiation TCR) to (pre-irradiation TCR) as a function of fluence for films sputtered in a reactive partial pressure of 2×10^{-5} torr nitrogen and 2×10^{-5} torr oxygen. The TCR was measured over the temperature range 303°K to 373°K (marked o), as well as from 33°K to 44°K (marked Δ).

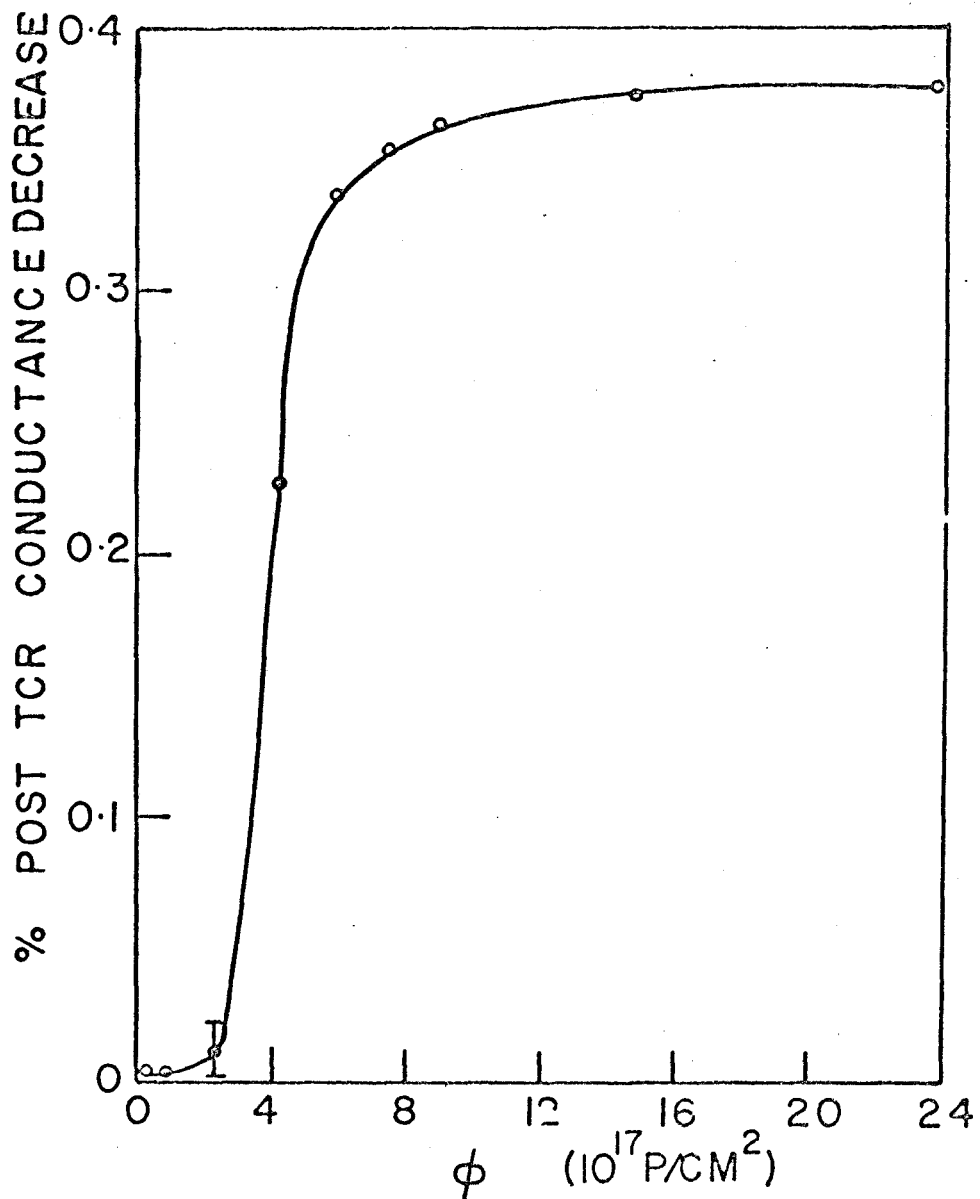


Figure 7-3

Curve showing the variation with fluence of the percent conductance decrease which occurs at 30°C after a post-irradiation TCR run in which the films were maintained at 130°C for 30 minutes. This curve was obtained for films sputtered in a reactive partial pressure of 2×10^{-5} torr nitrogen and 2×10^{-5} torr oxygen.

total reactive partial pressure, for equal oxygen and nitrogen reactive partial pressures. This conductance decrease becomes smaller as the total reactive partial pressure decreases.

After irradiation at 30°K, ten-minute isochronal annealing experiments were carried out for temperature increments of 5°K. Figure 7-5 shows the TCR measured from 33°K to 44°K as a function of annealing temperature, for a film which was sputtered in a reactive partial pressure of 1×10^{-5} torr nitrogen and 3×10^{-5} torr oxygen and irradiated to 2×10^{18} p/cm². The corresponding annealing results for the film conductance are included for comparison. For the TCR case, recovery occurs rapidly up to 150°K while from 150°K to 300°K relatively little TCR recovery occurs. For this film, the pre-irradiation TCR was -100 ppm/°C. In contrast to the TCR recovery, the conductance recovery rate is relatively independent of annealing temperature.

7.3 Discussion

7.3.1 Linear TCR Region

As discussed in Chapter III, the measured conductance of the films consists of two components, that due to tunneling and that due to metallic conduction via connected metallic islands. Thus, the film conductance g may be approximated by ⁸³

$$g = \gamma g_1 e^{-E/kT} + (1-\gamma) g_2 (1 - \alpha_m T) \quad (7-2)$$

where g_1 and g_2 are constants, E is the activation energy for

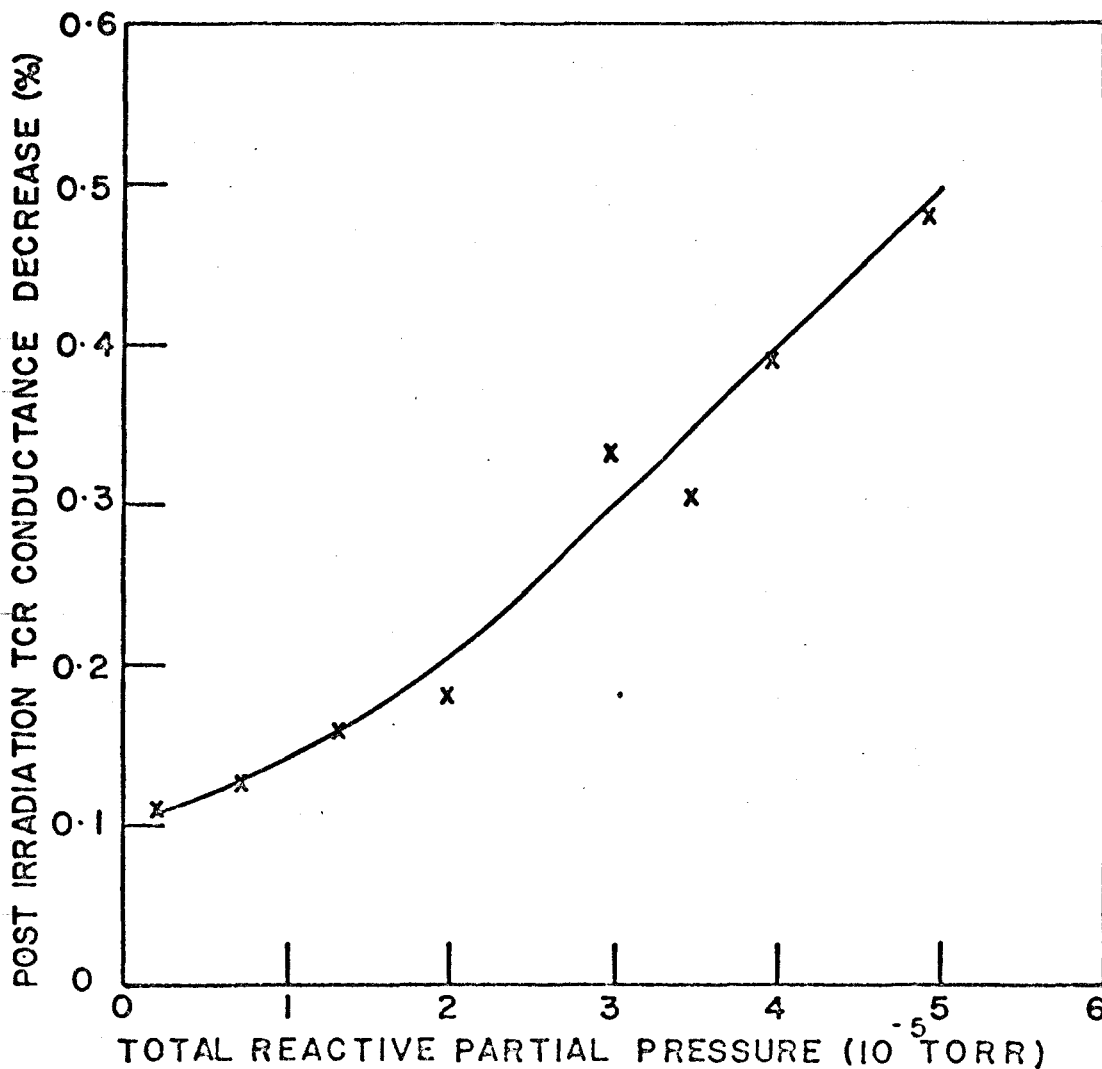


Figure 7-4

Curve showing the variation with total reactive partial pressure of the percent conductance decrease (measured at 30°C) which occurs after a post-irradiation TCR run in which the films are maintained at 130°C for 30 minutes. These films were sputtered in equal reactive partial pressures of oxygen and nitrogen.

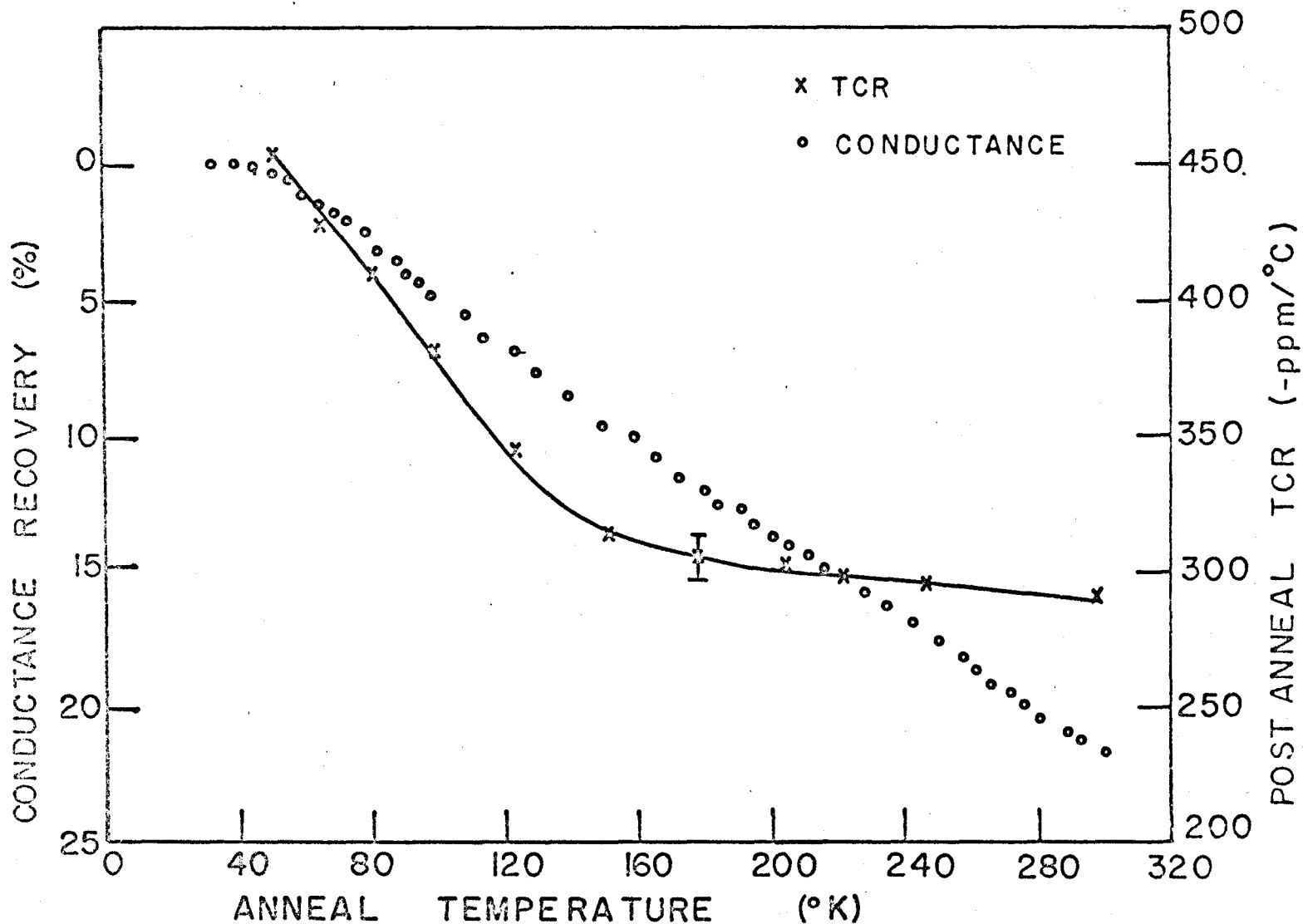


Figure 7-5

Curves showing the recovery which occurs in film conductance and film TCR as a function of temperature after irradiation to 2×10^{18} p/cm² at 34°K. This film was sputtered in a reactive partial pressure of 1×10^{-5} torr nitrogen and 3×10^{-5} torr oxygen.

the activated tunneling component, α_m is the TCR of the metallic component, and γ is the fraction of the total conductance due to the activated tunneling component.

From equations (7-1) and (7-2), the film TCR may be written as

$$\alpha = -\frac{1}{g} \left[\frac{E}{kT^2} \gamma g_1 e^{-E/kT} - \alpha_m g_2 (1 - \alpha_m T) (1 - \gamma) \right] \quad (7-3)$$

for $\alpha_m T < 1$.

In Chapter IV it was shown that the radiation-produced conductance increase for the film illustrated in Fig. 7-1 may be accounted for by an increased tunneling component occurring via radiation produced defect levels within the gap oxide regions, i.e., the effect on film conductance of damage in the metallic islands is very much less than the effect of damage within the oxide regions. In terms of the present notation, this means that $\gamma = \gamma(\phi)$ increases with fluence. However, a comparison of equations (7-2) and (7-3) shows that the ratio of the effect on film TCR of radiation-produced damage in the islands to damage in the gaps is increased by a factor of $\alpha_m kT^2/E$ relative to the ratio of the effect on film conductance of damage in the islands to damage in the gaps. Since this factor is expected to fall within the range of 10 to 100 for these discontinuous films, radiation-produced changes in the metallic component of TCR may not be negligible relative to radiation-produced changes in the tunneling component of TCR. Since E depends on the geometrical

structure of the film, E is expected to be independent of fluence. This was verified previously since the enhanced conductance could be accounted for over three orders of magnitude in fluence by $\gamma(\phi)$. If E were a function of fluence, this would not occur. Thus, from (7-3), the dependence of TCR on fluence may be written

$$\alpha(\phi) = - \frac{1}{g(\phi)} \left[\gamma(\phi) A - 1 - \gamma(\phi) B \right] \quad (7-4)$$

where

$$A = \frac{E g_1 e^{-E/kT}}{kT^2}$$

and

$$B = \alpha_m g_2 (1 - \alpha_m T)$$

It should be noted that α_m will be a function of fluence so long as damage occurs within the islands. Assuming the number of unstable sites ⁸ surrounding each defect to be 500, this damage is expected to saturate at about 10^{17} p/cm². Since much larger fluences (2×10^{18} p/cm²) are employed in the present case, α_m is considered to be constant for purposes of discussing the change in film TCR during irradiation.

For fluences less than that corresponding to the threshold for the conductance decrease, the enhanced conductance is proportional to $C(\phi)$, the concentration of radiation-produced defects through which enhanced tunneling can occur. Thus

$$\gamma(\phi) = \gamma_0 [1 + \epsilon C(\phi)] \quad (7-5)$$

where ϵ is the ratio of the enhanced conductance per unit defect concentration to the conductance of the unirradiated film. Combining equations (7-4) and (7-5), the ratio of the post-irradiation TCR to the pre-irradiation TCR as a function of fluence is given by

$$\frac{\lambda(\phi)}{\lambda(0)} = 1 + \frac{B \epsilon C(\phi)}{\gamma_0 A [1 + \epsilon C(\phi)] - B(1 - \gamma_0) [1 + \epsilon C(\phi)]} \quad (7-6)$$

Since $\epsilon C(\phi) < 1$, the numerator of the second term of equation (7-6) will be a greater function of fluence than the denominator of that term. Since $\epsilon C(\phi)$ increases with fluence, the TCR ratio is expected to increase with fluence, as observed.

For fluences in excess of the threshold for the conductance decrease, $\gamma(\phi)$ is no longer described by equation (7-5) since, in this fluence range, the height of the tunneling barrier, not defect levels within the barrier, account for the radiation-produced conductance change. From equation (7-4), the dependence of the TCR ratio on fluence is given by

$$\frac{\lambda(\phi)}{\lambda(0)} \propto \frac{[1 - \gamma(\phi)]}{g(\phi)} \left\{ \frac{A \gamma(\phi)}{1 - \gamma(\phi)} - B \right\} \quad (7-7)$$

In this region, $g(\phi)$ and $\gamma(\phi)$ decrease with ϕ . Thus, the term $[1 - \gamma(\phi)]/g(\phi)$ increases with increasing fluence, while $\frac{A \gamma(\phi)}{1 - \gamma(\phi)} - B$ decreases with increasing fluence. The net result of these two terms is that, for fluences in excess of the threshold for the radiation-produced conductance decrease, the TCR ratio increases very slowly with fluence. Physically,

the small rate of change in the TCR ratio for fluences in excess of the threshold for a radiation-produced conductance decrease may be attributed to the fact that the decrease in the proportion of the tunneling TCR component relative to the metallic TCR component is compensated for by a corresponding decrease in the magnitude of the reference conductance.

On the basis of the proposed model, the TCR ratio as a function of fluence, for fluences in excess of the threshold for the radiation-produced conductance decrease, would be expected to become less than unity if the proportion of the metallic TCR component could be increased sufficiently relative to the proportion of the tunneling component. If this occurred, the radiation-produced conductance decrease may be sufficient to allow the proportion of the metallic TCR component to become large enough to make the film TCR less negative. This postulate was verified experimentally by measuring the film TCR at low temperatures (33°K to 44°K) following room temperature irradiation since, as discussed in Chapter III, the proportion of the metallic TCR component increases as the film temperature decreases. Figure 7-2 shows that, for fluences in excess of the threshold for the radiation-produced conductance decrease, the TCR ratio does become less than unity, giving additional evidence for the proposed model. At sufficiently low temperatures the TCR ratio would be expected to become negative, i.e., the film TCR should become positive. The fact that this is not observed is attributed to the inability of the present equipment to attain sufficiently low temperatures.

The proposed model will also account for the observation that the magnitude of the TCR ratio for fluences less than the threshold fluence for the radiation-produced conductance decrease is smaller when the TCR ratio is measured from 33°K to 44°K than when measured from 303°K to 373°K. In the former case, the smaller proportion of the negative TCR component produces a smaller relative change in the film TCR than in the latter case.

According to the model proposed in Chapter IV, the enhanced tunneling mechanism in the films is inhibited by the trapping of free carriers by radiation-produced defects. Thus, it might be expected that the film conductance would be a function of temperature due to this mechanism if the fraction of the radiation-produced defects which are thermally occupied were a function of temperature. This temperature dependence would be expected to possess an activation energy of the order of the height of the tunneling barrier, or about ⁴⁸ 1 ev. The fact that this temperature dependence is not observed in irradiated films indicates that the carrier capture cross-section of the radiation-produced defects is much smaller than the capture cross-section of the oxygen vacancy donors. In this case, the free carriers would be captured by the donor levels rather than by the radiation-produced defect levels as the films are cooled; i.e., the free carrier concentration is determined principally by the oxygen vacancy donor concentration, with a small perturbation occurring due to the presence

of radiation-produced defects. During this cooling process, any carriers initially trapped in the radiation-produced defect levels would remain there. Thus, the fraction of thermally filled radiation-produced defects and the resulting enhanced conductance may be independent of temperature.

7.3.2 Nonlinear TCR Region

The permanent conductance decrease occurring in films heated above 100°C as the result of a post-irradiation TCR run is similar to that observed during room temperature conductance measurements as a function of fluence in that there is a threshold fluence above which this conductance decrease occurs. Analogously to the radiation-produced conductance decrease, the decrease produced by heating may be due to an increase in the height of the tunneling barrier resulting from a shift in the Fermi level. In the present case, this would occur if donor defects were able to annihilate at the gap-island interface between 100°C and 130°C . This would produce an excess of acceptor defects, with a resultant shift in the Fermi level.

Since the magnitude of the thermally-produced conductance decrease depends on the concentration of radiation-produced donor defects which can migrate to the gap-island interface during a post-irradiation TCR run, the magnitude of the conductance decrease is expected to increase as the gap size decreases. As shown by electron microscopy, the dimensions of the gap regions decrease as the total reactive partial

pressure increases. Thus, the magnitude of the thermally-produced conductance decrease is expected to increase as the total reactive partial pressure increases. As shown in Fig. 7-5, this is observed experimentally.

7.3.3 TCR Annealing

The difference in the conductance recovery and the TCR recovery as a function of temperature indicates that different recovery mechanisms are dominant in these two cases. As discussed previously in Chapter V, the conductance recovery is attributed mainly to the annihilation of defects produced within the inter-island oxide regions. In contrast to this, annealing of defects in both the oxide regions and the metallic island regions are expected to affect the TCR recovery.

As discussed previously in section 7.3.1, the metallic island TCR is expected to contribute significantly to the film TCR when this TCR is measured over the range 33°K to 44°K. As damage within the islands anneals, the metallic island contribution to the film TCR will become increasingly positive, causing the film TCR to become less negative. The rapid TCR recovery for temperatures below 150°K together with relatively little recovery for higher temperatures (150°K to 300°K) is generally characteristic of damage recovery in metals⁸ and is in agreement with the proposed model of a metallic conduction mechanism and a tunneling conduction mechanism acting concurrently.

7.4 Summary

Following irradiation at 286°K, the film TCR, as measured from 303°K to 373°K, becomes more negative with increasing fluence. This is consistent with an increase in the proportion of the tunneling component of negative TCR relative to the metallic component of positive TCR as the result of a radiation enhanced tunneling mechanism. The film conductance is a reversible function of temperature in this range, i.e., heating the films to 373°K does not produce any change in the conductance measured at 303°K. However, when the films are heated from 373°K to 403°K, a threshold fluence exists, above which the conductance measured at 303°K decreases after the films have been heated. This conductance decrease is attributed to an increase in the height of the inter-island tunneling barrier as a result of thermal annihilation of unequal concentrations of radiation-produced donors and acceptors at the gap-island interface. The threshold fluence corresponds to that value of fluence at which the concentration of uncompensated radiation-produced acceptors equals the initial concentration of ionized donors.

Following irradiation at 286°K, the film TCR was also measured over the range 33°K to 44°K as a function of fluence. These low temperature TCR measurements were carried out in order to increase the metallic contribution to the film TCR relative to the tunneling contribution. The variation of the film TCR

with fluence is qualitatively similar to the variation of film conductance with fluence, again suggesting that the radiation-produced change in film TCR is the result of a change in the proportion of the film TCR which is due to the tunneling mechanism: for fluences less than the threshold value for the radiation-produced conductance decrease, the film TCR becomes more negative due to an increase in the proportion of the tunneling mechanism relative to the metallic mechanism; for fluences in excess of the threshold for the radiation-produced conductance decrease, the film TCR becomes less negative due to a smaller contribution of the negative tunneling TCR to the film TCR. The fact that the film TCR does not become less negative when measured in the vicinity of room temperature indicates that, in this temperature range, the contribution of the metallic TCR component to the film TCR is insufficient to shift the film TCR toward a positive value.

Following irradiation at 30°K, the TCR as measured from 33°K to 44°K anneals much more rapidly from 50°K to 150°K than from 150°K to 300°K. This is attributed to an annealing of radiation-produced defects within interconnected metallic islands as well as within the gap oxide regions.

VIII

CONCLUSIONS

Due to their high resistivity and low TCR, reactively sputtered Ta films are used extensively as resistive elements in microelectronic circuitry. In many applications, where a circuit is operated in a radiation environment such as occurs during space flight, the stability of a circuit may be critically dependent on the stability of these resistors. The literature does not contain any information concerning the effects of radiation on the properties of reactively sputtered Ta thin film resistors. The present investigation was undertaken in an attempt to fill this void.

The films were prepared by reactive sputtering in oxygen and nitrogen simultaneously. Results of electron microscope investigations are consistent with a film structure consisting of connected metallic islands (typically 100 Å) largely surrounded by Ta₂O₅ (typically 50 Å). This oxide, initially amorphous for as-deposited films, crystallizes during heat treatment of the films at 500°C. Conductance measurements as a function of temperature are in agreement with this structure, suggesting that conduction occurs by activated inter-island tunneling (having a negative temperature coefficient of resistivity) acting concurrently with metallic conduction via

connected islands (having a positive temperature coefficient of resistivity). Electron microscopy shows that heat treated films reactively sputtered in a partial pressure of 7×10^{-6} torr nitrogen and 4.3×10^{-5} torr oxygen consist of polycrystalline Ta_2O_5 . Although the resistivity of these films is relatively high ($4 \times 10^4 \mu\Omega\text{-cm}$), the large TCR ($-2,000 \text{ ppm}/^\circ\text{C}$) generally prohibits these films from being used as resistors. However, these films are significant for the interpretation of radiation-damage experiments since they do not contain a large concentration of gap-island interfaces.

Results of room temperature irradiations to 10^{16} p/cm^2 are used as the basis for a model which is proposed to explain the conductance increase observed after irradiation of discontinuous films by 150-keV protons. For heat treated films, the linear conductance increase with fluence is attributed to an enhanced tunneling current occurring via radiation-produced defect levels within the inter-island oxide. The nonlinear conductance increase observed for non heat treated films is attributed to nonlinear defect production with fluence resulting from a trapping of radiation-produced defects. Other mechanisms of conductance increase were considered (sputtering of the surface oxide, hydrogen-ion implantation, and radiation-produced defect levels within the surface oxide), but these were found to be incompatible with experimental observations.

Low temperature (30°K) damage and isochronal annealing experiments were performed in order to provide further

insight into the damage mechanisms, thus forming a basis for the understanding of high fluence (2×10^{18} p/cm²) room temperature damage results. For non heat treated films, the observed linear decrease in damage rate with increasing damage concentration at 30°K is attributed to the production of unstable defects within the inter-island oxide due to a combination of spontaneous recombination and thermal annealing. Recovery occurs in two main stages: the low temperature stage (34°K to 150°K) is attributed to close-pair or correlated recombination, and the second stage (150°K to 300°K) is attributed to the migration of defects to sinks at the gap-island interface.

This thermal migration of defects to the gap-island interface accounts for the linear increase in inverse damage rate with increasing damage concentration which is observed for non heat treated films during room temperature irradiation for fluences in excess of 10^{16} p/cm². For fluences in excess of about 6×10^{17} p/cm², the conductance decreases as a function of fluence, approaching apparent saturation at about 2×10^{18} p/cm². This decrease in conductance is attributed to an increase in the height of the tunneling barrier as the result of a radiation-produced shift in the Fermi level. This shift is ascribed to the production of unequal concentrations of stable donor and acceptor defects as the result of annihilation of unequal concentrations of donor defects and acceptor defects at gap-island interfaces during irradiation.

The negative TCR (measured from 30°C to 100°C) of the unirradiated films becomes increasingly negative as the result of irradiation. This is ascribed to an increase in the proportion of the gap conduction mechanism of negative TCR relative to the metallic conduction mechanism of positive TCR.

Since the resistivity and TCR of these films changes by typically 1 percent at a fluence of 10^{16} p/cm², the films are relatively suitable for use as resistors in a radiation environment. In comparison, the gain of bipolar transistors will fall to unity at fluences which are typically about two orders of magnitude smaller. The use of these films as negative feedback elements in conjunction with such transistors is a simple and inexpensive method of reducing the radiation-sensitivity of a circuit since, in this configuration, the circuit properties are relatively independent of the properties of the transistor, but largely dependent on the properties of the resistors. 84

An interesting and useful result of employing thin film resistors is that massive shielding may not be required for satisfactory circuit operation since high energy radiation will simply pass through the films and produce little damage. Potentially damaging low energy particles will be effectively attenuated by almost any material surrounding the films and, thus, should not produce a significant amount of damage. In contrast to this, conventional bulk devices require a considerable amount of shielding since high energy radiation may possibly be stopped within the devices, thus causing a considerable amount of damage.

A P P E N D I X A

THE RELATIONSHIP BETWEEN THE CHANGE IN FILM CONDUCTANCE DUE TO ENHANCED TUNNELING AND THE RADIATION-PRODUCED DEFECT CONCENTRATION

It has been shown experimentally in Chapter III that electrical conduction in the present discontinuous films is consistent with inter-island tunneling. The current transmitted by tunneling in one direction through an oxide barrier between two islands to be called Island No. 1 and Island No. 2, is given by ⁵⁶

$$J_1 = e \int T(E_x) N_1(E_x) dE_x \quad (A-1)$$

where e is the electronic charge, $T(E_x)$ is the transmission coefficient for carriers of energy E_x in the tunneling direction, $N_1(E_x) dE_x$ given by

$$N_1(E_x) dE_x = v_x dP_x \int f_1 g_1 dP_y dP_z \quad (A-2)$$

is the number of electrons per unit area per unit time in the energy range E_x to $E_x + dE_x$ which are available to tunnel through the barrier, where f_1 is the Fermi function for metal 1 having a density of states g_1 , and $v_x = dE_x/dP_x$ is the x-directed velocity component of a carrier having momentum P_x . The net current between islands, given by the difference of the component currents in each direction, is

$$J = e \int T(E_x) dE_x \int g(f_1 - f_2) dP_y dP_z \quad (A-3)$$

Taking metal No. 1 as the reference level for an applied voltage V ,

$$f_1 = \left[1 + \exp(E-\eta)/kT \right]^{-1} \quad (\text{A-4})$$

where η is the Fermi level and E is the carrier energy, and

$$f_2 = \left[1 + \exp(E-\eta+eV)/kT \right]^{-1} \quad (\text{A-5})$$

Assuming free-electron metals and small applied voltages, substitution of equations (A-4) and (A-5) into (A-3) gives ⁵⁶

$$J = \frac{4}{h^3} \frac{me^2V}{3} \int T(E_x) \left[1 + \exp(E_x-\eta)/kT \right]^{-1} dE_x \quad (\text{A-6})$$

Penley ⁵⁶ has shown theoretically that the presence of an electronic trapping level in the oxide will enhance the tunneling current through the oxide. He has shown that, in analogy with equation (A-6), the net enhanced current for a trap located at position x is given by

$$J^t(x) = \frac{4}{h^3} \frac{me^2VA}{3} \int T^t(E_x) \left[1 + \exp(E_x -)/kT \right]^{-1} \frac{dE_x}{1+\beta\tau} \quad (\text{A-7})$$

where $T^t(E_x)$ is the transmission coefficient of a carrier through the barrier via the trapping level, A is the effective cross-sectional area of the trap, τ is the time the carrier spends in the trap, and β is a function of E_x and the position of the Fermi level.

If there are a number of traps in the barrier, the total tunneling current through the barrier will depend on the distribution as well as the concentration of traps. This total current

may be written ⁵⁶

$$J_{\text{total}}(V) = J(V) + \int C(x) J^t(V) dx \quad (\text{A-8})$$

where $J(V)$ is the current through a barrier which does not contain traps, and $C(x)$ is the concentration of unoccupied levels through which tunneling can occur. The total conductance of the barrier, g_{total} , is given by

$$\begin{aligned} g_{\text{total}} &= \frac{dJ_{\text{total}}}{dV} \\ &= g + \int C(x) g^t(x) dx \end{aligned} \quad (\text{A-9})$$

where g , the initial conductance before enhancement is given by

$$g = \frac{4\pi me^2}{h^3} \int T(E_x) [1 + \exp(E_x - \eta)/kT]^{-1} dE_x \quad (\text{A-10})$$

and $g^t(x)$, the enhanced conductance per unit defect concentration at position x is given by

$$g^t(x) = \frac{4\pi me^2 A}{h^3} \int T^t(x, E_x) [1 + \exp(E_x - \eta)]^{-1} \frac{dE_x}{1 + \beta \eta} \quad (\text{A-11})$$

From equation (A-8), the value of σ defined as $\frac{g_{\text{total}} - g}{g}$ is given by

$$\sigma = \frac{1}{g} \int C(x) g^t(x) dx \quad (\text{A-12})$$

A P P E N D I X B

DEFECT CONCENTRATION AS A FUNCTION OF FLUENCE

As the fluence ϕ increases by $d\phi$, the increase in the concentration of radiation-produced interstitial-vacancy pairs, dC_d , is given by ⁸

$$dC_d = N_a \nu \sigma_d d\phi \quad (\text{B-1})$$

where N_a is the atomic concentration, σ_d is the displacement cross-section, and ν is the average number of secondary knock-ons per primary knock-on. The increase in the concentration of stable defects is given by

$$dN_d = f(\phi) dC_d = N_a \nu \sigma_d f(\phi) d\phi \quad (\text{B-2})$$

where $f(\phi)$ is a function of magnitude equal to or less than unity that accounts for the fact that the concentration of stable defects may not be a linear function of fluence. The percent conductance change σ is given by $\sigma = \delta_1 N_d$ where δ_1 ($= \delta' (1 + P\sigma_c n\nu)^{-1}$) (see equation (4-6)) is the effective percent conductance change per unit defect concentration, i.e., δ_1 takes into account the fact that not all radiation-produced trapping levels are unoccupied and thus available for conductance enhancement. Therefore, from equation (B-2)

$$d\sigma/d\phi = \delta_1 \nu \sigma_d N_a f(\phi) \quad (\text{B-3})$$

For sufficiently low fluences $f(\phi)$ may equal unity, in which case

$$\sigma = \delta \nu \sigma_d N_a \quad (\text{B-4})$$

Now consider some specific cases where $f(\phi)$ is not unity.

1. Spontaneous Recombination and Close-pair Thermal Annealing

These mechanisms will occur at low irradiation temperatures if a newly-formed defect can be annihilated in the unstable zone of its anti-defect. Let the unstable zone contain m lattice sites and let the increase in the concentration of $i-v$ pairs produced by the irradiation, but not necessarily as stable defects, be dC_d . Then dC_d new interstitials may come to rest on a fractional concentration of either mN_v unstable sites or $(1-mN_v)$ stable sites, where N_v is the fractional vacancy concentration. Thus, the fraction of interstitials formed on stable sites is $(1-mN_v)$, and dN_i , the increase in the fractional concentration of stable interstitials is

$$dN_i = (1 - mN_v) \frac{dC_d}{N_a} \quad (\text{B-5})$$

Since defects can recombine only by mutual annihilation at low temperatures, $N_i = N_v = N_d$ and equation (B-4) becomes

$$\frac{d\sigma}{d\phi} = \delta \nu \sigma_d \left(1 - \frac{m\sigma}{\delta} \right) \quad (\text{B-6})$$

where δ is the percent conductance increase per fractional defect concentration.

2. Recombination at Unsaturation Traps

If long-range migration of defects (assumed to be interstitials) can occur during irradiation, these defects may become trapped, producing a nonlinear increase in defect concentration with fluence.

If N_i^m , N_t , and N_v are the fractional concentrations of migrating interstitials, of trapping sites, and of vacancies respectively, the rate of production of migrating interstitials is given by ⁷⁸

$$\frac{dN_i^m}{dt} = \nu\sigma_d\bar{\Phi} - K(r_t N_t + r_v N_v)N_i^m \quad (\text{B-7})$$

and the rate of production of stable vacancies is given by

$$\frac{dN_v}{dt} = \nu\sigma_d\bar{\Phi} - K r_v N_v N_i^m \quad (\text{B-8})$$

where $\bar{\Phi} = \phi/t$ is the proton flux density, r_v the capture cross-section of the vacancies, r_t the capture cross-section of the unsaturable traps, and K a constant proportional to the diffusion coefficient for interstitials. If the migration rate of interstitials is sufficiently rapid at the irradiation temperature, stationary conditions can be assumed ⁷⁸, i.e., $dN_i^m/dt = 0$. Thus, solving ⁷⁸ equation (B-7) and (B-8) gives

$$\frac{d\phi}{d\sigma} = \frac{1}{\delta\nu\sigma_d} \left(1 + \frac{\sigma}{\delta q_t N_t} \right) \quad (\text{B-9})$$

where $q_t = r_t/r_v$ and δ is the percent conductance increase per fractional defect concentration.

A P P E N D I X C

FUNCTIONAL DEPENDENCES OF FILM CONDUCTANCE

This Appendix summarizes the various functional dependences of film conductance which are discussed in the text of the thesis.

Conductance Equation

As shown experimentally in section 3.4.1, electrical conduction in the films can be considered to occur by a tunneling mechanism and a metallic conduction mechanism operating in parallel. If these mechanisms are independent, the film conductance g may be approximated by ⁸¹

$$g = g_t + g_m \quad (C-1)$$

where g_t and g_m represent the summations of the conductance over all gap regions and over all connected metallic islands. This approximation is valid regardless of the density, size, or composition of the islands and gaps.

Temperature Dependence

The experimental results show the tunneling component to possess an activation energy E . The metallic component is expected to possess a metallic TCR α_m , giving a temperature dependent film conductance ⁸³

$$g(T) = g_1 \exp(-E/kT) + g_2(1 - \alpha_m T) \quad (C-2)$$

for $\alpha_m T < 1$.

Dependence on Defect Concentration

For fluences less than the threshold for the radiation-produced conductance decrease, the film conductance may be approximated by

$$g = g_t [1 + \delta C_1(\phi)] + \frac{1}{R_m [1 + \rho C_2(\phi)]} \quad (C-3)$$

where $C_1(\phi)$ is the fractional concentration of empty radiation-produced trapping levels within the gap oxide regions, $C_2(\phi)$ is the fractional concentration of radiation-produced defects within the metallic islands, R_m is the resistance of the islands, δ is the percent conductance increase per fractional defect concentration within the gap regions, and ρ is the percent resistance increase per fractional defect concentration within the islands.

Dependence on Tunnel Barrier

The tunneling portion of the film conductance is proportional to the tunneling coefficient which may be approximated⁸² by $\exp(-dB^{\frac{1}{2}})$, where d is the tunneling distance in Å and B is the barrier height in eV. Thus,

$$g = g_2 \exp(-dB^{\frac{1}{2}}) + g_m \quad (C-4)$$

REFERENCES

1. R.C. Dorf, Modern Control Systems (Addison Wesley, Reading, 1967).
2. R.B. Marcus, J. Appl. Phys. 37, 3121 (1966).
3. R.B. Marcus and S. Quigley, Thin Solid Films 2, 467 (1968).
4. J. Sosniak, W.J. Polito, and G.A. Rozgonyi, J. Appl. Phys. 38, 3041 (1967).
5. M.H. Read and C. Altman, Appl. Phys. Letters 7, 5 (1965)
6. D. Gerstenberg and C.J. Calbick, J. Appl. Phys. 35, 402 (1964).
7. E. Krikorian and R.J. Sneed, J. Appl. Phys. 37, 3674 (1966).
8. M.W. Thompson, Defects and Radiation Damage in Metals (Cambridge University Press, Cambridge, 1969).
9. M.M. Ramsay, Thin Solid Films 1, 405 (1967).
10. K.L. Merkle and L.R. Singer, Appl. Phys. Letters 11, 35 (1967).
11. G.F. Ivanovskii and T.D. Radzhavov, Sov. Phys.-Solid State 8, 1013 (1966)
12. B. Navinsik and G. Carter, Can. J. Phys. 46, 719 (1968).
13. V. Teodosic, Appl. Phys. Letters 9, 209 (1966).
14. R.W. Berry, P.M. Hall, and M.T. Harris, Thin Film Technology (D. Van Nostrand Co., Princeton, N.J., 1968).
15. H.L. Olesen, Radiation Effects on Electronic Systems (Plenum Press, New York, 1966).
16. W.R. Hardy, J. Shewchun, D. Kuenzig, and C. Tam, Thin Solid Films 8, 81 (1971).
17. J. Shewchun, W.R. Hardy, D. Kuenzig, and C. Tam, Thin Solid Films 8, 101 (1971).
18. W.R. Hardy, P.P. Pronko, and J. Shewchun, Appl. Phys. Lett. 19, 174 (1971).

19. W.R. Hardy, P.P. Pronko, and J. Shewchun, J. Phys. Chem. Solids, Submitted.
20. W.R. Hardy and J. Shewchun, Rad. Effects, Submitted.
21. W.R. Hardy and J. Shewchun, Rad. Effects, Submitted.
22. W.R. Hardy, R. Yager, and J. Shewchun, Nucl. Inst. and Meth. 77, 331 (1970).
23. P.P. Pronko, W.R. Hardy, and J. Shewchun, Rad. Effects, In Press.
24. Hewlett-Packard, Catalogue No. 24, p. 124.
25. H. Hakansson and E. Erlandsson, Nucl. Inst. and Meth. 70, 205 (1969).
26. J.A. Walston and J.R. Miller, ed., Transistor Circuit Design (McGraw Hill, New York, 1963).
27. H.S. Carslaw and J.C. Jaeger, Conduction of Heat in Solids (Oxford University Press, London, 1959).
28. L.F. Lowe, C. Jiminez, and E.A. Burke, Rev. Sci, Instrum. 34, 1348 (1963).
29. ASTM Powder Index File Card 15-243.
30. ASTM Powder Index File Card 8-255.
31. ASTM Powder Index File Card 3-1212.
32. ASTM Powder Index File Card 4-0788.
33. C.J. Calbick and N. Schwartz, Trans. 9th Nat. Vac. Symp. (The MacMillan Co., New York, 1962).
34. P.H.G. Draper and J. Harvey, Acta Met. 11, 873 (1963)
35. C. Jech and R. Kelly, J. Phys. Chem. Solids 30, 465 (1969).
36. R.E. Pawel and J.J. Campbell, J. Electrochem. Soc. 111, 1230 (1964).
37. L.D. Calvert and P.H.G. Draper, Can. J. Chem. 40, 1943 (1962).
38. W.J. Ostrander and C.W. Lewis, Trans. 3th Vac. Symp. (Pergamon Press, New York, 1961).
39. K.L. Chopra, Thin Film Phenomena (McGraw Hill, New York, 1969).

40. E. Hollands and D.S. Campbell, J. Materials Science 3, 544 (1968).
41. H.J. Coyne and R.N. Tauber, J. Appl. Phys. 39, 5585 (1968).
42. E. Gebbhardt and H.D. Seghezzi, Z. Metallk 50, 521 (1959).
43. E. Gebbhardt, H. Seghezzi, and W. Durrschnabel, Z. Metallk 49, 577 (1958).
44. C.A. Steidel and D. Gerstenberg, J. Appl. Phys. 40, 3828 (1969).
45. R.H. Perkins, Tantalum Annealing and Degassing and Hardness Effects of Dissolved Gases, Los Alamos Scientific Laboratory, Report LA-2136.
46. J.G. Simmons, Phys. Rev. 155, 657 (1967).
47. G.L. Standley and L.I. Maissel, J. Appl. Phys. 35, 1530 (1964).
48. W.E. Flannery and S.R. Pollack, J. Appl. Phys. 37, 4417 (1966).
49. J.F. Henrickson, G. Krauss, R.N. Tauber, and D.J. Sharp, J. Appl. Phys. 40, 5006 (1969).
50. J.G. Simmons, J. Appl. Phys. 35, 2655 (1964).
51. J.G. Simmons, J. Appl. Phys. 34, 1793 (1963).
52. C.A. Neugebauer and M.B. Webb, J. Appl. Phys. 33, 74 (1962).
53. R.M. Hill, Proc. Roy. Soc. A309, 377 (1969).
54. D.A. McLean, N. Schwartz, and E.D. Tidd, Proc. IEEE 54, 1450 (1964).
55. H.J. Goldschmidt, Interstitial Alloys (Plenum Press, New York, 1967).
56. J.C. Penley, Phys. Rev. 128, 596 (1962).
57. J.W. Gadzuk, J. Appl. Phys. 41, 286 (1970).
58. R. Bube, Photoconductivity of Solids (John Wiley and Son, New York, 1960).
59. D.M. Smyth and T.B. Tripp, J. Electrochem. Soc. 110, 1264 (1963).

60. J. Lindhard, M. Scharff, and H.E. Schiott, Kgl. Danske Videnskab Selskab. Mat. Fys. Medd. 33, No. 14 (1963).
61. T.H. Amsbacher, Surface Sci. 14, 461 (1969).
62. O.A. Panchenko and Yu. G. Ptushinskii, Sov. Phys.-Solid State 9, 2782 (1968).
63. P. Sigmund, Phys. Rev. 184, 383 (1969).
64. L.W. Nghi and R. Kelly, Can. J. Phys. 48, 137 (1970).
65. P.J. Harrop, N. Wilkins, and J. Wanklyn, Corros. Sci. 7, 287 (1967).
66. G.W. Arnold and W.D. Compton, Appl. Phys. Lett. 4, 66 (1960).
67. A. Van Wijngaarden, B. Miremadi, E.J. Brimmer, and J.N. Bradford, Can. J. Phys. 48, 1026 (1970).
68. S. Lungu, Phys. Stat. Sol. 23, 147 (1967).
69. R.S. Nelson, United Kingdom Atomic Energy Authority Report AERE-R4283.
70. R. Kelly, C. Jech, and H.J. Matzke, Phys. Stat. Sol. 25, 641 (1968).
71. T.R. Waite, Phys. Rev. 107, 463 (1957).
72. A.C. Damask and G.J. Diennes, Point Defects in Metals (Gordon and Breach Science Publishers, New York, 1963).
73. E.F. Krimmel, Phys. Stat. Sol. 33, K63 (1969).
74. G. Burger, K. Isebeck, R. Kerler, J. Volkl, H. Wenzl, H.H. Kuhlmann, and H. Schultz, Phys. Lett. 20, 472 (1966).
75. S. Myhra and J.W. DeFord, Phys. Rev. 188, 1093 (1969).
76. J. Nihoul, Vacancies and Interstitials in Metals, ed. A. Seeger, D. Schumacher, W. Schilling and J. Diehl (North Holland Publ. Co., Amsterdam, 1969).
77. M.W. Thompson, Phil. Mag. 3, 278 (1960).
78. F. Dworschak, H. Schuster, H. Wollenberger, and J. Wurm, Phys. Stat. Sol. 29, 75 (1968).
79. J.S. Blakemore, Semi-Conductor Statistics (Pergamon Press, New York, 1962).

80. P. Kofstad and A. Hed, J. Electrochem. Soc. 115, 102 (1968).
81. T.J. Coutts, Thin Solid Films 4, 429 (1969).
82. R. Stratton, J. Phys. Chem. Solids 23, 1177 (1962).
83. J. Weber, IEEE Trans. on Component Parts 3, 14 (1967).
84. F. Larin, Radiation Effects in Semiconductor Devices (John Wiley and Son, New York, 1968).